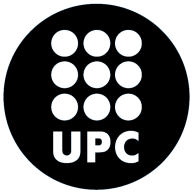

Universitat Politècnica de Catalunya

Enginyeria de Sistemes, Automàtica i Informàtica Industrial

Programa de Doctorat
Enginyeria Biomèdica

Contributions to Automatic and Unsupervised MRI Brain Tumor Segmentation: A New Fuzzy Approach

---

Author:
Nelly Gordillo Castillo

Advisors:
Eduard Montseny
Pilar Sobrevilla

May 2010

Resumen

Los tumores cerebrales son parte de un grupo de enfermedades comunes, no transmisibles, crónicas y potencialmente mortales que afectan a la mayoría de las familias en Europa [Albretha 2008]. La imagen juega un papel primordial en la gestión de los tumores cerebrales, desde su detección y clasificación hasta su posterior seguimiento.

Cada vez más, las imágenes de resonancia magnética (IRM) se utilizan en la gestión de posibles tumores cerebrales ya que, además de mostrar las estructuras cerebrales en gran detalle, tiene una gran sensibilidad para detectar la presencia o cambios en el interior de un tumor. Actualmente la mayor parte de los procesos relacionados con los tumores cerebrales como: el diagnóstico, terapia, y planificación de cirugías, están basados en su previa segmentación en IRM. La segmentación de tumores cerebrales en IRM es una tarea que involucra diferentes disciplinas, ya que los elementos a segmentar son estructuras anatómicas frecuentemente no rígidas y complejas en forma, que varían enormemente en tamao y posición, y muestran una considerable variabilidad de paciente a paciente. Además, la tarea de etiquetar tumores cerebrales en IRM es muy lenta y existe una variación significativa entre las etiquetas presentadas por diferentes expertos.

Los desafíos asociados con la segmentación automática de tumores cerebrales han dado lugar a muchos enfoques diferentes. Aunque la exactitud presentada por los métodos propuestos es prometedora, estos enfoques no han ganado una amplia aceptación entre los patólogos en la práctica clínica. Dos de las principales razones son la falta de procedimientos estandarizados, y la deficiencia de los métodos existentes para ayudar a la decisión médica siguiendo una línea de trabajo similar a la de un técnico.

Para que un sistema de segmentación de tumores cerebrales tenga aceptación entre los patólogos para la práctica clínica, debería apoyar la decisión médica

de manera transparente e interpretable, emulando el papel de un técnico y teniendo en cuenta su experiencia y conocimientos. Esto incluye conocimiento de la apariencia esperada, ubicación, variabilidad respecto de la anatomía normal, simetría bilateral, y conocimiento de las intensidades esperadas de los diferentes tejidos. Los problemas relativos a la imagen, así como la variabilidad en la distribución de los tejidos entre la población humana, implica la consideración de cierto grado de incertidumbre en los resultados de la segmentación.

Una posible solución para el diseo de sistemas complejos en los que se debe incorporar la experiencia de un experto, o los conceptos relacionados son inciertos, es el uso de técnicas de soft computing como los sistemas difusos. Una ventaja importante de los sistemas difusos es su capacidad para manejar información en la que hay vaguedad implícita.

En este trabajo se propone el desarrollo de un método para ayudar a los especialistas en el proceso de segmentación de tumores cerebrales. El objetivo principal es desarrollar un sistema que pueda seguir la misma línea de trabajo de un técnico, teniendo en cuenta su experiencia y conocimiento. En concreto, se presenta un sistema de segmentación, totalmente automático y sin supervisión, que considera el conocimiento humano. El método maneja exitosamente la ambigedad de las características de las IRM, siendo capaz de describir el conocimiento acerca de los tumores en términos vagos. El método fue desarrollado haciendo uso de las herramientas proporcionadas por la teoría de conjuntos difusos.

Esta tesis presenta, paso a paso, una metodología para la segmentación automática de tumores cerebrales en IRM. A fin de lograr la segmentación totalmente automática y sin supervisión, se definen medidas objetivas por medio de umbrales de histograma adaptativos, que delimitan las poblaciones tumor y no tumor. Además, para definir la población tumor, se lleva a cabo un análisis de simetría.

En el enfoque propuesto se introduce una nueva manera de definir automáticamente las funciones de pertenencia a partir del histograma. Las funciones de pertenencia propuestas están diseadas para adaptarse bien a los datos de las IRM y separar eficientemente las poblaciones. Puesto que no es necesario ningún post-procesado, y el único pre-procesado consiste en la extracción del cráneo, la técnica de segmentación propuesta permite reducir los tiempos de cálculo. El enfoque propuesto es cuantitativamente comparable a los métodos actuales más precisos, aun cuando la segmentación se lleva a cabo en 2D.

Abstract

Brain tumors are part of a group of common, non-communicable, chronic and potentially lethal diseases affecting most families in Europe [Albretha 2008]. Imaging plays a central role in brain tumor management, from detection and classification to staging and comparison.

Increasingly, magnetic resonance imaging (MRI) scan is being used for suspected brain tumors, because in addition to outline the normal brain structures in great detail, has a high sensitivity for detecting the presence of, or changes within, a tumor. Currently most of the process related to brain tumors such as diagnosis, therapy, and surgery planning are based on its previous segmentation from MRI. Brain tumor segmentation from MRI is a challenging task that involves various disciplines. The tumors to be segmented are anatomical structures, which are often non-rigid and complex in shape, vary greatly in size and position, and exhibit considerable variability from patient to patient. Moreover, the task of labeling brain tumors in MRI is highly time consuming and there exists significant variation between the labels produced by different experts.

The challenges associated with automated brain tumor segmentation have given rise to many different segmentation approaches. Although the reported accuracy of the proposed methods is promising, these approaches have not gained wide acceptance among the neuroscientists for every day clinical practice. Two of the principal reasons are the lack of standardized procedures, and the deficiency of the existing methods to assist medical decision following a technician way of work.

For a brain tumor segmentation system has acceptance among neuroscientists in clinical practice, it should support medical decision in a transparent and interpretable way emulating the role of a technician, considering his experience and knowledge. This includes knowledge of the expected appearance, location,

variability of normal anatomy, bilateral symmetry, and knowledge about the expected intensities of different tissues. The image related problems and the variability in tissue distribution among individuals in the human population makes that some degree of uncertainty must be considered together with segmentation results.

A possible solution for designing complex systems, in which it is required to incorporate the experience of an expert or the related concepts appear uncertain, is the use of soft computing techniques such as fuzzy systems. An important advantage of fuzzy systems is their ability for handling vague information.

In this work, it is proposed the development of a method to assist the specialists in the process of segmenting brain tumors. The main objective is to develop a system that can follow a technician way of work, considering his experience and knowledge. More concretely, it is presented a fully automatic and unsupervised segmentation method, which considers human knowledge. The method successfully manages the ambiguity of MR image features being capable of describing knowledge about the tumors in vague terms. The method was developed making use of the powerful tools provided by fuzzy set theory.

This thesis presents a step-by-step methodology for the automatic MRI brain tumor segmentation. For achieving the fully automatic and unsupervised segmentation, objective measures are delineated by means of adaptive histogram thresholds for defining the non-tumor and tumor populations. For defining the tumor population a symmetry analysis is conducted.

The proposed approach introduces a new way to automatically define the membership functions from the histogram. The proposed membership functions are designed to adapt well to the MRI data and efficiently separate the populations. Since any post-processing is needed, and the unique preprocessing operation is the skull stripping, the proposed segmentation technique reduces the computational times. The proposed approach is quantitatively comparable to the most accurate existing methods, even though the segmentation is done in 2D.

Agradecimientos

El desarrollo de esta tesis doctoral ha requerido grandes esfuerzos y mucha dedicación. Su finalización no hubiese sido posible sin la cooperación desinteresada de todas y cada una de las personas que a continuación cito.

Agradezco primeramente a Dios por fortalecer e iluminar mi mente y por permitir tener a mi lado a todas las personas que han sido mi soporte y compañía durante este periodo.

Deseo agradecer profundamente a mi esposo David por su apoyo incansable, porque estando a mi lado me ha permitido lograr mi máximo potencial en todos los aspectos.

Gracias a mis hijos David, Michel y Natalia por su amor, tiempo, paciencia y ánimo en esta dura tarea.

Agradezco los sabios consejos de mis directores de tesis Eduard Montseny y Pilar Sobrevilla quienes han guiando desde el inicio del doctorado mi formación no solamente académica, sino como persona, y sin lugar a duda las contribuciones presentadas en esta tesis, han sido producto de un esfuerzo conjunto. Gracias por conducir esta investigación de una manera abierta, generosa y de inmejorable disposición.

De igual manera mi más sincero agradecimiento a mi amada familia, a mis padres por enseñarme con sabiduría y darme seguridad en cada paso, a mis hermanos por todas sus oraciones.

Un agradecimiento especial a mis fieles amigos de Terrassa por su valioso apoyo y amistad.

Finalmente doy gracias por el apoyo otorgado para la realización de estos

estudios al Consejo Nacional de Ciencia y Tecnología de México.

Acknowledgments

The development of this thesis has required great effort and dedication. Its completion would not have been possible without the unselfish cooperation of each of those I quote below.

I first thank God for strengthen and enlighten my mind and for allowing me to be close to those who have been my support and companionship during this period.

I want to deeply thank my husband David for his untiring support, because being by my side he has allowed me to achieve my full potential in all aspects.

Thanks to my children David, Michel and Natalia for their love, time, patience and courage in this difficult task.

I appreciate the wise counsel of my thesis advisors Eduard Montseny and Pilar Sobrevilla who have guided my preparation since the beginning of the doctorate, not only academically, but as a person, and undoubtedly the contributions presented in this thesis have been the product of a joint effort. Thanks for conducting this research in an open, generous and of excellent disposition.

Likewise, my sincere thanks to my beloved family, to my parents for teaching me with wisdom and confidence in every footstep, to my brothers and sisters for all their prayers.

Special thanks to my faithful friends from Terrassa, for their precious support and friendship.

Finally I give thanks for the support granted to carry out this work to the National Council of Science and Technology of Mexico.

To David

All truth is independent in that sphere in which God has placed it, to act for itself, as all intelligence also; otherwise there is no existence.

D. and C. 93:30

Contents

List of Figures

List of Tables

Chapter 1

Thesis Overview

1.1 Introduction

Cancer is a group of common, non-communicable, chronic and potentially lethal diseases affecting most families in Europe, and a growing contributor to premature death within the European Union (EU) countries [Albretha 2008]. Around 2.3 million new cancer cases occurred in the 27 EU member states in 2006 [ECO 2009], and growing numbers of cancers are predicted for all countries in the region [Ferlay 2007]. One out of four deaths in the EU are attributable to cancer, and in the age range 4564 years, the number is almost one out of two deaths [WHO 2008].

Brain tumors are part of this group of extremely complex diseases. A brain tumor is any mass caused by abnormal or uncontrolled growth of cells that arise within or adjacent to the brain. In general, these tumors are categorized according to several factors, including location, type of cells involved, and the growing rate [Walter 2007]. Slowly growing tumors that lack of capacity to spread to distant sites are called benign, and rapidly growing tumors that can infiltrate surrounding tissues and spread to distant sites (metastasize) are called malignant. Primary brain tumors originate in the brain. Metastatic or secondary brain tumors are the most common types of brain tumors, and occur in 10-15 % of people with cancer.

The control of brain tumors faces several important challenges, including optimal exploitation of early detection and early treatment, and of the growing array of treatment options that can significantly improve survival [Albretha 2008]. Recent research is focused on finding new solutions to all aspects of

cancer management by: identifying new possibilities for: prevention, early detection, diagnosis and treatment. Imaging plays a central role in the management of brain tumors. People having tumors, or with potential tumors, are imaged for detection, classification, staging, and comparison. Detection can be subdivided into diagnosis, case finding, and screening, depending on the level of suspicion. Classification consists on making a tissue diagnosis to determine whether the tumor is a benign or malignant disease. Staging is performed to determine the extent of the disease, and it is important for the selection of an appropriate treatment. Imaging comparison is performed after treatment to determine the effect of treatment and to verify for tumor recurrence [Kundel 2002].

There exists a wide range of medical imaging modalities that allow neuroscientists to see inside a living human brain. Early imaging methods, invasive and sometimes dangerous, have been abandoned in recent times in favor of non-invasive, high-resolution modalities, such as computed tomography (CT), and specially magnetic resonance imaging (MRI). Increasingly, magnetic resonance imaging scan is being used instead of CT scan for suspected brain tumors, because MRI does not use ionizing radiation in the formation of its images. In addition, to outline the normal brain structures in great detail, the MRI has a higher sensitivity for detecting the presence of, or changes within, a tumor. Figure 1.1 shows a Magnetic Resonance Tomography and sequences of Magnetic Resonance (MR) images.

Most of the diagnosis, therapy, and surgery planning of brain tumors are currently based on its previous segmentation from magnetic resonance images. However, brain tumor segmentation from magnetic resonance images is a difficult task that involves various disciplines covering: pathology, MRI physics, radiologists perception, and image analysis. The process of segmenting tumors in (MR images, as opposed to natural scenes, is particularly challenging. The tumors to be segmented from medical images are true anatomical structures, which are often non-rigid, complex in shape, and exhibit considerable inter-patient variability. Brain tumors vary greatly in size and position, have a variety of appearance properties, and their intensities overlap those of normal brain tissues [Prastawa 2004]. In addition, often the expanding tumors can defect and deform nearby brain structures, making healthy tissues to have abnormal geometry.

Radiation oncologists, radiology technicians, and other medical specialists spend a substantial portion of their time to medical image segmentation. In particular, the task of labeling brain tumors in MR images is highly time con-

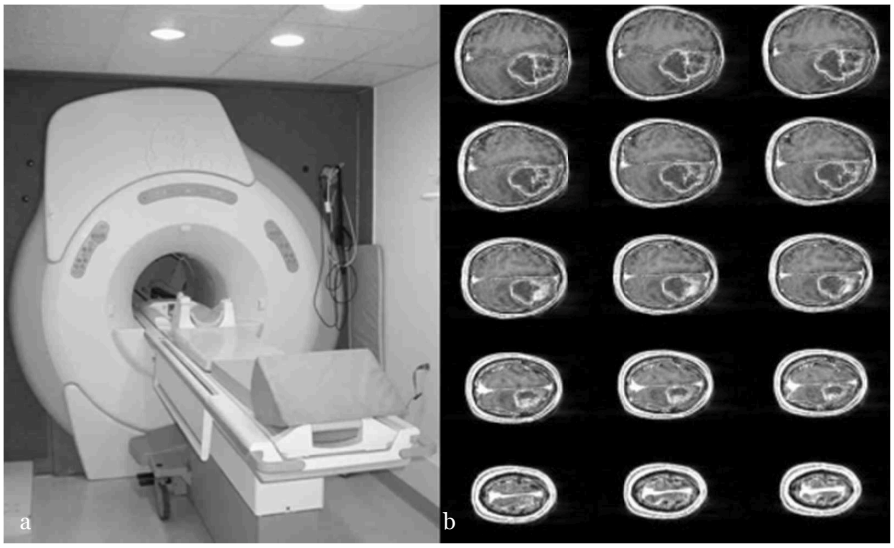

Figure 1.1: A Magnetic Resonance Tomography. (a) and samples of MR Images (b).

suming, and there exists significant variation between the labels produced by different experts [Mazzara 2004]. For these reasons an automated brain tumor segmentation method is desirable.

The challenges associated with automated brain tumor segmentation have given rise to many different segmentation approaches. Figure 1.2 shows examples of three images and their segmentation obtained using different approaches that will be described in Chapter 3, along with other segmentation methods.

Given the advantages of MRI over other diagnostic imaging methods, the majority of research in brain tumor segmentation is focused on MR images. Although there are numerous computer based techniques that have been examined for improving MRI brain tumor segmentation, nowadays it remains as an active research area.

Significant efforts on assisting brain tumor detection and segmentation have been focused on the application of diverse techniques such as threshold-based [ChangSun 2000, Gibbs 1996, Shanti 2007, Stad 2004], region-based [Battha 2008, Kaus 2001, Kong 2006, Ratan 2009, Salman 2009], pixel classification

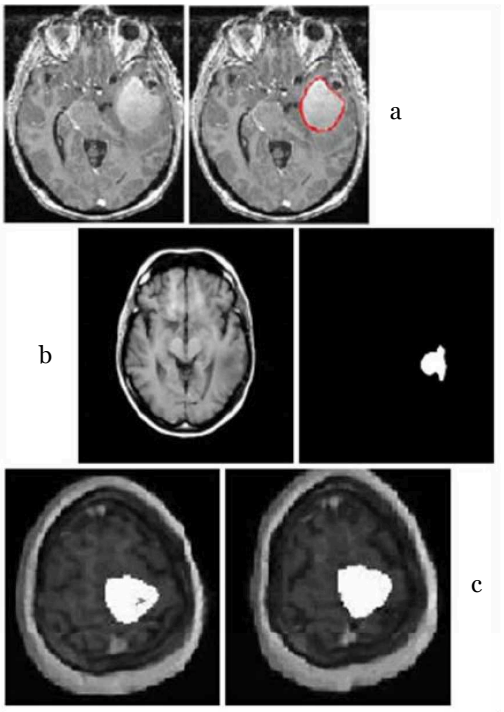

Figure 1.2: Diverse images and their segmentation obtained using different segmentation approaches. a) Deformable Model [Khotan 2008], b) Pseudo-Conditional Random Field Model [Lee 2008], and c) Modified Region Growing Method [Salman 2009].

[Fletcher 2001, Kannan 2008, Supot 2007, Tayel 2006, Veloz 2008], and deformable models and level sets [Chan 2001, Law 2002, Luo 2006, Khotan 2008]. Although the reported accuracy of the proposed computerized methods is promising, these approaches have not gained wide acceptance among the neuroscientists for every day clinical practice [Papage 2008]. Two of the main reasons might be the lack of standardized procedures [Archip 2007], and the deficiency of the existing methods to assist medical decision following a technician way of work. This has a negative effect on the perception of computer aided medical diagnosis, where the demand for reasoning and explanation is a priority.

A successful computer aided system for assisting brain tumor segmenta-

tion should support medical decision in a transparent and interpretable way, emulating the role of a technician, and considering expert's experience and knowledge. To do it, besides knowledge of the expected appearance, location, and variability of normal anatomy, it has to be also taken into account bilateral symmetry, expected intensities of different tissues, and appearance of regions of pixels and/or shapes present within the image [SchmiT 2005].

The MRI brain tumor segmentation involves several image related problems: visual patterns are inherently ambiguous, image features are corrupted during the acquisition process, knowledge about the tumors in images can be described only in vague terms, and the outputs of low-level processes provide vague, conflicting, or erroneous inputs to higher level algorithms. These problems, together with the variability in tissue distribution among individuals in the human population makes that some degree of uncertainty must be considered together with segmentation results.

A possible solution for designing complex systems in which it is required to incorporate the experience of an expert, or the related concepts appear vague or uncertain, is the use of soft computing techniques such as fuzzy systems. An important advantage of fuzzy systems, compared to the classical methods, is the ability of the obtained system to handle vague information.

Fuzzy logic techniques have been applied in different ways to brain imaging in order to recognize, represent, manipulate and interpret the enormous amount of information of complex brain functions. In general, researching works in this area are related to pattern recognition for localization of brain structures [Kannan 2008], tumor detection [Chen 2004, Khotan 2009, Veloz 2008], control of body movements [Wootton 2003], anesthesia [Zhang 2001], etc. Some studies have shown that the use of fuzzy techniques decrease the processing time and increase the robustness and efficiency against other conventional methods [Coifolo 2004, 2005]. In the literature there are several applications that have been improved using fuzzy logic techniques, such as the sensitivity for detecting and delineating brain lesions [Seghier 2008], or detecting atypical brain activations that may not be detected by other standard methods [Seghier 2007].

This work proposes the development of a method for assisting specialists in the process of brain tumor segmentation. The main motivation is to develop a system that follow a technician way of work. To achieve this goal, it is proposed the use of advanced techniques of soft computing such as fuzzy systems. In addition, to mimic the expert's way of working, the information provided by the technicians and the obtained from the images are put together to define a

set of rules. These rules are aimed to design a new brain tumor fuzzy segmentation approach in which segmentation is carried out in a transparent manner, and the results are easily interpretable by specialists.

1.2 Objectives

According to the motivation exposed in the introduction, the main objective of this thesis is:

> *To develop a system to assist brain tumor segmentation that follows the guidelines of the technician, considering his experience and knowledge.*

To achieve the main objective, it is necessary to define a number of sub objectives and requirements that must be taken into consideration for designing the brain tumor segmentation approach; these are:

- Develop a fully automatic and unsupervised segmentation method to assist neuroscientists in the segmentation of brain tumors in magnetic resonance images.
- The method has to consider and combine simultaneously diverse sources of human knowledge.
- The method must successfully manage the ambiguity of MR image features.
- The method has to be capable of describing, in vague terms, knowledge about the tumors appearing within images.

In order to fulfill the afore mentioned objectives, it is necessary to make use of the powerful tools provided by fuzzy set theory and fuzzy logic which are ideally suited for dealing with uncertainty. The flexibility provided by fuzzy set theory for knowledge representation makes fuzzy rule-based systems very attractive for computer vision in general, and for brain tumor segmentation in particular, when compared with traditional rule-based systems [Montseny 2001].

1.3 Outline of the Thesis

Here is given a description of the contents in each of the Chapters embodying this dissertation.

Chapter 1 : Thesis Overview.

General introduction.

Chapter 2 : MR Imaging of Brain Tumors.

Magnetic Resonance Imaging has evolved, in neuroradiology, in the last 30 years, becoming faster, more precise, and more specific. MRI is highly accepted as the most sensitive method for diagnosing brain tumors due to its high tissue contrast and its noninvasiveness. This is true for both, detection and description of the extent of the disease [Reiser 2008]. The small size of the brain along with the absence of motion makes high-resolution imaging routinely possible. Moreover, the MRI characteristics of white matter (WM), gray matter (GM), and cerebrospinal fluid (CSF) makes them ideal for optimizing contrast parameters. The paucity of air and fat reduces the artifacts in MR brain images often seen in other parts of the body. For these reasons, MRI of the brain has been the focus of most of the new technological developments. Such developments are often introduced in MRI of the brain before they are attempted in other parts of the body. These natural advantages create an excellent platform for the study and early diagnosis of brain tumors [Butman 2006].

Chapter 2 provides a general description of the basic physical principles of the Nuclear Magnetic Resonance Imaging (NMRI), as well as the practical aspects and MR Imaging appearances of the most common cerebral tumors. The standard on Digital Imaging and Communication in Medicine (DICOM) is presented as an introduction of how the medical imaging is handled and transmitted.

Chapter 3 : State of the Art Survey on Brain Tumor Segmentation

Image segmentation plays a crucial role in the extraction of attributes and useful information from images. The main objective of image segmentation is to partition an image into mutually exclusive and exhausted regions such that each region is spatially contiguous and the pixels within are homogeneous with respect to a predefined criterion [Bhandar 1997].

Brain tumor segmentation consists on separating the different tumor tissues (solid or active tumor, edema, and necrosis) from normal brain tissues (gray matter (GM), white matter (WM), and cerebrospinal fluid (CSF)). In brain tumor studies, the existence of abnormal tissues is easily detectable most of the times. However, accurate and reproducible segmentation and characterization of abnormalities are not straightforward.

In the past, many researchers in the field of medical imaging and soft computing have made significant survey in the field of brain tumor segmentation. Both semiautomatic and fully automatic methods have been proposed. Clinical acceptance of segmentation techniques has depended on the simplicity of the segmentation, and the degree of user supervision [Yao 2006]. Interactive or semiautomatic methods are likely to remain dominant, in practice, for some time, especially in these applications where erroneous interpretations are unacceptable [McIner 2000].

This chapter presents an overview of the most relevant brain tumors segmentation methods, conducted after the acquisition of the image. The chapter starts with an introduction of manual and automated segmentation. The concepts of unsupervised and supervised segmentation are also stated. Given the advantages of magnetic resonance imaging over other diagnostic imaging (Chapter 2), this survey is focused on MRI brain tumor segmentation. Semiautomatic and fully automatic techniques are emphasized.

Chapter 4 : A New Fuzzy Approach to Brain Tumor Segmentation

The existing work is a valuable source of insight for designing a new brain tumor segmentation system, since it is clear that these works contain a variety of different properties that can be exploited. However, since the goal of this work is to automate a task performed by human experts, the methods used by them have to be also considered, because provide insights into the problem. Human experts are able to incorporate complex information including: knowledge of the expected appearance, location, and variability of normal anatomy. Furthermore, humans are able to simultaneously consider and combine these diverse properties or sources of knowledge, and can consider previous experience in related tasks.

It is clear that improved results could be achieved if the system could consider, simultaneously, a variety of properties to perform brain tumor

segmentation. It is also obvious that, in cases where the discrimination between normal and abnormal areas is not trivial, a variety of sources have to be used for making a decision. However, in ambiguous cases, these complex interactions are difficult to represent with a set of "hard" manually determined rules.

Chapter 4 presents the proposed fuzzy approach for brain tumor segmentation. Considering the flexibility provided by fuzzy set theory for knowledge representation, the information provided by the technicians and the obtained from the images are put together to define a set of rules. These rules are aimed to design a new brain tumor fuzzy segmentation approach. A major focus of the proposed approach is the definition of a new method of acquiring fuzzy membership functions. The outcome is a segmentation carried out in a transparent manner, and the results are easily interpretable by specialists.

Chapter 5 : Experiments and Results

Chapter 5 presents three sets of experiments to prove the validity of the proposed method.

Chapter 6 : Conclusions and Future Work

Finally, general conclusions and an outline of some future directions are presented in Chapter 6.

1.4 Contributions of the Thesis

The main contributions of this thesis can be summarized as follows:

- Unsupervised and Fully Automatic Segmentation.
- Method based on fuzzy techniques.
  - Introduction of an easier way for automatically define the membership functions.
  - Proposed membership functions:
    - adapt well to the MRI data and experts knowledge.
    - efficiently separate populations (non-tumor vs. tumor).
- Simplification of the segmentation technique.

- No preprocessing in addition to skull stripping.
- No post segmentation refinement
- Short computational times.

Chapter 2

MR Imaging of Brain Tumors

2.1 Introduction

Neuroimaging is an essential part of the decision-making process for therapy, or planning of neurological interventions. Prior to neurosurgery, neuroimaging can precisely define the location and accurately delineate the lesion. It can also be of support in radiotherapy planning, by correctly defining the lesion margins [Essig 2008]. In addition, neuroimaging is mandatory after therapeutic intervention to monitor disease and possible side effects.

Magnetic Resonance Imaging in neuroradiology has evolved in the last 30 years, becoming faster, more precise, and more specific. As exposed in [Reiser 2008], MRI is highly accepted as the most sensitive method for diagnosing brain tumors, due to its high tissue contrast and its noninvasiveness. This is true for both, detection and description of the extent of the disease. The small size of the brain, along with the absence of motion, makes high-resolution imaging routinely possible. Moreover, the characteristics of white matter (WM), gray matter (GM) and cerebrospinal fluid (CSF) makes them ideal for optimizing contrast parameters. The paucity of air and fat within the brain reduces the artifacts often seen in other parts of human body. For these reasons, MRI of the brain has been the focus of most new technology developments, which are often introduced in brain MRI before attempting to apply them to other parts of the body. These natural advantages create an excellent platform for the study and early diagnosis of brain tumors [Butman 2006].

In 2003, there were approximately 10,000 MRI units worldwide, since then, and approximately 75 million MRI scans were performed per year [Hornak 2008]. Currently, eight million MRI examinations are carried out per year in Europe [ESTRO 2009]. In the past years, it has become generally recognized that MRI would be the imaging study of choice in the evaluation of intracranial tumors if availability and cost were not an issue [Albreth 2008].

In this chapter, the basic principles of magnetic resonance imaging are described. The chapter provides a general overview of the basic physical principles of the Nuclear Magnetic Resonance Imaging (NMRI) and the practical aspects and Magnetic Resonance (MR) imaging appearances of the most common cerebral tumors. To better understand how medical imaging is handled and transmitted, the chapter will start presenting The Digital Imaging and Communication in Medicine (DICOM) standard.

2.2 Outline of Chapter

Section 2.3 introduces the DICOM standard including data structures, network services, media exchange, and conformance statement. Section 2.4 provides a broad description of the nuclear MRI phenomena. Section 2.5 presents an introduction of the practical aspects of MRI brain tumors, as well as a description of the appearances, in MR images, of the most common cerebral tumors. Finally, in Section 2.6, the chapter conclusions are briefly presented.

2.3 Digital Imaging and Communications in Medicine (DICOM)

Digital Imaging and Communications in Medicine (DICOM) is a standard for handling, storing, printing, and transmitting information in medical imaging. Since the seventies, when computed tomography was introduced as the first digital modality, the importance of digital medical image processing has increased permanently. The emerging idea of sharing a digital image archive (the Picture Archiving and Communication System PACS), and electronic image distribution, created in hospitals the need to exchange digital images between medical devices of different manufacturers.

In 1983, the American College of Radiology (ACR), and the National Electrical Manufacturers Association (NEMA) formed a working group in order to develop a standard for image exchange. The collective work resulted in the ACR-NEMA standard, which was published in 1985, and revised several times until 1988. Due to certain conceptual weaknesses (no network support, and different proprietary "dialects"), the ACR-NEMA standard was not adopted in hospitals. As a consequence, the DICOM standard was developed on the basis of the experiences with the ACR-NEMA standard. The main objective of this new standard was to create an open (vendor independent) platform for the communication of medical images and related data. Moreover, the new standard should support PACS networks and guarantee interoperability of arbitrary DICOM devices and programs. DICOM was published in 1993 and is continuously being actualized. In 1995, DICOM was accepted as a formal standard in Europe.

The diverse digital modalities of DICOM standard are shown in Table 2.1.

The content of the DICOM standard goes far beyond of the definition of an exchange format for these medical image modalities. What DICOM defines is:

- Data structures (formats) for medical images and related data.
- Network oriented services, e. g.
  - image transmission,
  - query o an image archive (PACS),
  - print (hard copy), and
  - RIS - PACS - modality integration

Table 2.1: Application areas of DICOM standard.

Modality	**Description**
BI	Biomagnetic Imaging
CR	Computed Radiography
CT	Computed Tomography
DG	Diaphangraphy
EM	Electron Microscope
ES	Endoscopy
GM	General Microscopy
LS	Laser Surface Scan
MG	Mammography
MR	Magnetic Resonance
NM	Nuclear Medicine
OT	Other
PT	Positron Emission Tomography
RF	Radio Fluoroscopy
RG	Radiographic Imaging
RT	Radiation Therapy
SC	Secondary Capture
SM	Slide Microscopy
TG	Thermography
US	Ultra Sound
VL	Visible Light
XA	X-Ray Angiography
XC	External Camera (Photography)

- Formats for storage media exchange.
- Requirements for conforming devices and programs.

The following sections briefly explain these four points.

2.3.1 DICOM Data Structures

A DICOM image consists of a list of data elements (attributes) containing a multitude of image related information:

- Patient information (name, sex, identification number).
- Modality and imaging procedure information (device parameters, calibration, radiation dose, contrast media).
- Image information (resolution, windowing).

For each image modality, DICOM precisely defines the data elements that are required, optional (i.e. may be omitted) or required under certain circumstances (i.e. only if contrast media was used). This powerful flexibility is at the same time, a crucial weakness of DICOM standard; because practical experience shows that image objects are frequently incomplete, due to required fields are missing or contain incorrect values. These problems can lead to subsequent problems when exchanging data.

2.3.2 DICOM Network Services

The DICOM network services are based on the client/server concept. In case two DICOM applications want to exchange information, they must establish a connection and agree on the following parameters:

- Who is the client and who the server.
- Which DICOM services are to be used.
- In which format data are transmitted (e. g. compressed or uncompressed).

Only if both applications, the client and the server agree on a common set of parameters, the connection can and will be established. In addition to "image transmission" (or in DICOM terminology: "Storage Service Class"), which is the most basic DICOM service, there are a number of advanced services, for example:

- DICOM image archive service ("Query/ Retrieve Service Class") that allows to search images in a PACS archive by certain criteria (patient, time of creation of the images, modality etc.), and to selectively download images from this archive.
- DICOM print service ("Print Management Service Class") that allows to access laser cameras or printers over a network, so that multiple modalities and workstations can share one printer.
- DICOM modality work list service, that allows to automatically downloading up-to-date work lists which include a patient's demographic data, from an information system (HIS/RIS) to the modality.

2.3.3 Media Exchange

In addition to the exchange of medical images over a network, media exchange has become another application which was integrated into the DICOM standard in 1996. Fields of application are, for example, the storage or cardiac angiography films in cardiology, or the storage of ultrasound images. In order to make sure that DICOM storage media are really interchangeable, the standard defines application profiles which explicitly are:

- Images from which modalities may be present on the medium (e. g. "only X-Ray Angiography images").
- The encoding formats and compression schemes that may be used (e. g. "only uncompressed or loss-less JPEG").
- The storage medium that is going to be used (e. g. "CD-R with ISO file system").

Aside from the image files, each DICOM medium contains a "DICOM directory". This directory contains the most important information (patient name, modality, unique identifiers etc.) for all images which are captured on the medium. With the necessary help of this directory, it is possible to quickly browse or search through all images on the medium without having to read the

complete image files.

2.3.4 Conformance Statement

DICOM requires that a Conformance Statement has to be written for each device or program claiming to be DICOM conformant. The format and content of a Conformance Statement is defined in the standard itself. In general, the statement shall explain which DICOM services and options are supported, which extensions and peculiarities have been implemented by the vendor, and how the device communicates with other DICOM systems. In theory, comparing two conformance statements allows to determine whether two DICOM compliant devices are able to communicate with each other or not.

In practice, however, conformance statements are only comprehensible by experts and are frequently inadequated since often only a minimum set of features is documented. Interoperability problems typically tend to occur because some details do not go together.

Once explained the standard for handling, and transmitting information in medical imaging, next section presents the basic principles of magnetic resonance.

2.4 Magnetic Resonance Imaging

Magnetic resonance imaging (MRI) is a non-invasive technique, which uses the interaction between radio frequency pulses, a strong magnetic field, and biologic tissue. MRI produces high quality sectional images, which have equivalent resolution in any projection from internal anatomy. Biological tissues, when placed within a strong magnetic field, can be induced to emit a detectable signal immediately following stimulation by a pulse of radio frequency energy.

MRI is based on the principles of nuclear magnetic resonance (NMR), a spectroscopic technique used to obtain microscopic chemical and physical information about molecules. As appeared in [Hornak 2008], the technique was called magnetic resonance imaging, rather than nuclear magnetic resonance imaging (NMRI), because of the negative connotations associated with the word nuclear in the late seventies.

One of the main advantages of MRI, unlike similar anatomic imaging modalities as computerized axial tomography (CAT), is that does not use ionizing radiation in the formation of its images.

MRI, as all medical imaging techniques, is a relatively new technology which foundations began at 1946. Felix Bloch [Bloch 1946] and Edward Purcell [Purcell 1946] independently discovered the magnetic resonance phenomena at this year, and were awarded for its discovering the Nobel Prize in 1952. Until the seventies MRI was being used for chemical and physical analysis. Afterwards, in 1971, Raymond Damadian [Damadian 1971] showed that nuclear magnetic relaxation times of tissues and tumors were different, motivating scientists to use MRI to study disease. With the advent, in 1973, of the computed tomography, by Hounsfield [Hounsf 1946], and echo-planar imaging, in 1977 by Mansfield [Mansfield 1977], over the next 20 years many scientists developed MRI into the technology that we now know today.

The first human being MRI examination did not occur until 1977. Since then faster computing has made the MRI process much faster. The most significant advancement in MRIs occurred in 2003, when the Nobel Prize was won by Paul C. Lauterbur and Peter Mansfield [Nobel 2003] for their discoveries of using MRIs as a diagnostic tool.

2.4.1 Nuclear Magnetic Resonance

Nuclear Magnetic Resonance is a physical phenomenon of the magnetic property of nuclei, which have a positive nuclear spin quantum number. Under the influence of an external static magnetic field, these nuclei will precess about the direction of the magnetic field with an angular frequency, the Larmor frequency. Through absorption (excitation) and emission (relaxation) of radio frequency energy at the resonance frequency, the Larmor equation, and the processing of this raw data by the Fourier transformation, physical, chemical, electronic, and structural information about molecules can be obtained.

An ample explanation of the nuclear magnetic resonance phenomena, and the Magnetic Resonance Image formation is given in Appendix A.

2.5 MRI of Brain Tumors

The term "tumor", which literally means swelling, can be applied to any pathological process that produces a lump or mass in the body. Brain tumors are a major manifestation of a vast and varied group of diseases called neoplasms or, more commonly, cancers [Kundel 2002]. Neoplasms derive from normal body cells that, after a series of transformations, lose the capability of responding to the usual physiological mechanisms that control growth. Uncontrolled growth leads to the formation of a tumor. Slowly growing tumors that lack of capacity to spread to distant sites are called benign; while rapidly growing tumors, which can infiltrate surrounding tissues and spread to distant sites (metastasize) are called malignant. Primary brain tumors originate in the brain, while metastatic, or secondary brain tumors (cancer that spreads from other parts of the body to the brain), are the most common types of brain tumors.

People with tumors, or potential tumors, are imaged for detection, classification, staging, and comparison. Detection can be subdivided into diagnosis, case finding, and screening; depending on the level of suspicion. Tumor classification consists, ideally, on making a tissue diagnosis or at least a determination of whether the tumor is a manifestation of a benign or malignant disease. The radiologist is required to classify all the suspicious regions in an image. Staging is performed to determine the extent of the disease, both local and distant, and it is important for the selection of an appropriate treatment and for estimating prognosis. Imaging comparison is performed after treatment to determine its effect and to check for tumor recurrence. The diagnostic problem frequently involves discriminating between changes caused by the treatment and by recurrent tumor.

MRI is the imaging method with highest sensitivity for brain tumors detection. This is true for detection as well as for description of the extent of disease. The use of a MRI standard protocol for cerebral neoplasms allows high resolution imaging and characterization of lesions. The diverse types of MR images obtained from the excitation sequences can provide different image intensity information for a given anatomical region and subject. Since a tumor consists of different biological tissues, radiology experts combine the multispectral MRI information of a patient to take a decision about location, extension, prognosis and diagnosis of the tumors. At least three types of MRI, generally T1-weighted (T1), T2-weighted (T2), and proton density (PD) are used as the routine sequences in practice.

Brain tumors are difficult to classify and segment because they have a wide

range of appearance and effect on surrounding structures. Some of the general characteristics of brain tumors are [Prastawa 2003]:

- Vary greatly in size and position,
- Vary greatly in image intensities, as seen by MRI,
- May have overlapping intensities with normal tissue,
- May be space occupying (new tissue that moves normal structure) or infiltrating (changing properties of existing tissue),
- May enhance fully, partially, or not at all, with contrast agent, and
- May be accompanied by surrounding edema (swelling).

The following sections provide a brief explanation of the effect of exogenous contrast agents in MR images of brain tumors. It is also included an overview of the World Health Organization (WHO) classification of brain tumors, and a description of the practical aspects and MR imaging appearances of the most common cerebral tumors.

2.5.1 Exogenous Contrast Agents in Brain Tumors

Signal contrast in MRI can be modified by the use of exogenous contrast materials. MR contrast agents do not contribute to the signal directly; rather, they alter the signal of surrounding water protons via their effect on relaxation rates. The contrast agents, currently used in clinical and laboratory, can be roughly divided into two types: those incorporating paramagnetic ions, such as gadolinium or manganese, and those containing superparamagnetic iron oxide (SPIO) particles.

Paramagnetic ions are typically chelated to organic ligands or bound to macromolecules, such as albumin. This minimizes their toxicity and reduces their tumbling rates, thereby increasing their effectiveness or "relaxivity". When water molecules bind to the agent and tumble with it in solution, they experience randomly oscillating magnetic fields that stimulate longitudinal relaxation, thereby shortening T1 relaxation. Although only a small fraction of the water can bind to the agent at any time, the bound fraction is in continuous exchange with the free water, so that the T1-shortening effect is distributed throughout the bulk fluid. This results in an enhancement of signal on T1-weighted images.

SPIO particles have much stronger magnetic moments than individual paramagnetic ions, and, therefore, alter the magnetic field over a much longer range. They induce rapid dephasing of water protons, causing strong signal attenuation on T2 and T2* weighted images. Although SPIO particles are primarily T2 agents, they also shorten T1 relaxation times and can be used to produce enhancement on T1-weighted images. In such applications, the concentration of the agent and the TE of the sequence must be chosen to minimize T2 and T2* effects, so that they do not counteract the T1-related signal enhancement.

MR imaging of brain tumors requires a higher contrast for lesions than for imaging central nervous system (CNS), which depends on the signal intensity of the lesion relative to that of the surrounding normal tissue [Muroff 1995]. Furthermore, detailed information on the internal morphology of the lesion is essential for differential diagnosis, grading, and for the selection and planning of therapy. For most diseases, and for many of the currently available functional MR Imaging methods, the use of MR contrast media is mandatory.

Contrast enhanced MRI also helps in distinguishing tumors from other pathologic processes, and depicts basic signs of tumor response to therapy such as: change in size, morphology, and degree of contrast material enhancement.

Due to the presence of the bloodbrain barrier (BBB), currently available MR contrast media do not leak into the brain tissue [Neuwelt 2004]. The BBB serves as an effective physical barrier to the entry of lipophobic substances into the brain, and consists on a complex of capillary endothelial cells, pericytes, and astroglial and perivascular macrophages. The integrity of the BBB can be altered by a variety of circumstances that increase its permeability, for both contrast media and drug delivery. While the integrity of the barrier is often compromised within the tumor, this alteration in permeability is variable and dependent on the tumor type and size. Though the BBB is frequently leaky in the center of malignant brain tumors, the edge of the tumor has been shown to have variable and complex barrier integrity [Guru 2002]. Figure 2.1 [Reiser 2008] shows an example of a contrast-enhanced MRI in a patient with cerebral metastasis. The use of contrast material substantially increased the number of visible cerebral metastases. In (a) only one tumor can be appreciated, after using a triple dose of contrast (b), three tumors were displayed.

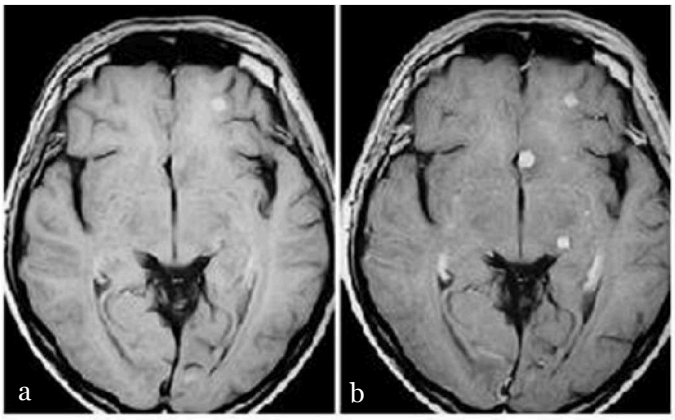

Figure 2.1: Contrast-enhanced MRI in a patient with cerebral metastasis. Increasing the amount of contrast material from a single dose (a) to triple dose (b) substantially increased the number of visible cerebral metastases.

2.5.2 The WHO Classification of Brain Tumors

In 1993 the World Health Organization ratified a new comprehensive classification of neoplasms affecting the central nervous system. The classification of brain tumors was based on the premise that each type of tumor results from the abnormal growth of a specific cell type.

To the extent that the behavior of a tumor correlates with basic cell type, tumor classification dictates the choice of therapy and predicts prognosis. The WHO classification also provides a parallel grading system for each type of tumor. In this Trading system, most named tumors are of a single defined grade. The new WHO classification provides the standard for communication between different centers around the world. An outline of this classification is provided in Table 2.2.

The WHO Grading of central nervous system tumors also establishes a malignancy scale based on histologic features of the tumor. The histologic grades are as follows:

- WHO grade I. Includes lesions with low proliferative potential, a frequently discrete nature, and the possibility of cure following surgical resection alone.

Table 2.2: The World Health Organization list of brain tumors.

1	**Tumors of neuroepithelial tissue**
1.1	Astrocytic tumors
1.2	Oligodendroglial tumors
1.3	Ependymal tumors
1.4	Mixed gliomas
1.5	Choroid plexus tumors
1.6	Neuroepithelial tumors of uncertain origin
1.7	Neuronal and mixed neuronal-glial tumors
1.8	Pineal parenchymal tumors
1.9	Embryonal tumors
2	**Tumors of the cranial and spinal nerves**
2.1	Schwannoma
2.2	Neurofibroma
2.3	Malignant peripheral nerve sheath tumor
3	**Tumors of the meninges**
3.1	Tumors of meningothelial cells (meningiomas)
3.2	Mesenchymal non-meningothelial tumors
3.3	Primary melanocytic lesions
3.4	Tumors of uncertain histogenesis
4	**Lymphomas and hematopoietic neoplasms**
5	**Germ cell tumors**
6	**Cysts and tumor-like lesions**
7	**Tumors of sellar region**
8	**Local extensions from regional tumors**
9	**Metastatic tumors**
10	**Unclassified tumors**

- WHO grade II. Includes lesions that are generally infiltrating and low in mitotic activity but recur. Some tumor types tend to progress to higher grades of malignancy.
- WHO grade III. Includes lesions with histologic evidence of malignancy, generally in the form of mitotic activity, clearly expressed infiltrative capabilities, and anaplasia.
- WHO grade IV. Includes lesions that are mitotically active, necrosis-prone, and generally associated with a rapid preoperative and post operative evolution of disease.

2.5.3 Practical Aspects and MR Appearances of the Most Common Cerebral Tumors

This section presents a summary of the most common brain tumors. Some examples of their MR appearances are included. All images showing cerebral tumors were obtained from the book "Magnetic Resonance Tomography," [Reiser 2008].

Astrocytic Tumors

Astrocytic tumors (1.2 of Table 2.2) account for up to 80 % of glial neoplasms and refer to a diffuse infiltrating tumor originating from glial cells. The tumor border on both imaging (T1 and T2) and histology is ill defined, with an infiltration that usually does not destroy the anatomic cerebral structures. [Ohgaki 2005]. The two most common *astrocytic tumors* are the *Pilocytic astrocytoma* and the *glioblastoma multiforme* (GBM).

*Pilocytic astrocytom*a (WHO grade I) is a well-circumscribed mass that commonly has a large cyst and a focal mural nodule. The typical appearance of an *infratentorial pilocytic astrocytoma* in the T1 and T2 channels is shown in Figure 2.2 where both channels present a partly solid and cystic tumor with surrounding edema and mass effect. The tumor can also be solid, with or without cystic degeneration.

Malignant astrocytoma (WHO grade IV), also known as GBM, may develop from a *diffuse astrocytoma* or an *anaplastic astrocytoma*. *Glioblastoma* is the most frequent brain tumor and accounts for approximately 1215 % of all brain tumors and 5060 % of all astrocytic. The usual appearance of a GBM or *anaplastic astrocytoma* on MRI is that of a contrast-enhancing lesion causing

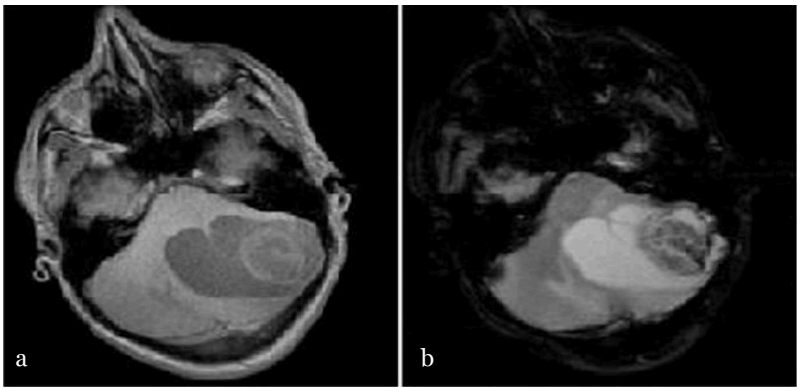

Figure 2.2: Typical appearance of an *infratentorial pilocytic astrocytoma*. (a) The non-enhanced T1 and T2 (b) present a partly solid and cystic tumor with surrounding edema and mass effect [Reiser 2008].

mass effect as the large GBM shown in Figure 2.3. In (a) the T1 -weighted image shows strong enhancement, and in (b), a heterogeneous signal pattern is shown on T2-weighted MRI. GBMs usually exhibit heterogeneous signal intensity on both T1- and T2 -weighted images caused by cysts, necrosis, and hemorrhage commonly seen with GBM. Up to 95 % of GBMs demonstrate contrast enhancement, and they are usually associated with high signal on T2-weighted imaging tumors.

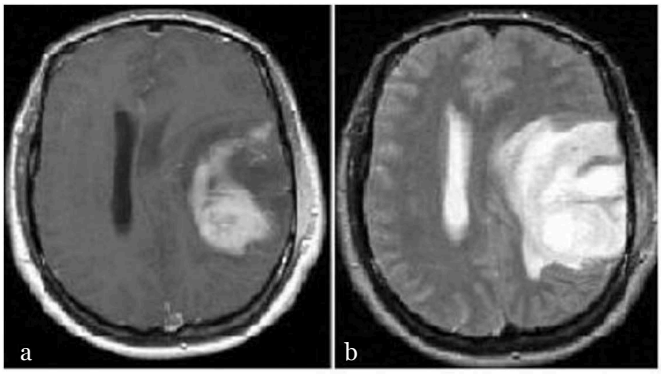

Figure 2.3: Large GBM presenting a large mass lesion, (a) with strong enhancement, and (b) a heterogeneous signal pattern on T2-weighted MRI.

Oligodendroglial Tumors

Oligodendroglioma (WHO grade II) is a kind of Oligodendroglial Tumor (1.2 of Table 2.2). In MRI, *oligodendrogliomas* appear iso- to hypointense on T1 with very low intensity, representing the calcified areas.

In Figure 2.4, the tumor has the appearance of a heterogeneous mass lesion with cystic components and hypointensities both on T1-(a) and T2-weighted imaging (b).

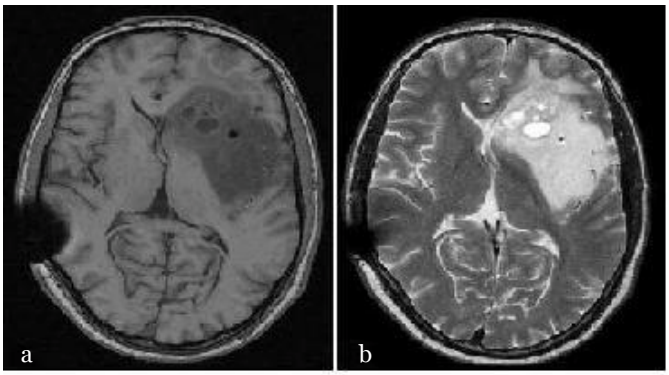

Figure 2.4: MRI of an *Oligodendroglioma*. (a) T1-weigted, and (b) T2-weighted imaging.

On T2 the tumors are typically hyperintense with a not-well delineated margin. Compared to *astrocytomas*, the lesions present with a lower signal on T2, which is related to the high cellular density.

The most useful finding, however, is the typical cortical infiltration and marked cortical thickening. Small cystic lesions and hemorrhage is also a common finding. Enhancement is common and tends to be more intense in the *Anaplastic* or *malignant oligodendrogliomas*.

Figure 2.5 shows an Anaplastic oligodendroglioma, the unenhanced T1-weighted image (a) does not show any hemorrhage, with a strong enhancement of the solid parts after contrast (b).

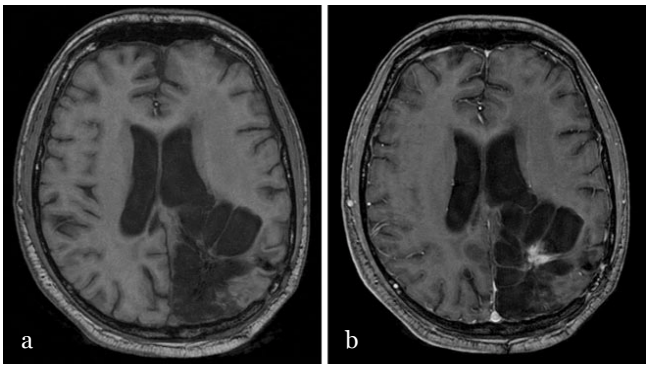

Figure 2.5: *Anaplastic oligodendroglioma*. (a) The unenhanced T1-weighted image does not show any hemorrhage, with a strong enhancement of the solid parts after contrast (b).

Ependymal Tumors

Ependymal tumors (1.3 of Table 2.2) are common in children, accounting for about 10% of pediatric CNS neoplasms and 5% of all intra-axial tumors. MR imaging of *Ependymomas* (WHO grade II) shows the heterogeneity of the tumors which reflects areas of necrosis, bleeding, and cysts.

Figure 2.6 shows an *Ependymoma* appearing as a large mass lesion in (a) and in (b), and with rim enhancement and cystic necrosis in (c). On T2 the tumors are not as high in signal intensity as other *gliotic tumors* due to the high cellular density.

Embryonal Tumors

Medulloblastoma (WHO grade IV) is a malignant, invasive Embryonal Tumor (1.9 of Table 2.2) of the cerebellum that occurs primarily in children. The characteristic appearance on MRI is an intraventricular mass lesion in a midline or paramedian location with isointense signal to gray matter on T2-weighted imaging. The enhancement is intense with some heterogeneity and sometimes ring enhancement.

Figure 2.7 presents a *Medulloblastoma* showing the inhomogeneous mass on T1 (a) and T2-weighted imaging (b).

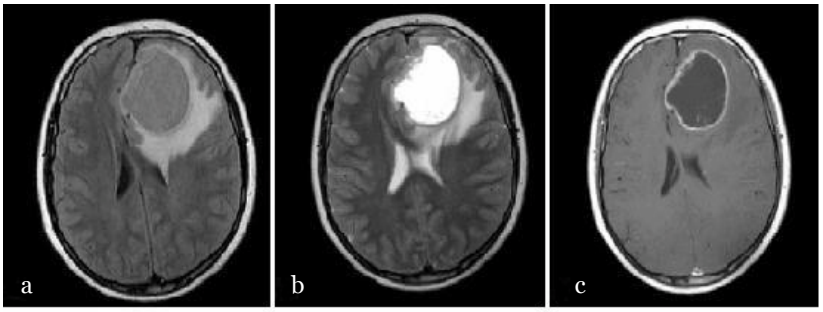

Figure 2.6: *Ependymoma*. (a) and (b), the tumor appears as a large mass lesion. (c) Shows the tumor with rim enhancement and cystic necrosis.

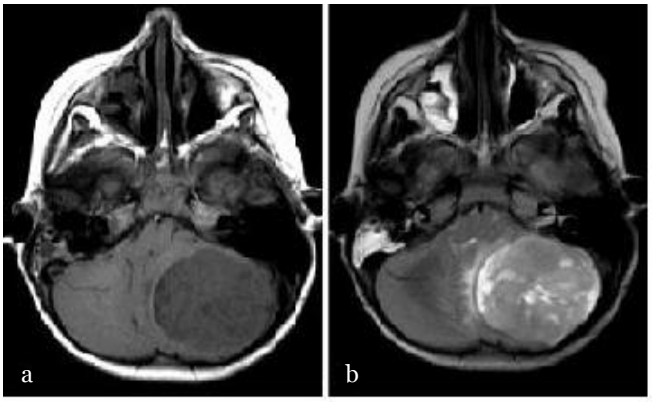

Figure 2.7: *Medulloblastoma*. The inhomogeneous mass on T1 and T2-weighted imaging (a,b).

Meningiomas

Meningiomas (3.1 of Table 2.2) are the most common primary nonglial intracranial tumors. They are typically slow-growing, benign, WHO grade I tumors attached to the dura mater and composed of neoplastic meningothelial (arachnoidal) cells. *Meningiomas* are estimated to comprise between 13 and 26% of primary brain tumors.

Figure 2.8 shows a *Meningioma* before and after contrast. *Meningioma* hypointense on T1-weighted imaging (a), and (b) presents a homogeneous intensive contrast enhancement.

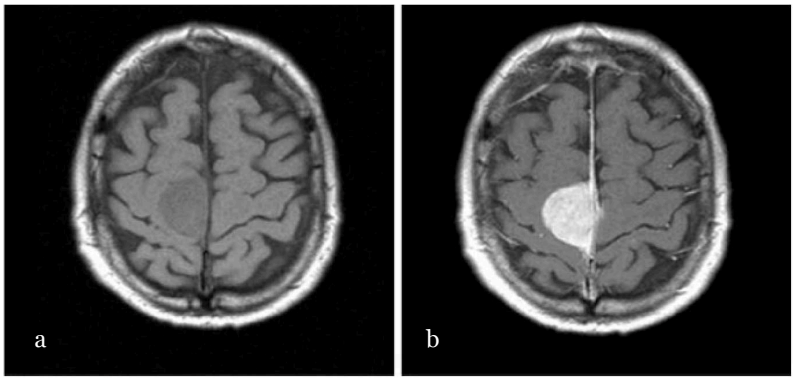

Figure 2.8: *Meningioma* on the T1 channel, before and after contrast. (a) *Meningioma* hypointense on T1-weighted imaging, and (c) presents a homogeneous intensive contrast enhancement.

Tumors of Uncertain Histogenesis

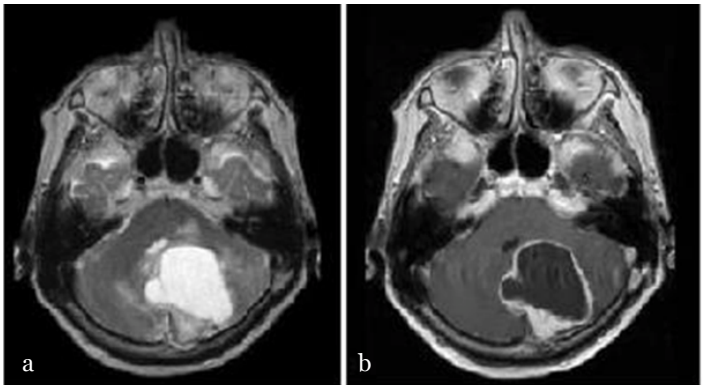

Figure 2.9: *Capillary hemangioblastoma* in a patient with *von Hippel-Lindau* (VHL) disease. The tumor presents as a large cystic mass (a), after contrast administration (b), the solid tumor parts show intensive enhancement.

Capillary hemangioblastoma (WHO grade I) is a tumor of uncertain histogenesis (3.4 of Table 2.2). It occurs sporadically and is associated with the familial tumor syndrome *von Hippel-Lindau* (VHL) disease. Because of the high protein content of the cysts, they are slightly hyperintense to CSF on T1-weighted MR images. They generally present without surrounding edema.

In Figure 2.9 the tumor presents as a large cystic mass (a), after contrast administration (b), the solid tumor parts show intensive enhancement.

2.6 Conclusions

Brain tumor imaging is an essential part of the decision-making process for therapy and later for precise planning of surgical or radiological interventions. The goals and requirements for brain tumor imaging are multiple and complex. They involve providing a diagnosis and a differential diagnosis, and, if possible, a specific diagnosis, as well as accurate grading of the tumor.

Magnetic Resonance Imaging is a powerful visualization technique that allows images of internal anatomy, metabolism, and function to be acquired in a safe and non-invasive way. It is based on the principles of Nuclear Magnetic Resonance, and allows a vast array of different types of visualizations to be performed. This imaging medium has been of particular relevance for producing images of the brain, due to the ability of MRI to record signals that can distinguish between different soft tissues such as gray matter and white matter.

MRI of the brain is a vital part of modern oncology. It is used in tumor diagnosis, monitoring tumor progression, planning treatments, and monitoring responses to treatment. From the very beginning, the technical development of MRI has progressed quickly, and it seems to be continuing at an ever-increasing pace. As a result, over the last 30 years there has been an explosion in the number of clinical applications of MRI.

Due to its high tissue contrast and its noninvasiveness, MRI is accepted as the most sensitive method for diagnosing brain tumors. The very accurate MR Imaging, generally T1-weighted, T2-weighted and proton density, add diagnostic value. In visualizing brain tumors, a second T1-weighted image is often acquired after the injection of a contrast agent. These contrast-agent compounds usually contain an element whose composition causes a decrease in the T1 time of nearby tissue (gadolinium is one example).

Chapter 3

State of the Art Survey on Brain Tumor Segmentation

3.1 Introduction

The ultimate goal of brain tumor imaging analysis is to extract the patient-specific important clinical information, and their diagnostic features. This information embedded within the multidimensional image data, can guide and monitor interventions after the disease has been detected and localized, and ultimately leading to knowledge for clinical diagnosis, staging, and treatment of disease [Wong 2005]. These processes can be represented diagrammatically as a pyramid, as illustrated in Fig. 3.1. At each level of the pyramid, specific techniques are required to process the data, extract, label, and represent the information. Moreover it is necessary a high level of abstraction in order to obtain relevant clinical knowledge or datasets from which medical diagnosis and decision can be made.

Effective management, processing, visualization, and analysis of the obtained datasets cannot be accomplished without high-performance computing infrastructure that should be composed of high-speed processors, storage, network, image display unit, as well as software programs. Development and implementation of the related techniques requires detailed understanding of the underlying problems, and knowledge about the acquired data, as: nature of data, goal of the study, and scientific or medical interest, etc.

The effective extraction of all information and features contained in different types of multidimensional images are of increasingly importance in image

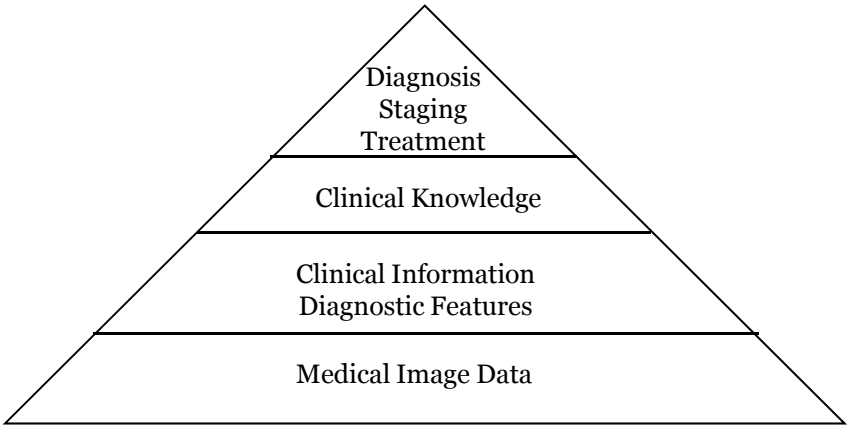

Figure 3.1: The steps and ultimate goal of medical image analysis in a clinical environment [Wong 2005].

segmentation, because it plays a crucial role in extraction of useful information and attributes from images. As Bhandar states [Bhandar 1997]: The main objective of image segmentation is to partition an image into mutually exclusive regions such that each region is spatially contiguous and the pixels within the region are homogeneous with respect to a predefined criterion.

In the particular case of brain tumor, segmentation consists on separating the different tumor tissues such as solid or active tumor, edema, and necrosis, from normal brain tissues, such as gray matter (GM), white matter (WM) and cerebrospinal fluid (CSF). In brain tumor studies, the existence of abnormal tissues is easily detectable most of the time. Nevertheless, accurate and reproducible segmentation and characterization of abnormalities are not straightforward.

In the last years many researchers in the field of medical imaging and soft computing have made significant survey in the field of brain tumor segmentation [Capelle 2000, Clark 1998, Corso 2008, Dam 2004, Dou 2007, Fletcher 2001, Gibbs 1996, Ho 2002, Iftek 2009, Kaus 2001, Khotan 2008, Lee 2005, Prastawa 2004]. Both semiautomatic and fully automatic methods have been proposed. Clinical acceptance of segmentation techniques have depended on the simplicity of computation and the degree of user supervision [Yao 2006]. Interactive or semiautomatic methods are likely to remain dominant in practice for some years, especially in applications where erroneous interpretations are

unacceptable [McIner 2000].

This chapter presents an overview of the most relevant existing brain tumors' segmentation methods applied after the acquisition of the image. Given the advantages of magnetic resonance imaging (MRI) over other diagnostic imaging techniques (as has been explained in Chapter 2) this survey is focused on MRI brain tumor segmentation. Semiautomatic and fully automatic techniques are emphasized.

3.2 Outline of the Chapter

This chapter is divided into four sections. First, section 3.3 gives an introduction of manual and automated segmentation methods. Then, in section 3.4, the concepts of unsupervised and supervised segmentation are presented. Subsequently, the most relevant existing methods for the segmentation of brain tumors are introduced in Section 3.5. Finally, some conclusions are summarized in Section 3.6.

3.3 Manual and Automated Brain Tumor Segmentation

Brain tumor segmentation methods can be classified into three categories according to the degree of required human interaction as exposed by Foo et al. [Foo 2006], Olabarriga et al. [Olaba 2001], snd Yao [Yao 2006]:

- manual segmentation,
- semiautomatic segmentation, and
- fully automatic segmentation.

Next sections give a description of each category, some of their principal advantages and inconveniences are delineated.

3.3.1 Manual Segmentation

Manual segmentation of brain tumors involves manually drawing the boundaries of the tumor and structures of interest, or painting the region of anatomic structures with different labels [Yao 2006]. In manual segmentation, human experts not only make use of the information presented in the image but also make use of additional knowledge such as anatomy.

Manual delineation requires software tools with sophisticated graphical user interfaces to facilitate drawing regions of interest and image display. In practice, the selection of the tumor region, which is the region of interest (ROI), is a tedious and time-consuming task. As explained in Chapter 2, MRI scanners generate multiple two-dimensional cross-sections (slices), and the human expert has to go through the dataset slice by slice for choosing the most representative ones from which the relevant regions are carefully delineated [Wong 2005]. Manual segmentation of brain tumors is also typically done based on a single image with intensity enhancement provided by an injected contrast agent [Prastawa 2003].

The task of marking the tumor regions slice by slice sometimes limits the human rater's view and generates jaggy images as in Figure 3.2 where the tumor was manually segmented slice by slice in axial direction. As a result, the segmented images are less than optimal showing a "stripping" effect [Prastawa 2003]. Needless to say, manual ROI delineation is also operator dependent and

the selected regions are subject to large intra and inter rater variability [White 1999].

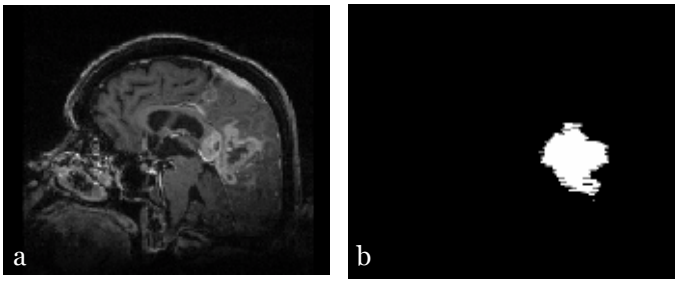

Figure 3.2: a)Sagittal view of gadolinium contrast enhanced T1-weighted MR image and the manual tumor segmentation result. b). "Striping" effect due to segmenting the tumor slice by slice in axial direction can be appreciated [Prastawa 2003].

For example, a recent study [Mazzara 2004] quantified an average of 28% 12% variation in quantified volume between individuals performing the same brain tumor segmentation task (the variation ranged from 11% to 69%), and quantified a 20% 15% variation within individuals repeating the task three times at 1 month intervals. Figure 3.3 gives an example presented in [Luo 2003] of inter rater variability, where four different experts performed a manual segmentation of a glioma on the same slice and patient. The resulting segmentation of each expert presents notable differences.

In spite of the possible intra and inter rater variability, manual segmentation is habitually used as validation ground truth for semi and fully automatic segmentation methods; in which segmentation results are qualitatively and quantitatively evaluated by comparison with manual segmentations. Figure 3.4 shows a graphical representation of the resulting segmentation from an automated method (inner contour displayed in black) as compared with the resulting manual segmentation from a physician (outer contour displayed in white).

Methodologies providing semi automated or, ideally, fully automated segmentation will present clear advantages over the manual delineation. However, manual segmentation is still widely used in clinical trials, especially where a lot of human knowledge and expertise is required to distinguish tissues.

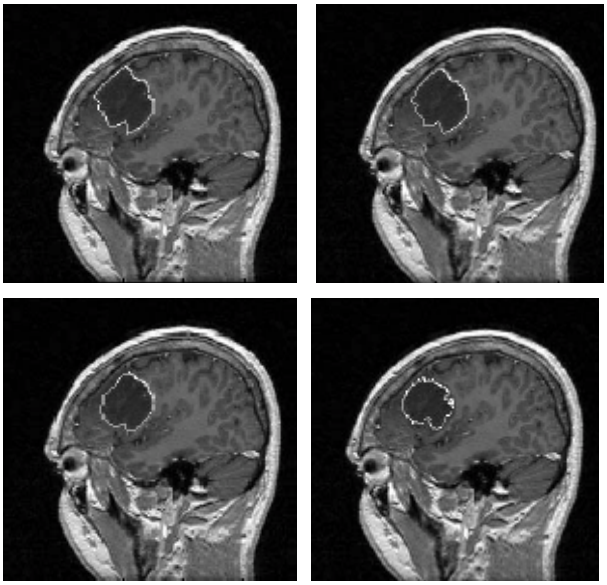

Figure 3.3: Manual segmentation by four different experts of a glioma on the MRI [Luo 2003].

3.3.2 Semiautomatic Segmentation

In semiautomatic brain tumor segmentation, the intervention of a human operator is often needed to initialize the method, to check the accuracy of the result, or even to correct the segmentation result manually. Most of the current research is targeted at semiautomatic segmentation of brain tumors with the intention of having as least human interaction as possible.

According to Olabarriaga et al [Olaba 2001], the main components of an interactive brain tumor segmentation method are the computational part, the interactive part, and the user interface. A representation of these components is depicted in Figure 3.5. Computational part corresponds to one or more pieces of program capable of generating a delineation of the tumor given some parameters. The interactive part is responsible for mediating information between the user and the computational part. It translates the outcome produced by the computational part into visual feedback to the user and the data input by

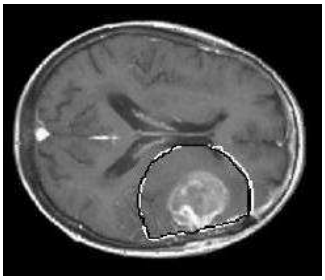

Figure 3.4: Planning target volume resulting from k-nearest neighbors segmentation method (inner contour displayed in black) compared with PTV of a Physician (outer contour displayed in white) [Beyer 2006].

the user into parameters for the program. The actual communication between the computer and the user is done via the output and input devices controlled by the user interface. The user analyses the visual information displayed on the screen and reacts accordingly, providing feedback for the computation.

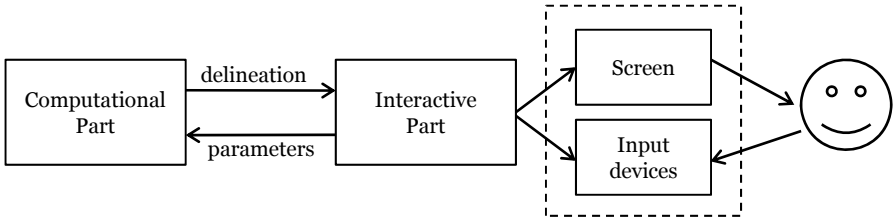

Figure 3.5: Main components of an interactive brain tumor segmentation method, according to Olabarriaga et al. [Olaba 2001].

The user interaction in brain tumor segmentation was recently grouped by Foo [Foo 2006] into three main categories: initialization, intervention or feedback response, and evaluation. Most methods will consist of one or more types of interaction and can be summarized as:

- Initialization
  - Input of arguments or parameters. Either from keyboard, mouse or other forms of input devices.

  - Some pre-processing of image data to enhance quality (sharpening or noise removal).
  - Evaluation of the complexity of the image data to improve decision making during input of arguments/parameters.
  - User selecting the object from the first slice of the data set to be processed or from a three-dimensional representation.

- Intervention / Feedback response
  - Steering of the process continuously or intermittently towards a desired result.
  - Giving a response to feedback data from process.
  - Stopping the process midway when undesired results are obtained to make corrections, and then resume the process.

- Evaluation
  - Evaluating the final result of the process to determine if it is correct or satisfactory. If not satisfactory, necessary changes are made to the arguments or parameters and the process is repeated, make modifications to the results, or in some cases results are simply rejected.

Since the semiautomatic methods use different strategies to combine computers and humans' expertise, the outcome of these methods depends on the strategy as much as on computation. Olabarriaga et al. [Olaba 2001] presented a summary of strategies that are necessary to be considered for the design of efficient brain tumor and medical imaging semiautomatic segmentation methods, for generating accurate and repeatable results, these are

- Design an integrated process for interaction and computation.
- Use pictorial input to the computational process.
- Minimize the amount of interaction by presenting options for user selection.
- Involve the user in the initialization of segmentation process to provide information that can bootstrap or lead the method to the desired segmentation result more quickly.
- Properly visualize the working of the computational part to enable an effective user's response.

- Keep the user in the control during the whole process to generate accurate results.
- Emphasize computation after each interaction to generate repeatable results.
- Add intelligent behavior to elevate the abstraction of interaction; and
- Add intelligence to learn from interaction and reduce the need of future interventions.

Although it is true that by using these strategies efficient brain tumor semi-automatic segmentation methods can be obtained, semi automatic segmentation like manual segmentation is subjected to variations both between expert users and within the same user.

3.3.3 Fully Automatic Segmentation

In fully automatic methods, the computer determines the segmentation of tumor without any human interaction. Fully automatic methods generally incorporate human intelligence and prior knowledge in the algorithms, and are usually developed making use of soft computing and model-based techniques such as deformable models. Soft computing techniques such as fuzzy systems, and deformable models will be reviewed in Section 3.5.

The study of automatic brain tumor segmentation represents an interesting research issue in Machine Learning and Pattern Recognition, since it represents a problem that humans can learn to do effectively. However, developing highly accurate automatic methods remains a challenging problem. This is easily explained by the fact that humans must use high-level visual processing, and must incorporate specialized domain knowledge to perform this task [Prastawa 2003], which makes developing fully automatic methods extremely difficult. Although this is true for many pattern recognition and vision problems, brain tumor segmentation has several properties that reduce the advantage that humans have over machines.

For example, from the brain anatomical properties can be emphasized that the head's appearance in MR images is relatively predictable, the brain is well quantified structurally, and the behavior of different tissue types in different MR channels is well characterized. Additionally, there is no temporal component and the brain remains stationary, therefore being able to visually track

Table 3.1: Summary of related methods in automatic brain tumor segmentation.

Authors	**Description**
[$Dou2007$]	Fuzzy Region Growing Framework
[$Khotan2008$]	Model-based Fuzzy classification
[$Prastawa2004$]	Knowledge-based / outlier detection
[$Vijaya2007$]	Self Organizing Maps
[$Ho2002$]	$3D$ Level Sets
[$Iftek2009$]	Self Organizing Maps
[$Lee2005$]	Discriminative Random Fields and Support Vector Machines

objects over time has no advantage. Another property which reduces the advantage of humans over machines is that the viewpoint is known and that humans view the data as a series of two-dimensional slices. Therefore the ability of humans to use three-dimensional information in segmentation is also reduced in this task since there is no three-dimensional modeling of structures based on a large range of views of the object. Concerning the illumination, there are robust algorithms for correcting intensity inhomogeneity, making the ability to compensate for differences in illumination less of an advantage.

The use of implicit or explicit anatomical knowledge such as size, shape, location, expected appearance of the tumor, and bilateral symmetry to guide the segmentation are especially important for robust automatic methods. This knowledge may be incorporated into the segmentation model in the form of initial conditions, constraints on the model shape parameters, data constraints, or into the model fitting procedure. For automatic segmentation, it is essential to have a model that not only describes the size, shape, location and appearance of the tumor but that also permits expected variations in these characteristics.

However, no completely automatic segmentation algorithm has yet been adopted in the clinic environment. Table 3.1 gives a list of the prior art in fully automatic tumor segmentation. These approaches will be reviewed in section 3.5 according to their segmentation method.

Currently, fully automatic segmentation methods are desirable in processing large batch of images and are mainly restricted to the research environment. However, it must be pointed out that these methods have not gained wide ac-

ceptance among the pathologists for every day clinical practice. It has been mainly due to the lack of interpretability and transparency in the segmentation process, two characteristics that make a segmentation method a convenient tool for every day clinical practice [Papage 2008].

3.4 Unsupervised and Supervised Segmentation

As previously mentioned, the main objective of image segmentation is to partition an image into mutually exclusive and exhausted regions which are homogeneous with respect to a predefined criterion. In the case of brain tumors, the segmentation consists on separating the different tumor tissues such as solid or active tumor, edema, and necrosis, from the normal brain tissues such as gray matter (GM), white matter (WM) and cerebrospinal fluid (CSF). The brain tumor segmentation requires of an objective measure that can be used to define the homogeneity of each tissue. There exist two ways of obtaining the objective measure, namely the unsupervised and supervised segmentation methods [ScmiT 2005]. The difference between them is that unsupervised methods do not make use of training data that have been manually labeled, as is the case of supervised methods.

Figure 3.6 summarizes the difference between the unsupervised and supervised approaches. In unsupervised segmentation (left side of figure 3.6) the number of classes is automatically specified by an algorithm that groups numerically similar pixels. The right side of figure 3.6 emphasizes that the number of classes is manually specified. Next sections give a description of unsupervised and supervised segmentation methods.

3.4.1 Unsupervised Segmentation

When image data are unlabeled, the image can be segmented using clustering algorithms. In this case, no human finds and labels subsets of training data. Instead, the entire set of pixel vectors is submitted to a cluster analysis scheme, and the clusters are found algorithmically. Moreover, once found, algorithmic clusters (regions that have the same labels) must somehow be assigned physical (tissue) labels [Bezdek 1993]. Unsupervised segmentation can be performed using an anatomic objective measure or an image-based objective measure to assess segmentation quality. In the former the goal is to segment the image into regions that have homogeneous and known anatomic properties, whereas in image-based objective the segmentation quality is based on the evaluation

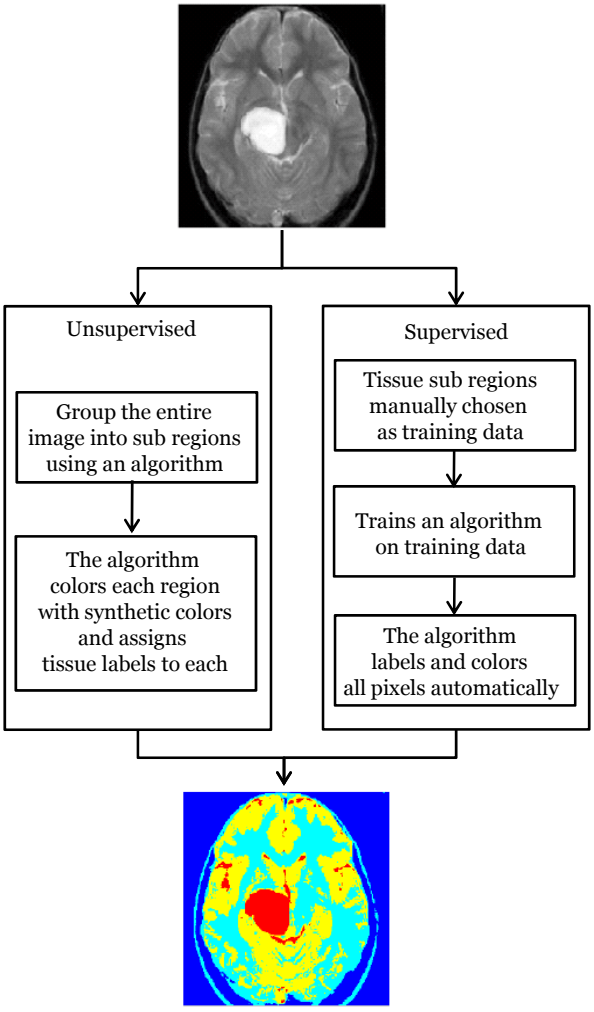

Figure 3.6: Unsupervised and supervised brain tumor segmentation schemes.

of regions having similar intensities or textures.

Brain tumor unsupervised segmentation approaches that use an anatomic objective measure aim to segment the image into at least two anatomically meaningful regions, one of which is tumor or edema. These approaches have been of limited applicability; because most of the proposed methods have been focused solely on the segmentation of enhancing tumor areas [Gibbs 1996, Ho 2002, Sammou 1996, Zhu 1997]. This limitation is primarily due to the difficulty in translating the visual processing and anatomic knowledge used by human experts into operations that yield the desired results.

The unsupervised segmentation methods that use image-based features, rather than dividing the image along anatomically meaningful distinctions, divide the images into homogeneous regions using image-based features such as intensities and/or textures. These methods can handle more complicated cases, for example producing an accurate segmentation of the different regions present in a heterogeneous tumor [Wiselin 2005]. Because of the lack of intensity prior knowledge on the tumors, makes it challenging to proceed in an unsupervised manner [Popuri 2009], for this reason there has been narrow research effort directed towards techniques for unsupervised brain tumor segmentation in MR images that do not use an anatomic objective measure. Three major disadvantages have been pointed out [SchimiT 2005] when using unsupervised segmentation methods using image-based features: the number of regions often needs to be pre-specified, tumors can be divided into multiple regions, and tumors may not have clearly defined intensity or textural boundaries. These disadvantages were reduced in [Cappelle 2004, Clark 1999, Shanti 2007, Zhuang 2006] making use of an automatic preprocessing operation named "skull stripping". Intracranial segmentation commonly referred to as skull stripping, aims to segment the brain tissue from the skull and non-brain intracranial tissues in magnetic resonance images of the brain. Skull stripping is an important preprocessing step in neuroimaging analysis because brain images must typically be skull stripped before other processing algorithms can be applied. In chapter 4 a broad description of this preprocessing operation is given.

3.4.2 Supervised Segmentation

Image segmentation supervised methods differ from unsupervised methods through the use of labeled training data. Supervised classification involves both a training phase that uses labeled data to learn a model that maps from features to labels (Figure 3.7 a and c), and a testing phase that is used to assign labels to

unlabeled data based on the measured features (Figure 3.7 b and d).

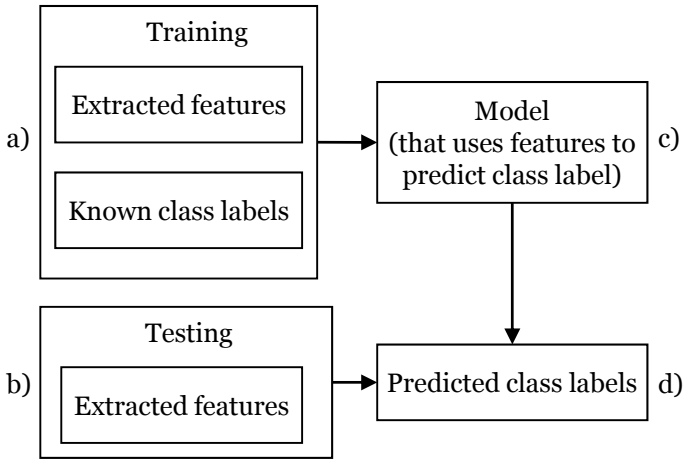

Figure 3.7: Overview of supervised learning framework. The training phase uses labeled data and extracted features to generate a model mapping from the values of the features to the labels. The testing phase uses this model to predict labels from extracted features where the label is not known [SchmiT 2005].

In supervised segmentation the choice of accurate training data is crucial because different training sets can lead to great disparities in training time, as well as potential differences in segmentation results [Bezdek 1993]. In the supervised manner, the operator decides, based on the MR data being inspected, how many tissue classes exist in the image.

When formulating the brain tumor segmentation task as a supervised classification problem, one straightforward method is to use the labels normal and tumor as classes, and to use the intensities in the different MR images as features. Under this formulation the training phase consists on learning a model that uses the MR image intensities to discriminate between normal and tumor pixels. The testing phase would consist on using this model for classifying unlabeled pixels into one of the two classes based on their intensities.

The source of the training and test data has a major influence on the performance of a supervised method. Two mayor sources of training and test are

patient-specific training, and inter-patient training. In patient-specific training, the training data are obtained from the images to be segmented. Several of the subclasses of patient-specific training that will be examined include: training and testing data are the same, training uses a subset of the pixels within the test slice, and training is performed based on slices that are adjacent to the test slice. Inter-patient training is to perform training on several patients, and testing in one [Cobzas 2007]. Subclasses for inter-patient training include: training and testing data are the same, training on the same slice and tumor type from different patients, and Training on the same tumor type from different patients.

A major advantage of using a supervised formulation is that supervised methods can perform different tasks simply by changing the training set. Supervised methods have the potential of reducing the manual engineering task by providing labeled data, appropriate features, and appropriate parameters for the learning algorithm.

Although highly effective and versatile, supervised methods for brain tumor segmentation in MR images often suffer from the disadvantage of requiring patient-specific training. The exceptions that were able to perform inter-patient classification focused on relatively simplified tasks, and required a large amount of training data, as in [Dickson 1997]. The human variability associated with manual training data, could also be a disadvantage.

3.5 Segmentation Methods

Detection, localization, diagnosis, staging, and monitoring treatment responses are crucial procedures in clinical medicine and oncology. Early detection and localization of the diseases, and accurate disease staging could lead to changes in patient management that will impact on health outcomes. Accurate quantification of regional physiology depends on accurate delineation or segmentation of the tumor structure or region of interest in the images. According to Wong [Wong 2005], the fundamental roles of segmentation are: (1) permit quantification, (2) reduce the dataset by focusing the quantitative analysis on the extracted regions that are of interest, and (3) establish structural correspondences for the physiological data sampled within the regions.

A wide variety of brain tumor segmentation techniques has been proposed. However, there is no standard segmentation technique that can produce satisfactory results for all imaging applications. Quite often, methods are optimized to deal with specific imaging modalities such as magnetic resonance imaging.

In general, segmentation techniques have been divided for diverse authors [Yao 2006, Wong 2005, Farag 2005, Xu 2000] into four major classes:

- Threshold-based techniques
- Region-based techniques
- Pixel classification techniques
- Model-based techniques

Threshold-based, region-based and pixel classification techniques are commonly employed in two-dimensional image segmentation [Battha 2008, Iftek 2009, Vijaya 2007, ChangS 2000, Shanti 2007]. Model based techniques such as parametric and geometric deformable models (level sets), are mostly employed in volumetric ($3D$) image segmentation [Chang 2008, Ho 2002, Xie 2005].

There has been a large amount of research effort directed towards the segmentation methods. Many of the approaches that will be discussed here represent prototypical examples of state of the art methods in the general area of brain tumor segmentation. A review of threshold-based, region-based and pixel classification techniques will be given in this section. Model-based techniques such as parametric and geometric deformable models (level sets), as well as their applications, will be introduced and discussed latter in this chapter. Semiautomatic and fully automatic image segmentation techniques are emphasized.

3.5.1 Threshold-Based Methods

Thresholding is a simple and effective region segmentation method, in which the objects of the image are classified by comparing their intensities with one or more intensity thresholds. These thresholds can be either global or local. If the histogram of an image expresses a bimodal pattern, the object can be separated from the background in the image by a single threshold called global thresholding. However, if the image contains more than two types of regions, corresponding to different objects, the segmentation must be carried out using local thresholding. The image may be segmented by applying several individual thresholds or by using a multi-thresholding technique.

Global Thresholding

The simplest property that pixels in a region can share is intensity. So, a natural way to segment such regions is through thresholding, the separation of light and dark regions. Thresholding creates binary images from gray-level ones by turning all pixels below some threshold to zero and all pixels about that threshold to one. If $g(x, y)$ is a thresholded version of $f(x, y)$ at some global threshold T,

$$g(x,y) = \begin{cases} 1 & \text{if } f(x,y) \geq \rho \\ 0 & \text{otherwise} \end{cases} \tag{3.1}$$

in which pixels with value of 1 correspond to the ROI, while pixels with value 0 correspond to the background.

The major problem with thresholding is that only the intensity is considered, not any relationships between the pixels. There is no guarantee that the pixels identified by the thresholding process are contiguous. Extraneous pixels that are not part of the desired region can easily be included, and sometimes isolated pixels within the region (especially near the boundaries of the region) are ignored. These effects get worse as the noise gets worse, simply because it is more likely that a pixel intensity does not represent the normal intensity in the region. When thresholding is used, it is necessary to play with it, sometimes losing too much of the region and sometimes getting too many extraneous background pixels. Shadows of objects in the image are also a problem, not just where they fall across another object but where they mistakenly get included as part of a dark object on a light background. Another problem with global thresholding is that changes in illumination across the scene may cause some parts to be brighter (in the light) and some parts darker (in shadow) in ways that have nothing to do with the objects in the image.

Global thresholding performs well if the image contains objects with homogeneous intensity or the contrast between the objects and the background is high. However, it may not lead itself to fully automatic segmentation, and may fail when two or more tissue structures have overlapping intensity levels. The accuracy of the ROI is also questionable because it is separated from the background based on a single threshold value which may be subject to very large statistical fluctuations. With the increasing number of regions or noise levels, or when the contrast of the image is low, threshold selection will become

more difficult.

Gibbs et al. [Gibbs 1996] presented an unsupervised approach for the segmentation of enhancing tumor pixels from T1-weighted post-contrast images. The system first applied an intensity threshold to a manually selected region of interest, and represents a clearly justified approach for segmenting image objects that are different in intensity from their surroundings.

Although the requirement of manual slice or region of interest selection is a disadvantage, a more severe drawback is that the method does not effectively take into account the presence of hyper-intense pixels representing normal structures in T1 post-contrast images.

Figure 3.8 shows in a) and in c) the T1-weighted post-contrast images. In b) and in d) the resulting segmentation using global thresholding, it can be observed false positive areas including non-tumor structures that have short T1 times (locations of bone and fat) in addition to normal structures that may also uptake the contrast agent.

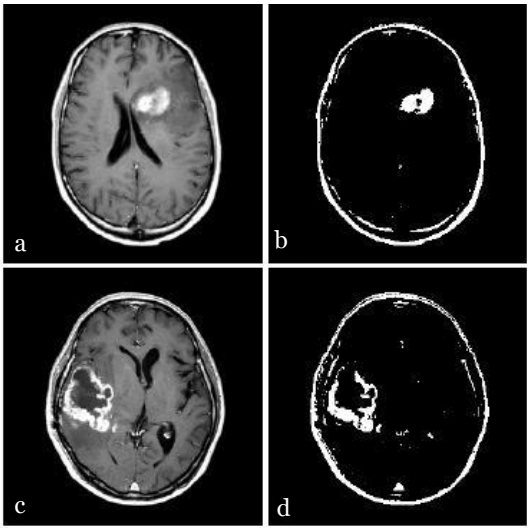

Figure 3.8: Segmentation by Global thresholding (a,c) T1-weighted post-contrast image, (b,d) image after intensity thresholding. The binary segmentation fails in locations of bone and fat (false positives).

Local Thresholding

Apart from global thresholding, there are several thresholding methods which can be classified as local thresholding. A local threshold is determined adaptively in a local region around a pixel. These techniques maybe useful when a thresholding value cannot be determined from a histogram for the entire image or a single threshold cannot give good segmentation results. Local threshold can be determined by estimating a threshold value for the different regions from the intensity histogram. According to Yao [Yao 2006] the values of thresholds are generally estimated by the prior knowledge.

Local threshold values can also be estimated using the local statistical properties such as the mean intensity value as in [Shanti 2007] or by calculating partial volumes of each region to determine the threshold for the segmentation of each component on a brain MR image [ChangSun 2000].

Stadlbauer et al. [Stad 2004] used the Gaussian distribution of data values in normal brain as threshold. The limit threshold value for normal brain tissue was the mean plus three times the standard deviation. Based on this threshold, an area was calculated which was delineated as pathologic tissue.

Generally threshold-based segmentation methods, local or global, are considered unable to exploit all the information provided by MRI, and are used as a first step in the segmentation process.

3.5.2 Region-Based Methods

Region-based segmentation approaches examine pixels in an image and form disjoint regions by merging neighborhood pixels with homogeneity properties based on a predefined similarity criterion [Wong 2005]. These methods can be sketched in a general way as follows: Let X be an image that is segmented into N regions, each of which is denoted as R_i where $i = 1, 2, , N$. The original image can be exactly assembled by putting all regions together (Eq.3.2) and there should be no overlapping between any two regions R_i and R_j for $i \neq j$ (Eq. 3.3). The logical predicate $L(\cdot)$ contains a set of rules (usually a set of homogeneity criteria) that must be satisfied by all pixels within a given region (Eq. 3.4), and it fails in the union of two regions since merging two distinct regions will result in an inhomogeneous region (Eq. 3.5). The regions must satisfy the following properties:

$$X = \bigcup_{i=1}^{N} R_i \tag{3.2}$$

$$R_i \cap R_j = 0 \quad \forall i, j = 1, 2, \ldots, N \tag{3.3}$$

$$L(R_i) = TRUE \quad for \quad i = 1, 2, \ldots, N \tag{3.4}$$

$$L(R_i \cup R_j) = FALSE \quad for \quad \forall i, j = 1, 2, \ldots, N; i \neq j \tag{3.5}$$

where $L(\cdot)$ is a logical predicate.

The region growing and the watershed segmentation method are part of the region-based methods [Yao 2006], and are the most commonly used for brain tumor segmentation. Next sections give a description of these methods, and some applications in the literature for brain tumor segmentation.

Region Growing

The simplest region-based segmentation technique is the region growing, which is used to extract a connected region of similar pixels from an image [Adams 1994]. Region growing starts with at least one seed that belong to the structure of interest. Neighbors of the seed are checked and those satisfying the similarity criteria are added to the region. The similarity criteria are determined by a range of pixel intensity values or other features in the image. Seeds can be chosen manually or provided by an automatic seed-finding procedure. The procedure iterates until no more pixels can be added to the region. The advantage of region growing is that it is capable of correctly segmenting regions that have similar properties and generating connected region.

Kaus et al. [Kaus 2001] implemented a region growing technique for segmenting MR Images of brain tumors. The technique involved the iteration of statistical classification to divide an image into different tissue classes on the basis of the signal intensity value. Objects of interest were identified on the classified images with local segmentation operations (mathematic morphology and region growing).

Recent studies [Salman 2005, Vincent 2004, SalBad 2005] have proved that the region growing is an effective approach and less computation intensive than other non region-based methods for brain tumor segmentation, especially for the homogeneous tissues and regions. The primary disadvantage of region growing method is the partial volume effect [Sato 2000, Lakare 2000] which limits the accuracy of MR brain image segmentation. Partial volume effect blurs the intensity distinction between tissue classes at the border of the two tissues types, because the voxel may represent more than one kind of tissue types [Links 1998].

S. Lakare et. al. [Lakare 2000] introduced the modified region growing method (MRGM), which is used to remove the partial volume effects and to incorporate gradient information for more accurate boundary detection and filling holes occurred after segmentation.

Recenlty Salman [Salman 2009] presented a comparative analysis of the traditional region growing segmentation and the MRGM, addressed to brain tumor segmentation in $3D$ images. In his study Salman proved that the MRGM increases the accuracy of the volumetric measurements of brain tumors, producing lower relative errors than traditional region growing method when compared with manual segmentation.

As matter of example, Figure 3.9 shows the results of the traditional and modified region growing segmentation methods. It can be observed that some false negatives (center of tumor in Figure 3.9a) were detected by using the MRGM (Figure 3.9 b). Figure 3.10 shows a graphical representation of the relative errors of tumor volume segmentation using the traditional and modified region growing methods compared to the expert manual tracing.

Other recent approaches incorporate the region growing process as a refinement step. A good example is the work presented by Dou et al. [Dou 2007], wherein they proposed a fuzzy information fusion framework for the automatic segmentation of tumor tissues of human brain from multiple MR image sequences. This framework consists on the registration of multispectral images, the creation of fuzzy models (based on a priori knowledge), fuzzy feature fusion and an adjustment by fuzzy region growing. Rexilius et al.[Rexilius 2007] propose a fast multispectral segmentation of brain tumors by means of a probabilistic intensity model, followed by an iterative refinement of the initial segmentation. The refinement step is performed by a progressive region growing that combines probability and distance information.

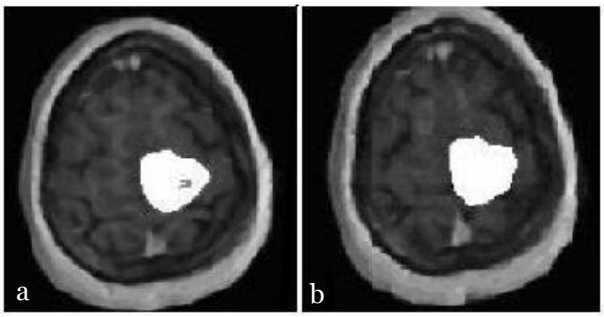

Figure 3.9: Comparison of the modified region growing segmentation method against the traditional method. (a) Results of traditional region growing segmentation; some false negatives in the interior of tumor volume (b) Results of modified region growing segmentation method [Salman 2009].

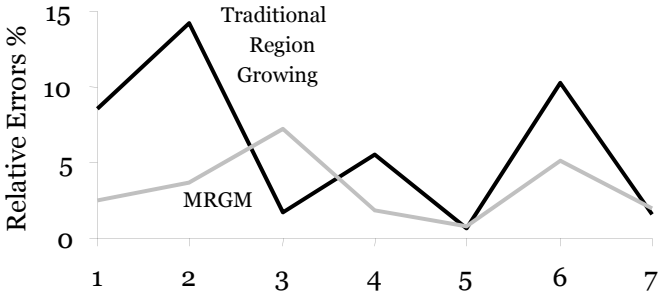

Figure 3.10: Relative errors for traditional region growing segmentation (gray) and modified region growing segmentation method (black) compared with manual segmentation method [Salman 2009].

Watershed

Basic watershed segmentation method can be explained by a metaphor based on the behavior of water in a landscape. When it rains, drops of water falling in different regions will follow the landscape downhill. The water will end up at the bottom of valleys. For each valley there will be a region from which all water drains into it. In other words: each valley is associated with a catchments basin, and each point in the landscape belongs to exactly one unique basin. At points where water coming from different basins meet, dams will be built. When the water level has reached the highest peak in the landscape, the process is stopped. As a result, the landscape is partitioned into regions separated by dams, called watershed lines or watersheds. It produces a complete contour of the images and avoids the need for any kind of contour joining.

Watershed applications have been widely used in brain tumor segmentation, for example, Letteboer et al. [Letteboer 2001] and Dam et al. [Dam 2004] performed segmentation of brain tumors using multi-scale watershed transformation. Dam presented an interactive method for brain tumor segmentation, the method builds blocks at different scales that the user can select (and deselect) in order to sculpt the desired anatomical object. Supervised learning is used to predict which building blocks are to be included in the segmentation.

Cates et al. [Cates 2005] performed an analysis of user-assisted hierarchical watershed segmentation of brain tumors from MRI data. The quantitative and qualitative results showed improvements on the segmentation time and precision over manual segmentation. The analysis also identified some failures in the watershed technique, where edges were poorly defined in the data, and noted a trend in the manual segmentation results toward systematically larger segmentations. The analysis raised questions about the wisdom of using expert segmentations to define ground truth.

Batthacharya and Das [Battha 2008] implemented a marker-based improved watershed algorithm utilizing the prior knowledge of the test images for the segmentation of brain tumors; seeded region-growing method was used as the marker of ROIs.

Recently Ratan et al. [Ratan 2009] proposed a watershed segmentation based algorithm that has been used for detection of tumor in $2D$ and in $3D$ brain MRI. A simple supervised block-based and image-based (shape, texture, and content) technique has been used to analyze MRI brain images with relatively lower computational requirements.

The watershed transform usually suffers from over-segmentation. As any local maximum in the image will generate a shape boundary (or part of) it is obvious that watershed segmentation has a strong potential for over segmentation, if not for other reasons then because of noise. To avoid over-segmentation some pre or post processing methods have been proposed in order to produce a more reasonable segmentation that reflects the layout of objects [Bleau 2000, Gies 2004, Haris 1998]. Kong et al. [Kong 2006] applied on brain tumor MRI a merging process for the over segmented regions using Fuzzy C-Means clustering algorithm. This algorithm will be broadly explained at section 3.5.3.

3.5.3 Pixel Classification Methods

Another type of segmentation methods is based on pixel classification. Pixels in an image can be represented in feature space using pixel attributes that may consist of gray level, local texture, and color components for each pixel in the image. In the case of single-channel (or single-frame) image, pixel classification is typically based on gray level and image segmentation can be performed in a one-dimensional feature space. For multichannel (multiple-frame) images or multispectral (multimodality) images the segmentation can be performed in multidimensional feature space.

In brain tumor segmentation the methods based on pixel classification are constrained to the use of supervised or unsupervised classifiers to cluster pixels in the feature space. Clustering is the process of grouping similar objects into a single cluster, while objects with dissimilar features are grouped into different clusters based on some similarity criteria. The similarity is quantified in terms of an appropriate distance measure. An obvious similarity measure is given by the distance between two vectors in the feature space which can be expressed as:

$$d(x_i, x_j) = \left(\sum_{k=1}^{n} \parallel x_i - x_j \parallel^p \right)^{\frac{1}{p}} \tag{3.6}$$

where $x_i = \left(x_i^1, \ldots, x_i^n\right) \in R^n$ and $x_j = \left(x_j^1, \ldots, x_j^n\right) \in R^n$ are the two vectors in the feature space. It can be seen that the above measure corresponds to Euclidean distance when $p = 2$ and Mahalanobis distance when $p = 1$.

Another measure that is commonly used as similarity criterion is the normalized inner product, which is given by:

$$nd(x_i, x_j) = \frac{x_i^T x_j}{\|x_i\|\|x_j\|} \tag{3.7}$$

where T denotes the vector transpose operation. This measure provides information regarding the cosine between the vectors x_i and x_j in the feature space.

Each cluster is represented by its centroid (or mean) and variance, which indicates the compactness of the objects within the cluster, and the formation of clusters, is optimized according to a cost function that typically takes into account the similarity within individual cluster and dissimilarity between clusters.

There are many clustering techniques proposed in the literature. Basic techniques include unsupervised methods such as: Fuzzy C-Means (FCM), k-means, and statistical methods as Markov Random Fields (MRF) among others. The supervised methods include Bayes and Artificial Neural Networks (ANN). In this section the FCM, MRF and ANN clustering techniques are presented and analyzed.

Fuzzy C-Means

In many situations, it is not easy to determine if a pixel should belong to a region or not due to the features considered for determining the homogeneity within each region do not have sharp transitions at region boundaries [Bezdek 1999]. To alleviate this situation fuzzy set concepts can be introduced into the segmentation process, as is the case of Fuzzy C-Mean technique. FCM clustering is a very popular technique in the area of unsupervised image segmentation by pixel classification, particularly in the case of brain tumor segmentation [Kong 2006, Supot 2007].

When the FCM method is applied for brain tumor segmentation, the first step consists on determining a set of tissue classes. Each pixel is then assigned membership values to the tissue classes according to its attributes. The fuzzy membership functions, constrained to be between 0 and 1, reflect the similarity degrees between the data value at a specific location and the prototypical data value, or centroid, of its class. Thus, a membership value near one means that the data value at that location is close to the centroid of the class.

Let $X = \{x_k|1 = k = N, andx_kR^d\}$ represents the observed image where d is one in the case of gray-level images, three for color images, and d greater than three for multi-spectral ones. Then, mathematically, the standard FCM must optimize an objective function for partitioning a dataset X into c clusters is given by:

$$J_m = \sum_{i=1}^{c} \sum_{k=1}^{N} \pi_{ik}^m \|x_k - v_i\|^2 \tag{3.8}$$

where $\{v_i\}_{i=1}^c$ are the centroids or prototypes of the clusters, the parameter m is a weighting exponent on each fuzzy membership and determines the amount of fuzziness of the resulting classification and the array of membership functions $\Pi = [\pi_{ik}]$ is a fuzzy partition matrix satisfying:

$$\Pi \in \left\{ \pi_{ik} \in [0,1] \mid \sum_{i=1}^{c} = 1, \forall k, 0 < \sum_{k=1}^{N} \pi_{ik} < N, \forall i \right\} \tag{3.9}$$

If the initialization can be carried out by accurate estimation of cluster centers, the algorithm converges faster and the clustering results are improved. Supoot et al. [Supot 2007] applied the splitting technique of discrete curve evolution (DCE) in order to find the most accurate estimation of cluster centers for MR brain image segmentation.

Phillips et al. [Phillips 1995] gave an early proof-of-concept fuzzy clustering for brain tumor by operating on the raw multisequence data. They visually demonstrated that even with multisequence data the intensity distributions for tumor and normal tissues overlap. This led to other researchers to incorporate additional knowledge into the feature vectors being clustered using FCM.

Clark et al. [Clark 1998] integrated knowledge-based techniques and multispectral histogram analysis to segment glioblastoma multiforme (GBM) tumors in a multichannel feature space. The level of correspondence between ground truth measurements and isolated tumor pixels was incremented by their segmentation method. Fletcher-Heath et al. [Fletcher 2001] also implemented a knowledge-based fuzzy clustering approach for the segmentation of non-enhancing tumors followed by $3D$ connected components to build the

tumor shape.

Veloz et al. [Veloz 2008] applied Fuzzy C-Means and Mathematical Morphology to extract patterns of intensities of the GBM and to select seed points automatically to perform the Fuzzy Spatial Growing. Additionally, a Fuzzy similarity criterion was considered to measure the memberships degrees of the voxels to the tumor.

Many authors have considered that standard FCM for MR image segmentation is not efficient by itself, as it fails in dealing with the significant strong correlation of neighboring pixels that is given in MR images. Ignoring this specificity leads to strong noise sensitivity and several other imaging artifacts. Recently, several solutions have been proposed to overcome this problem [Pham 1999, Ahmed 2002, Pham 2003, Siyal 2005, Chuang 2006, Kannan 2008]. Most of the proposed improvements involve the consideration of local spatial information based on the fact that besides to the gray level value of the considered pixel, the information provided by its neighbors also contribute to its assignment to a given cluster [Szilgyi 2007].

Since Fuzzy C-Means is an iterative algorithm, it is considered a very time consuming clustering technique [Lazaro 2005, Yong 2004]. Aiming at reducing the execution time, several particular implementations have been developed. Szilagyi et al. [Szilgyi 2003], and Chen and Zhang [Chen 2004] proposed to evaluate the neighborhoods of each pixel as a pre-filtering step, and perform FCM afterwards. This latter quick approach, combined with an averaging prefilter, is referred to as enhanced Fuzzy C Means (EnFCM) [Cai 2007].

Markov Random Fields

Most clustering methods do not take into account spatial information of the image, the dependency between the pixels in the image surface. The unsupervised clustering method of Markov Random Field (MRF), first discussed by Besag [Besag 1986] and later improved by Qian and Titterington [Qian 1991], provides a way to integrate spatial information into the clustering process. In many cases, this reduces both the possible problem of clusters overlapping and the effect of noise on the clustering result [Tran 2005].

Let S be a set of lattice sites (or pixels). In order to define MRFs, a neighborhood system over the lattice S has first to be defined. A neighborhood system η related to a lattice S is defined as:

$$\eta = \{\eta_{ij} \subset S \mid (i,j) \in S\} \tag{3.10}$$

where η_{ij} is the neighbourhood of site (i,j). This neighbourhood is such that:

$$(i,j) \notin \eta_{ij}\,(k,l) \in \eta_{ij} \quad implies \quad (i,j) \in \eta_{kl} \tag{3.11}$$

Let $X = X_{ij}$ be a random field; that is, a collection of random variables, one at each site of the lattice S. X is said to be a Markov random field with respect to (S,η) and $P(X = x) > 0$ for all x if and only if

$$P\left(X_{ij} \mid X_{kl}, (k,l) \in \Omega\right) = P\left(X_{ij} \mid X_{kl}, (k,l) \in \eta_{ij}\right) \tag{3.12}$$

where Ω is any subset of sites of S containing completely η_{ij} but not (i,j).

In the particular case of brain tumor segmentation, if a pixel is strongly labeled as tumor, it suggests that its neighbors will have a tumor label. Similarly non-tumor pixels tend to be next to other non-tumor pixels. This has motivated some researchers [Li 2001] to apply Markov Random Fields and Conditional Random Fields (CRFs) [Lafferty 2001] to various segmentation tasks. MRF and CRF techniques are able to represent complex dependencies among data instances, giving a high accuracy on brain tumor's segmentation task [Lee 2005].

Gering et al. [Gering 2002] proposed a method that detects abnormalities in the brain using a multi-layer MRF framework. The information layers included pixel intensities, structural coherence, spatial locations, and user input. In their work, it was considered that a given voxel would change its high-level classification in the evolving presence of tumor if the attributes of lower-level layers shared strong similarities.

Cappelle et al. [Cappelle 2000] presented an unsupervised approach by means of a Markov Random Field model that statistically uses influences that neighboring pixels should have on each other's labels removing the need of morphological operations. In their work the authors assumed that the tissue

classes: gray matter, white matter, CSF, tumor, and edema could be modeled by a Mixture Model (of Gaussians), and trained the Markov Random Field with the Iterated Condition Modes (ICM) algorithm.

However, these previous random field approaches are based on computationally intractable formulations. There are approximation techniques that can deal with these computational challenges. Conditional Ramdom Field variants such as Discriminative Random Fields (DRFs) [Kumar 2006] and Support Vector Machines (SVMs) [Zhang 2004, Schmi 2005] are coupled with a set of knowledge-based features to perform the segmentation and classification.

One difficulty associated with MRF models is the proper selection of the parameters that control the strength of spatial interactions. A setting that is too high selection can result in very soft segmentation and a loss of structural details. In addition, MRF methods usually require algorithms computationally intensive. Despite these disadvantages, the Markov Random Fields are widely used not only for modeling classes of segmentation, but also to model texture properties and inhomogeneities of the intensities.

Artificial Neural Networks

Another relevant supervised clustering method is the Artificial Neural Network (ANN) technique. This classifier feeds the features through a series of nodes, where mathematical operations are applied to the input nodes and a classification is made at the final output nodes.

A flowchart of the ANN architecture is given in Figure 3.11, wherein multispectral intensities represent the input to the network, linear combinations of the intensities (weighted along the edges with values $w(i)$) are input to the "hidden" nodes of the layer, while the output node values are obtained from linear combinations of the results of the hidden layer transformations. Pixels are assigned to the class whose output node has the highest value.

The training step for this technique consists on determining the values of the parameters considered (or involved) in the mathematical operations such that the error in the predictions made by the output nodes is minimized. Since no parametric distribution (such as a Gaussian distribution) is assumed for the data, ANN approaches are non-parametric techniques. Moreover, the use of "hidden" layers of nodes allows the modeling of non-linear dependencies in the features. Although ANN training is complex, the ability to model non-trivial distributions offers clear practical advantages. This is noteworthy in the case of

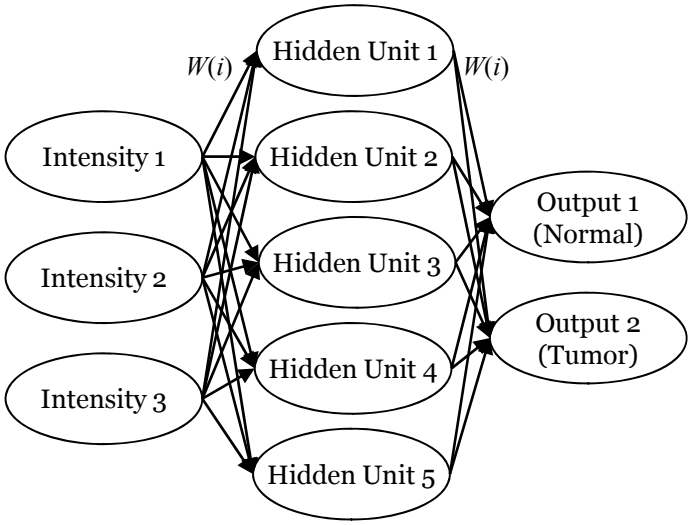

Figure 3.11: Example of the ANN architecture. Linear combinations of the intensities are input to the hidden layer of nodes. The output node values are formed from linear combinations of the results of the hidden layer transformations.

tumor segmentation since assuming the data follows a simple Gaussian distribution may not be appropriated for segmenting heterogeneous tumors [ScmiT 2005].

Clarke [Clarke 1991] was one of the first researchers in introducing a supervised classification using an ANN approach for brain tumor segmentation in MR images. Ozkan et al. [Ozkan 1993] also made use of ANN classification methods. Their system first used patient-specific training of a neural network classifier on a single slice. When segmenting an adjacent slice, this neural network was first used to classify all pixels in the adjacent slice, after that the locations of pixels that received the same label in both slices were then determined. These pixels in the adjacent slice were used as a new training set for the neural network classifier used to classify the adjacent slice.

Dickson and Thomas [Dickson 1997] presented one of the uncommon supervised methods that do not require patient-specific training. The authors used a set of 50 hand-labeled MR slices from the same area of the head from different patients with acoustic neuromas, and learned to automatically label this type

of tumor without patient specific training. The features used in this system included not only the pixel intensities, but also the intensities of neighboring pixels and the pixel location within the image.

Implementing Artificial Neural Networks for brain tumor segmentation involve problems of complexity and it is a time consuming task: the size of network becomes very large, training time is unacceptable, and large number of images is required for training the network. Some methods to solve these problems has been introduced, as it is the case of the neuro difference fuzzy proposed by Tayel [Tayel 2006], which purpose reducing complexity, time, and storage space in determining the critical points of ROI contour using an ANN.

A particular case of ANN is the self-organizing map (SOM). It is a neural network model developed in 1980 by Teuvo Kohonen [Kohonen 2000]. In contrast with other neural network models, it has a strong physiological inspiration, as it is based on the topological map that exists in the brain cortex. The cortex is organized so that topologically closer neurons tend to produce answers to the same kind of stimulus; this is one of the reasons why SOM technique is largely employed in visual pattern recognition [Vijaya 2007]. The self-organizing map training method is based on competitive learning, which is a type of neural network unsupervised learning.

Reddick et al. [Reddick 1997] developed a pixel-based two stage approach where a SOM was trained to segment multispectral MR images which were subsequently classified into white matter, gray matter, etc., by a feed-forward ANN. In a recent work Vijayakumar et al. [Vijaya 2007] proposed a method based on SOM to segment tumor, necrosis, cysts, edema, and normal tissue in MRI. Their approach also graded the tumors simultaneously. The overall sensitivity and specificity of the Vijayakumar's method was observed as 0.86 and 0.93, respectively. More recently, Iftekharuddin et al. [Iftek 2009] presented a work where the effectiveness of two novel fractal and fractal-wavelet features is exploited to segment and classify tumor and non-tumor regions along with intensity values in multimodal MR images. The features are fused and the segmented tumor clusters are obtained exploiting a SOM neural network.

The researchers in the field of MRI brain tumor segmentation have used SOM or FCM separately as segmentation process tools. In [Muruga 2007] Murugavalli and Rajamani implemented a hybrid technique combining the advantages of a Hierarchical Self Organizing Map (HSOM) and FCM to detect various tissues like white matter, gray matter, CSF and tumor in MR images.

HSOM is the combination of self organization and topographic mapping techniques. This technique combines the idea of regarding the image segmentation process as one of data abstraction where the segmented image is the final domain independent abstraction of the input image. Figure 3.12 shows the comparison of execution time and variation of the total number of tumor pixels detected in an image with various segmentation techniques. The value of the tumor pixels detected with both implementations, HSOM and SOM combined with FCM, is about 3223, this value is higher than the number of tumor pixels detected for the SOM k-means and HSOM k-means, 2772. This increment is due to the abstraction level and fuzzy clustering process.

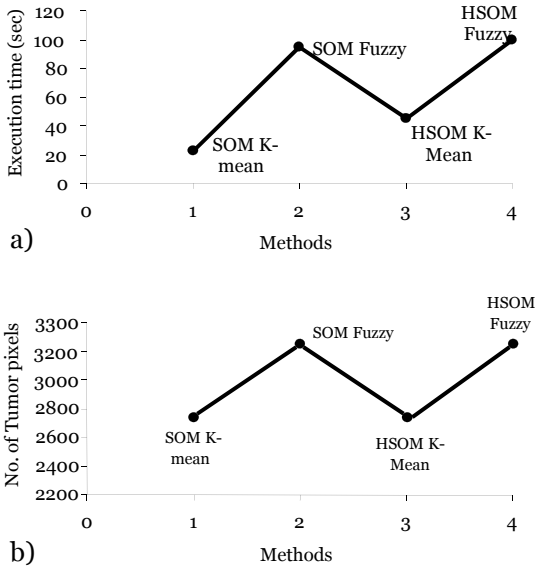

Figure 3.12: Comparison for various segmentation techniques of: (a) execution time, and (b) variation of the total number of tumor pixels detected in an image [Muruga 2007].

3.5.4 Model-Based Segmentation Techniques

In Section 3.4 the most successful solutions for the extraction of brain tumor boundary were analyzed, mainly for $2D$ MRI data. The segmentation of volumetric ($3D$) image data is a challenging problem that has been mainly

approached by model-based segmentation techniques as parametric deformable models and geometric deformable models or level sets.

In model-based segmentation, a connected and continuous model is built for a specific anatomic structure by incorporating a priori knowledge of the object such as shape, location, and orientation. Some models incorporate prior statistical information drawn from a population of training datasets [Yao 2006]. The statistical parameterization provides global constraints and allows the model to deform only in ways implied by the training sets.

Segmenting structures from medical images and reconstructing a compact geometric representation of these structures is difficult due to the sheer size of the datasets and the complexity and variability of the anatomic shapes of interest [McIner 2000]. The challenge is to extract boundary elements belonging to the same structure and integrate these elements into a coherent and consistent model of the structure.

Deformable models involve the formulation of a propagating interface (a closed curve in $2D$ and a closed surface in $3D$) that moves under a speed function determined by local, global and independent properties [Osher 2003]. Given the initial position of a propagating interface, and the corresponding speed function, deformable models track the evolution of the interface during the segmentation process. Existing deformable models can be broadly divided into two categories: parametric and geometric.

The following sections explain the parametric and geometric deformable models including some approaches appearing in the literature for brain tumor segmentation.

Parametric Deformable Models

The strength of parametric deformable models (also known as active contour models or snakes) stems from their ability to segment, match, and track images of anatomic structures by exploiting constraints derived from the image data together with a priori knowledge about the location, size, and shape of these structures. Parametric deformable models are capable of accommodating the often significant variability of biological structures over time and across different individuals [McIner 1996]. Furthermore, these models support highly intuitive interaction mechanisms that allow medical scientists and practitioners to bring their expertise to bear on the model-based image interpretation task

when necessary [McIner 2000].

Deformable models are parametrically defined curves or surfaces that move under the influence of weighted forces that have two components named internal and external forces. The internal forces are used to assure the smoothness of the model during deformation process, while external forces are defined to push/pull the model toward the boundaries of the structure. Parametric representations of the models allow accurate and compact description of the object shape, while the continuity, connectivity, and smoothness of the models compensate the irregularities and noise in the object boundaries. The active contour model, or snake, is defined as an ordered collection of n points in the image plane $V = \{v_1, \ldots, v_n\}, v_i = (x_i, y_i), i = \{1, \ldots, n\}$.

The points in the contour iteratively approach the boundary of an object through the solution of an energy minimization problem. For each point in the neighborhood of v_i, an energy term is computed:

$$E_i = \alpha E_{int}(v_i) = \beta E_{ext}(v_i) \tag{3.13}$$

where $E_{int}(v_i)$ is an energy function dependent on the shape of the contour and $Eext(vi)$ is an energy function dependent on the image properties, such as the gradient, near point v_i. α and β are constants providing the relative weighting of the energy terms.

E_i, E_{int}, and E_{ext} are matrices. The value at the center of each matrix corresponds to the contour energy at point v_i. Other values in the matrices correspond (spatially) to the energy at each point in the neighborhood of v_i. Each point, v_i, is moved to the point, v_i', corresponding to the location of the minimum value in E_i. If the energy functions are chosen correctly, the contour, V, should approach, and stop at, the object boundary.

Contour deformable models have been widely used for its sensitivity in searching the boundary of brain tumors [Chan 1996, Kang 1999, Law 2001]. In fact, the sensitivity of the boundary found by the snake is better than the conventional edge detection methods, such as the Sobel and Laplacian [Kass 1987]. The external energy of snake function is only positive in homogeneous regions, and zero at the edges [Chan 2001].

A number of methods have been proposed to improve the snake's performance, a review of the most relevant methods can be found in [McIner 1996, Bamford 1998]. Luo et al. [Luo 2003] implemented two of these improved methods for tumor segmentation on $2D$ brain MRI: the balloon model [Cohen 1989, Cohen 1993], and the Gradient Vector Flow snake (GVF) [Xu 1998, XuPrince 1998]. The improvement provided by these methods are that the balloon model permits to enlarge the snake's capture range, and the GVF uses a spatial diffusion of the gradient of an edge map of the image, instead of using image gradients as an external force. Latter in [Luo 2006], Luo et al. extended their approach to $3D$.

Law et al. [Law 2002] presented a modified deformable region model for the extraction of brain tumor boundary in $2D$ MR images. The model used a point sampling technique in order to reduce the number of boundary points processed. The time required for the extraction of brain tumor boundary in MR image was greatly reduced compared with traditional active contour models.

In some applications, the initial position of the model needs to be manually placed close enough to the desired boundary to avoid converging to wrong boundaries. Khotanlou et al [Khotan 2008] proposed a parametric deformable model constrained by spatial relations as refinement step to provide an accurate estimation of the boundaries of any type of brain tumors on MRI.

Geometric Deformable Models or Level Sets

One disadvantage when using parametric deformable models for the segmentation of volumetric ($3D$) image, is the difficulty of naturally handling topological changes for the splitting and merging of contours. This problem was solved by Osher and Sethian [Osher 1988] introducing the use of geometric deformable models, or level sets. The main component of the level set method is the implicit representation of the interface. If the interface is given by Γ, Γ is represented as the zero level set $\{\phi = 0\}$ of a level set function ϕ. The function is a surface defined over the image area with the following property:

$$\phi(x, y, t = 0) = \pm d(x, y) \tag{3.14}$$

where d is the distance function from (x, y) to $\Gamma(t = 0)$, and the plus (minus) sign is chosen if the point (x, y) is outside (inside) the initial interface. Thus, the surface ϕ evolves along its normal direction with speed F as:

$$\frac{\partial \phi}{\partial t} + F|\nabla \phi| = 0 \quad given \quad \phi\,(x, y, t = 0) \tag{3.15}$$

and at any time the propagating front is given by the zero level set:

$$\Gamma(t) = \{(x, y)|\phi(x, y, t) = 0\} \tag{3.16}$$

The speed F can be a function of various arguments, including the curvature gradient, normal direction, etc. A common choice for F is [Hao 2006]:

$$F = g(x, y)\,(1 - \varepsilon\kappa) \tag{3.17}$$

where g is a property function of the image $I : \Re^2 \to \Re$, $I(x, y)$ is the image intensity, $0 < \varepsilon < 1$ is a constant, and κ is the curvature. The property g is meant to stop the front on the object's boundaries. For example, if the edge is modeled as pixels with high gradients, the feature image g can be defined as

$$g(x, y) = \frac{1}{1 + |\nabla I(x, y)|^2} \tag{3.18}$$

which yields minimal value on the boundaries while bigger value in other area. Thus with an appropriate g, the evolution is driven to stop on the boundaries, and the image is segmented.

Caselles et al. [Caselles 1993] and Malladi et al. [Malladi 1995] proposed a geometric deformable contour with an image gradient stopping force based upon the OsherSethian [Osher 1988] level set framework. Although the Caselles method notably improved the initialization of parametric active contours, provided that the initial contour was placed symmetrically with respect to the

boundaries of interest, in practice this is not easy to achieve since many medical image segmentation problems are not dealing with regularly shaped objects.

Figure 3.13 shows the difficulty of using the CasellesMalladi deformable contour to segment the brain with convoluted shapes in T2-weighted MR images. Note that the initial contour was not symmetrically placed with respect to the brain (Figure 3.13a). It was not easy to choose an appropriate stopping force required to achieve satisfactory results (Figure 3.13b). The contour was confined inside by the high intensity structures when using a stronger stopping force (Figure 3.13c), and the contour leaked past the brain boundaries when using a weaker stopping force (Figure 3.13d).

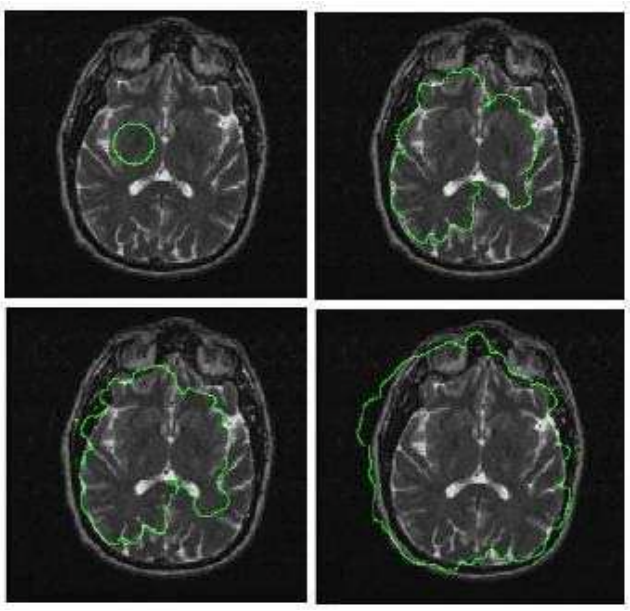

Figure 3.13: Difficulty of using the CasellesMalladi deformable contour in segmenting the brain in T2-weighted MR images. (a) The initial contour that was not symmetrically placed. (b) The contour was confined inside the brain by the inner high intensity structures using a strong stopping force. (c) Some of the contours were crossed over the brain boundaries while some contours were restricted inside, using a slightly weaker stopping force. (d) The contour leaked past the brain boundaries using a weaker stopping force [Chang 2008].

Diverse approaches were proposed to overcome aforementioned problem. So, Kichenassamy et al. [Kichen 1995] and Yezzi et al. [Yezzy 1997] added a term to efficiently attract the evolving contour to the desired feature. Siddiqi et al. [Siddiqi 1998] subsequently modified the speed function by adding a term based upon the gradient flow derived from a weighted area functional so that the contour could more flexibly evolve toward the desired edges.

Chang and Valentino [Chang 2006] used the simulation of a charged fluid framework, governed by Poisson's equation, as a deformable model to perform general image segmentation. Later Chang et al. [Chang 2008] proposed the Charged Fluid Model (CFM), a new deformable model that extends and modifies the charged fluid framework for brain tumor segmentation.

Ho et al. presented in [Ho 2002] a method for automatically segmenting blobby-shaped tumor structures in MR images. The segmentation was performed using a probability map of tumor versus background to guide a level set snake propagation. Prastawa et al. [Prastawa 2004] presented a knowledge-based detection/segmentation algorithm, which is based on learning pixel-intensity distributions and uses level set snakes, for normal brain matter and detecting outlier pixels that are considered tumor, The distributions were learned with kernel-based density estimation methods, and the initial outlier detection were followed by a region competition algorithm. The input for the snake was obtained by sampling specific regions based on the probabilistic brain atlas, which is represented as the zero level set of the implicit function (Eq. 3.14).

Xie et al. [Xie 2005] exploited a hybrid level set segmentation method driven by region and boundary information simultaneously. Region information served as a propagation force, and boundary information served as stopping functional. In this approach, the user selects a ROI and then a level set method is applied to segment the tumor.

Lefohn et al. [Lefohn 2003] proposed a semi-automatic method for tumor segmentation using level sets in which the user selects the tumor region to initialize the segmentation. Based on a visual inspection of the results, they tune the level set parameters and the segmentation process is repeated.

Recently Cobzas [Cobzas 2007] and Popuri [Popuri 2009] presented a variational method for brain tumor segmentation. Their approaches used prior knowledge of the appearance of anatomical structures in the normal brain, in the form of templates and atlases. These templates and atlases were fully in-

tegrated into a level set variational segmentation.

3.6 Summary of Brain Tumor Segmentation Methods

In this section it is provided a summary table enhancing the advantages and disadvantages of the presented methods. This section concludes with a general discussion of the analyzed brain tumor segmentation methods is presented.

Threshold-based techniques offer the possibility of conducting a simple and fast segmentation when good threshold values are defined. Although with restrictions, these techniques are generally used as a first step in the segmentation process.

Region-based techniques for brain tumor segmentation are mainly used as refinement step for defining a connected boundary of the tumor [Dou 2007, Rexilius 2007]. Some region-based approaches such as watershed transform, have reported very accurate results in segmenting tumors, but generally these approaches are constrained to be semi-automatic [Cates 2005].

Pixel classification techniques for brain tumor segmentation are limited to clustering nevertheless they are the most frequently used for brain tumor segmentation. The unsupervised technique of FCM, which is the most popular for medical image segmentation [Kong 2006, Supot 2007], permits the use of vague concepts in the definition of clusters, and gives highly accurate results in cases of non homogeneous tumors. The unsupervised method of MRF provides a way to integrate spatial information into the clustering process, reducing the overlapping of clusters and the effect of noise on the result [Tran 2005]. A mayor difficulty in MRF is the selection of the parameters that control the strength of spatial interactions, which can result in very soft segmentation and a loss of structural details. The supervised clustering method of ANN has the ability to model non-trivial distributions offering clear practical advantages [Vijaya 2007, Iftek 2009]. Implementing ANNs for brain tumor segmentation involve problems of complexity and it is a time consuming task.

Model-based techniques have been widely used for its sensitivity in searching the boundary of brain tumors. However, as in the case of region-based methods, these models are mainly used as refinement step in brain tumor segmentation [Khotan 2008]. Segmenting tumors by making use of geometric

Table 3.2: Summary Table of Segmentation Methods

Segmentation Method	**Advantages**	**Disadvantages**
	Threshold-based	
Global and Local Thresholding	Simple and computationally fast.	Limited applicability to enhancing tumor areas [Gibbs 1996].
	Region-based	
Region-growing	Simple and capable of correctly segmenting regions that have similar properties and generating connected region [Salman 2005].	Partial volume effect [Sato 2000, Lakare 2000]. Noise or variation of intensity may result in holes or over-segmentation.
Watershed	Segments multiple regions at the same time. It produces a complete contour of the images and avoids the need for any kind of contour joining [Dam 2004].	Over-segmentation [Gies 2004].
	Pixel-based	
Fuzzy C Means	Unsupervised. Always converge the boundaries of tumor.	Long computational time [Lazaro 2005, Yong 2004], sensitivity to noise [Kanan 2008].
Artificial Neural Netwoks	Ability to model non-trivial distributions and non-linear dependences [ScmiT 2005].	Gathering training samples is not straightforward and learning phase is slow [Iftek 2009].
Markov Random Fields	Are able to represent complex dependencies among data instances [Zhang 2004].	Difficulty when selecting the parameters that control the strength of spatial interactions. Usually require algorithms computationally intensive [Cappelle 2004].
	Model-based	
Parametric Deformable Models	Capable of accommodating to the variability of biological structures over time and across different individuals [McIner 2000].	The model may converge to wrong boundaries in case of inhomogeneities [Luo 2003].
Level Sets	Topological changes are naturally possible [Osher 1988].	Extremely computationally expensive [Cobzas 2007].

deformable models or level sets, permits the development of fully automatic and highly accurate segmentation approaches as in [Ho 2002]. Unfortunately, these methods are still extremely computationally expensive [Cobzas 2007].

Based on the existing literature, several general conclusions can be drawn with regard to elements of a system that can be used to improve performance in brain tumor segmentation. First of all, it is important to address the segmentation towards a fully automated method. This can be done incorporating within the algorithms human intelligence and prior knowledge about intensity and other tissue information, shape, size, symmetry, and normal anatomic variability to improve segmentation results. Furthermore, it would be desirable to have an unsupervised fully automatic segmentation method to avoid the use of patient-specific training. The use of some pre- or post-processing methods has demonstrated to provide more reasonable segmentation results, which reflect the layout of regions of interest, as is the case of intracranial segmentation commonly referred to as skull stripping.

3.7 Conclusions

Detecting the existence of brain tumors from MRI in a fast, accurate, and reproducible way is a challenging problem. Medical image processing is a very active and fast-growing field that has evolved into an established discipline. Brain tumor segmentation techniques have already shown great potential in detecting and analyzing tumors in clinical images and this trend will undoubtedly continue into the future.

Medical image analysis needs to address real-world issues that have been outside the realm of computer vision [Shen 2006]. These issues come largely from the fact that the end systems are mostly used by the physician. The human factor is essential, since any successful solution will have to be accepted by a physician and integrated into the medical procedural work flow. This put strong constraints on the type of applicable methods. Due to it, there has been a discrepancy between the advanced frameworks presented in computer vision and the low-level methods used by researchers working on real medical application solutions.

One major goal in tumor imaging research is to accurately locate the cancer. Segmentation techniques have been applied according to the characteristics that allow distinguish tumors from normal tissues. When tumors can be distinguished from normal tissues by their image intensity, threshold-based [Shanti

2007] or region growing [Dou 2007] techniques have been employed. Other tumors can be identified by their shapes so that a model-based technique [Chang 2008, Popuri 2009] was applied for the segmentation.

Although the reported accuracy on brain tumor segmentation of the proposed automated methods is quite promising, these approaches have not still gained wide acceptance among the pathologists for every day clinical practice. One of the principal reasons might be the lack of standardized procedures. Another two reasons could be the substantial differences with the traditional specialists' way of work, and the deficiency of the existing methods in assisting medical decision with a transparent and interpretable way. The latter two are very important for computer aided medical diagnosis where the demand for reasoning and explanation is of main priority.

Chapter 4

A New Fuzzy Approach for Automatic and Unsupervised Brain Tumor Segmentation

4.1 Introduction

Chapter 3 presented a variety of approaches proposed in the literature for automate brain tumor segmentation on magnetic resonance images. These techniques have already shown great potential in detecting and analyzing tumors. Based on the existing literature, several general conclusions were drawn with respect to elements of a segmentation system that can be used to improve performance:

- Some pre- or post-processing steps and methods can produce a more reasonable segmentation that reflects the layout of regions of interest.
- Intensity and other tissue information can be combined to improve discrimination between the classes.
- Information about shape, size, symmetry, and normal anatomic variability can improve segmentation results.

The existing work is a valuable source of insight in designing a new system to perform brain tumor segmentation, since there are a variety of different

properties of the problem that can be exploited. However, since the goal of this work is to automate a task performed by human experts, the methods used by human experts also provide insights into the problem. It is clear that human experts do not build an internal intensity-based pixel classifier, but are able to incorporate much more complex information. This includes knowledge of the expected appearance, location, and variability of normal anatomy, and also includes bilateral symmetry, and knowledge about the expected intensities of different tissues present within the image. Furthermore, humans are able to simultaneously consider and combine these properties, and can consider previous experience in related tasks.

It is obvious that in cases where the discrimination between normal and abnormal areas is not trivial, a variety of properties are used in making a decision. As outlined in Chapter 3 improved results could be achieved if a system could consider a variety of properties simultaneously in performing segmentation. Although the goal of the knowledge-based systems discussed in Chapter 3 was to find ways to meaningfully incorporate different sources of knowledge as rules, these systems do not meet this goal in ambiguous cases, because the patterns are complex and involve interactions between the sources. These complex interactions are difficult to represent with a set of "hard" manually determined rules.

As stated in the introduction of Chapter 1, a possible solution for designing complex systems in which it is required to incorporate the experience of an expert, or where the concepts appear vague or uncertain, is the use of fuzzy sets-based systems. Fuzzy systems permit the development of methods and algorithms that can perform tasks normally associated with intelligent human behavior.

This chapter presents the proposed fuzzy approach to brain tumor segmentation. Considering that the human factor is essential, the expert knowledge and the features derived from the MR images are coupled to define rules aimed to the design of the new fuzzy approach. Two main characteristics of the proposed approach are: 1. it is fully automatic and 2. it is unsupervised. To assess the unsupervised and fully automatic segmentation, intensity-based objective measures are defined, and a new method for obtaining membership functions to suit the MRI data is introduced. As a result, accurate brain tumor segmentation is achieved in a transparent manner, and the results are easily interpretable by specialists.

4.2 Outline of the Chapter

Next, the main aspects discussed in each Section of the chapter are summarized. In Section 4.3 intensity features for the definition of rules are extracted by means of histogram analysis. Section 4.4 presents the different elements of the fully automatic brain tumor segmentation framework. This Section also introduces a new skull stripping algorithm and the proposed membership function acquisition method. Finally in Section 4.4 the chapter conclusions are presented.

4.3 General Domain Information

Before beginning the design of the proposed approach, it was necessary to obtain domain information in the form of general principles of MR imaging, discussions with experts, anatomy of the brain, and knowledge useful for tumor segmentation from the intensity distributions of the different tissues.

The general principles of MR imaging, are contained in Appendix A, this appendix provides a broad description of the nuclear MR phenomena, and image formation. The brain tumor MRI materials used in this system are described in Section 4.3.1. Knowledge useful for tumor segmentation was extracted from the available MRI materials, discussions with experts, the intensity distributions of individual pixels, and the distributions of the different tissues in feature space. A training set was created to extract heuristic rules. The process of knowledge extraction was performed by means of intensity histogram analysis; it is described in Section 4.3.2. The extracted rules are presented in Section 4.3.3.

4.3.1 MR Image Materials

A "slice" is defined as a multispectral MR image recorded at the intersection of a subject brain, and a specific $2D$ plane created by an MR coil [Appendix A]. The slices considered here were taken from the transaxial plane, a plane roughly perpendicular to the long axis of the human body [Novell 1987].

Although most authors do not specify the number of slices used for feature extraction, in practice, these sets are usually composed of 15-25 slices [Chang 2008, Corso 2008, Bhatta 2008, Iftek 2009]. A set greater than 50 slices is considered to be large [SchmiT 2005] since each image has a large number of pixels and training times can grow large as feature sets and the number of training

pixels increases.

The set considered for feature extraction consisted of 20 T1-weighted contrast-enhanced slices (176 x 256 pixels each) presenting a glioblastoma multiforme (GBM, Chapter 2) brain tumor. It is important to emphasize that this training set is required to establish knowledge constrains, and does not generate labeled training data. Therefore in the case here presented, the concepts of patient-specific and inter-patient training (Chapter 3.4.2) do not concern. However in the GBM dataset, the algorithm was trained on a subset of the patient's data, and then tested on another (disjoint) subset. This is similar to the approach taken in many other studies of automatic brain tumor segmentation such as [Garcia 2004, Zang 2004].

The GBM tumor type was addressed because of its relative compactness and tendency to enhance well with paramagnetic substances, such as gadolinium. GBM are the most common primary tumors of the central nervous system [Smirnio 1999], and the median postoperative survival time is extremely short (eight months) with a five-year recurrence-free survival rate of nearly zero [Patel 2004].

In the case of glioblastoma multiforme brain tumor, the heterogeneous processes in study are the tumor comprising a necrotic (dead) part and an active part, and the brain tissue. Given a contrast enhanced T1-weighted MRI containing a GBM tumor, the primary tissue types that can be observed are:

- Cerebrospinal Fluid (CSF).
- Brain Parenchyma (white matter and gray matter).
- Necrotic part of tumor.
- Gadolinium-enhanced tumor (active part of tumor).
- Outside brain region: arachnoid / dura mater, air, bone, muscle, fat and connective tissue.

Figure 4.1-a shows a $2D$ transversal MRI sample slice in the T1-weighted channel presenting an enhancing GBM brain tumor. In 4.1-b, the outside brain region, the brain parenchyma, the CSF and the active and necrotic parts of the GBM tumor are emphasized.

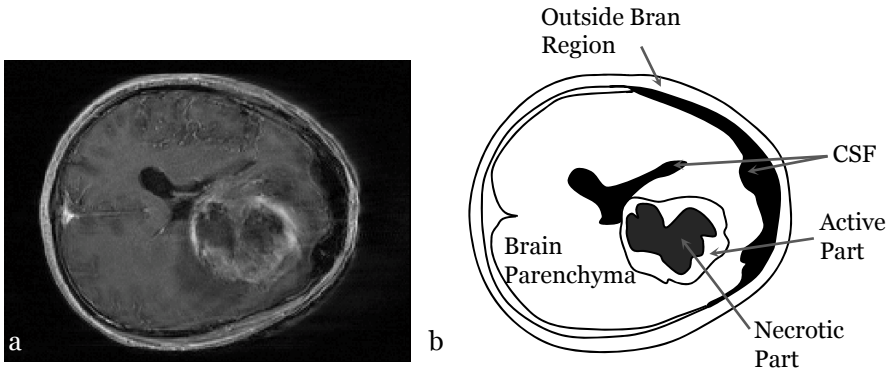

Figure 4.1: A sample slice of image materials. a) A transversal T1-weighted MRI presenting an enhancing GMB tumor. b) Scheme representing the outside brain region, the brain parenchyma, the cerebrospinal fluid, and the active and necrotic parts of GBM tumor in a).

The following section describes the process of knowledge extraction from the image material here presented.

4.3.2 Knowledge Extraction by Histogram Analysis

The system presented here is a knowledge-based system. "Knowledge is any heuristic or chunk of information that helps discriminate one class type from another" [Giarra 2004]. In the domain of MRI, the primary source of knowledge is pixel intensity in feature space based on tissue characteristics [Clark 1999].

Histogram analysis is a simple and practical approach for automatically extracting intensity information from an image. This information is explicit and can be used in subsequent decision making processes [Vernon 1991]. The gray-level histogram of an image often contains relevant information to allow analysis of the image content and, in particular, to discriminate between objects. It has the distinct advantage that it is not necessary to segment the image first and it is not dependent on the location of the object in the image. The analysis is based exclusively on the visual appearance of the scene or image as a whole.

In medical imaging, histogram analysis has been widely used to extract fea-

Table 4.1: T1 Signal intensity in different tissue types.

Effect (Signal Intensity)	**Tissues**
Short T1 relaxation (bright)	Fat, bone, Lipid-Containing Molecules, Proteinaceous Fluid, Paramagnetic Substances (Gadolinium)
Long T1 relaxation (dark)	Neoplasms, Edema, CSF, Pure Fluid, Inflammation

tures of the anatomical structures and tissues. Early approaches of MRI brain segmentation were achieved using histogram analysis for gray-level thresholding, providing a first estimation of the brain volume [Allain 1992]. Recently the use of histogram analysis is the basis of a variety of applications, accomplishing very promising results. The analysis is not only focused on gray level but has been extended to texture features and diverse measures like mean diffusivity and fractional anisotropy among others [Filippi 2005, Kato 2007, Valsasina 2005].

In this work, the histogram analysis is achieved by extracting intensity features which are descriptive of the shape of the histogram. The aim of this analysis is to define the gray-level characteristics of tissues found in MRI materials, in order to extract knowledge that can be implemented as heuristics/rules.

The first step in the histogram analysis is to know which part of the histogram corresponds to each tissue in the image. Given the T1-weighted MRI data set, the signal intensity of different tissues can be represented in Table 4.1. For example, Table 4.1 indicates that paramagnetic substances (used to enhance brain pathology) will have a short/bright T1-weighted signal, while CSF will have a relatively long/dark T1-weighted signal.

Based on the fact that pixels belonging to the same tissue type will exhibit similar relaxation behaviors, they will then also have approximately the same location in feature space (the intensity histogram) [Clark 1999]. The intensity distributions of brain tissues has been investigated by a number of researchers [Corso 2008, Gering 2002, Mayer 2009, Shanthy 2007], and forms an important foundation in the knowledge obtained for this system.

One of the most important pieces of knowledge for detecting enhancing-

pathology is the blood-brain barrier (BBB, Chapter 2). In a normal brain, the BBB acts as an extremely selective filtering device, allowing only a limited number of naturally occurring substances, such as oxygen and glucose, to migrate from the blood supply into the brain itself and excludes many other compounds, including paramagnetic substances like gadolinium. The presence of tumors and other brain pathologies, however, damage brain tissues and alter the BBB. This "breakdown" of the BBB allows paramagnetic substances to enter the tumor and enhance it in MR images [Ott 1988, Vander 1990]. The heuristics obtained later in this section, rely heavily on this fact.

Next section describes the analysis of the intensity distributions in the image histograms, and presents the heuristics obtained from this analysis.

Histogram Analysis

For extracting the features, on each training image, a subset of pixels from four different tissue types, namely populations CSF (Cerebrospinal Fluid), BP (Brain Parenchyma), TUM (Gadolinium-enhanced tumor), and OBR (outside brain region), was manually selected, and its correspondent intensity histogram was obtained.

A typical slice with enhancing pathology is shown in Figure 4.2. The histogram distributions of the tumor TUM, and the other tissue populations CSF, BP, and OBR, were manually overlaid on the histograms of the training images (excluding the background). Specific dimensions are not given in Figure 4.2, since they will change from slice to slice and the primary concern is the relative location of enhancing pathology within the histogram. By observing the distributions of populations, TUM is among the populations BP and OBR. Moreover, it can be observed that the majority of enhancing tumor is found to the right of the signal intensity bin having the greatest number of pixels, the histogram "highest peak", P_{HIGH} in Figure 4.2.

An analysis of the intensity distributions of these populations was conducted in order to obtain intensity information. The values of the lowest (GL_{min}) and highest (GL_{max}) gray levels, as well as the mean gray level (GL_{mean}) for each population were obtained. For each sample image, the relevant peaks of the gray-level histogram were acquired. This was achieved using the peak-finding algorithm proposed by Cheng and Ying [Cheng 2000]. This algorithm finds the relevant peaks of the histogram, and determines if a peak is relevant considering its size, the proximity with other peaks and the depth of its valley. The first peak and valley found, were designated as the background peak P_{BACK},

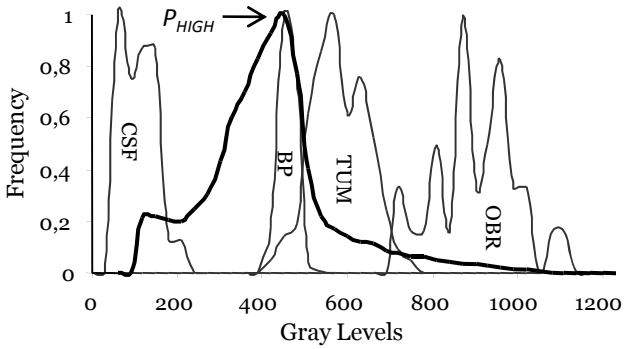

Figure 4.2: Gray-level histograms of CSF, BP, TUM, and OBR populations, and general image histogram (darker line). The relative location of enhancing tumor is found among the populations BP and OBR, and to the right of the signal intensity bin having the greatest number of pixels, the histogram "highest peak", P_{HIGH}.

and the background valley V_{BACK}. P_{BACK} and V_{BACK} were discarded taking into consideration only the relevant peaks of the higher levels. After the background peak was discarded, a new highest peak and its corresponding valley were found in the gray-level histogram namely the highest peak and valley, P_{HIGH} and V_{HIGH}.

A summary of the gray-level information obtained for populations CSF, BP, TUM, and OBR is given in Table 4.2. The columns refer the image slice number. From first to twelfth row, the values of GL_{min}, GL_{mean}, and GL_{max} for each population are given. Rows 13 and 14 are the values of P_{BACK} and V_{BACK}, respectively. In rows 15 and 16, the values of highest peak P_{HIGH}, and its corresponding valley V_{HIGH} are presented.

Since the target population in the problem of segmenting tumors is the tumor itself, a simple set of additional features to use are the intensities of neighboring populations. As other authors [Dickson 1997, Clark 1999, Garcia 2004], the endeavor is to specify the gray-level relations between TUM population and its neighboring populations. The distributions of populations CSF, BP, TUM, and OBR were examined and interviews were conducted with experts concerning the general makeup of tumorous tissue, and the behavior of gadolinium enhancement in the T1 channel. From these sources, a set of heuristics were extracted:

Table 4.2: An extract of the gray-level histogram information extracted from training images

	Slice Number						
	35	45	55	65	75	85	Row
$CSFGL_{min}$	36	34	38	65	69	49	1
$CSFGL_{mean}$	119	157	129	153	121	112	2
$CSFGL_{max}$	301	259	215	271	198	209	3
$BPGL_{min}$	439	436	480	378	409	410	4
$BPGL_{mean}$	524	521	537	466	462	461	5
$BPGL_{max}$	602	624	601	539	611	540	6
$TUMGL_{min}$	612	556	512	576	563	496	7
$TUMGL_{mean}$	701	653	632	761	648	576	8
$TUMGL_{max}$	76	769	775	842	752	737	9
$OBRGL_{min}$	663	701	724	721	691	875	10
$OBRGL_{mean}$	977	948	898	892	861	902	11
$OBRGL_{max}$	1335	1260	1045	1035	955	940	12
P_{BACK}	79	24	23	25	24	23	13
V_{BACK}	197	218	140	168	157	124	14
P_{HIGH}	468	446	439	420	400	452	15
V_{HIGH}	598	583	579	574	571	541	16

Figure 4.3: T1 signal intensity of CSF, BP, TUM, and OBR populations.

H1 The background pixels occupy the lower part of the histogram. The values of PBACK are lower than those of the gray-level mean GL_{mean} of populations CSF, BP, TUM, and OBR.

H2 If the populations are sorted by their gray levels, the order is always as follows: CSF, BP, TUM, and OBR.

H3 The CSF gray levels (rows 1 to 3 of Table 4.2) occupy the lower part of the histogram after excluding the background.

H4 The CSF gray levels are always lower than the BP gray levels (compare rows 3 and 4).

H5 The BP gray levels fall within the range of the gray levels of V_{BACK} and V_{HIGH}. Moreover, the values of the highest peak after excluding the background, P_{HIGH} (row 15) are close to the lowest gray levels GL_{min} of BP population.

H6 The TUM gray levels (rows 7 to 9 of Table 4.2) are higher than those of the BP (rows 4 to 6), and they are lower than the OBR gray levels (rows 10 to 12).

H7 The mean values of TUM gray levels are always higher than the next valley situated after the highest peak V_{HIGH}. In all cases the values of GL_{mean} of tumor population (row 8), are higher than V_{HIGH} (row 16).

H8 The OBR gray levels are always higher than the next valley situated after the highest peak V_{HIGH}. In all cases the lowest gray-level values of OBR, GL_{min} (row 10), are higher than V_{HIGH} (row 16).

H9 The OBR gray levels are higher than the tumor gray levels (rows 10 to 12 of Table 4.2).

H10 The highest gray levels (rows 10 to 12) are those of the outside brain region.

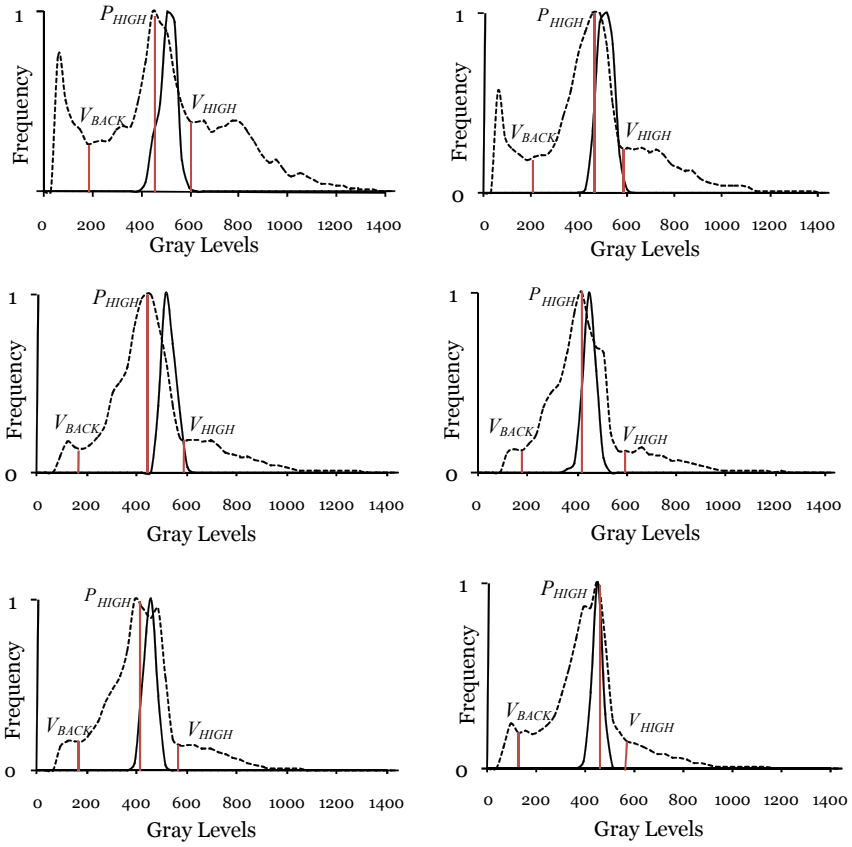

Figure 4.4: Diverse training images showing the relation of BP population histogram (dark line) with the gray-level values of the highest peak P_{HIGH} and valley V_{HIGH}, and the background valley V_{BACK} of the image histogram (dotted line).

After obtaining these heuristics, the aim was to analyze them in order to define effective rules for gross separation of tumor from non-tumor pixels that work across slices, even those with varying degrees of gadolinium enhancement.

4.3.3 Definition of Rules

A rule based system consists of three fundamental elements: a working memory of facts from which inferences are derived, a knowledge base of rules to guide the inferences, and the inference engine to draw conclusions and fire rules [Giarra 2004]. Rules resemble IF-THEN statements and have the basic form:

$$\langle ANTECEDENT \rangle \Longrightarrow \langle CONSEQUENT(S) \rangle$$

The left hand side of the rule,$\langle ANTECEDENT \rangle$, contains the set of conditions required for the rule to fire, while the right hand side, $\langle CONSEQUENT(S) \rangle$, is a set of one or more resultant actions. When all of the left hand conditions of a rule are satisfied by the facts in working memory, the rule is fired by the inference engine and all of its right hand actions are executed, which may modify the working memory.

When domain specific knowledge is available, an "expert system" is one of the most common implementations of rule based systems. Domain knowledge is explicitly integrated into the rule based system (stored as rules) through a process called "knowledge engineering" [Luger 2008].

Knowledge discussed as heuristics in previous section are examples that were manually extracted and integrated into the system in the form of rules, and these are described below.

As stated in the heuristic $H1$, the background pixels occupy the lower part of the histogram. When the relevant peaks of the gray-level histogram were acquired using the peak-finding algorithm of Cheng and Ying [Cheng 2000], the first peak and valley found were designated as the background peak P_{BACK}, and the background valley V_{BACK}. The V_{BACK} value was found to be effective threshold for background pixels working across slices. Therefore, Rule 1 can be expressed as:

Rule 1 *By applying the peak-finding algorithm, all pixels whose gray level is lower than the first valley found, are considered background.*

When applying *Rule 1*, inside the intracranial region there will not be pixels with gray levels darker than V_{BACK}. Figure 4.5 shows two training images before and after applying *Rule 1*. In (b) and in (d), all pixels considered background were discarded. It can be observed that in addition to the background pixels, some of the CSF pixels were also discarded.

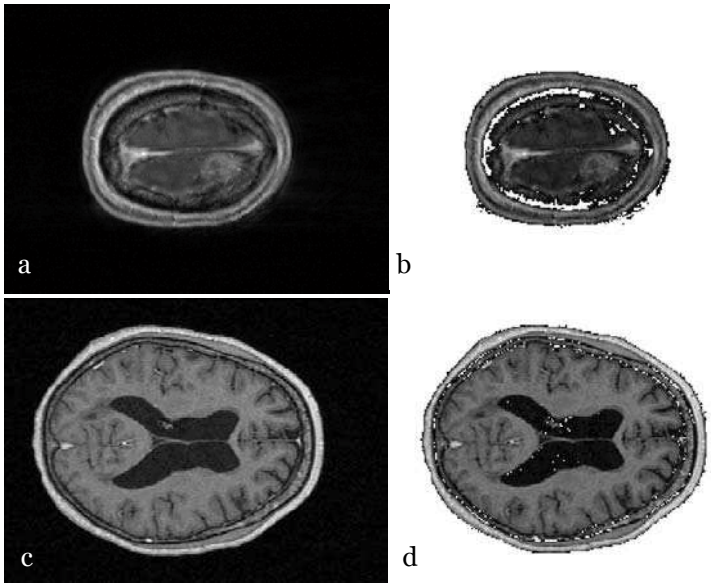

Figure 4.5: Training images before (a,c) and after (b,d) applying *Rule 1.* In (b) and in (d), it can be observed that in addition to the background pixels, some of the CSF pixels were also discarded.

Considering heuristics $H2$,$H3$, and $H4$, which state that the CSF gray levels are in the lower part of the histogram after excluding the background, and they are lower than the BP gray levels, in the future, the CSF population will not be considered for the segmentation process.

Making reference to heuristic $H5$, the brain parenchyma gray levels fall within the range of V_{BACK} and V_{HIGH}. Based on this correspondence, the brain parenchyma population can be defined in the image histogram with V_{BACK} as the lowest gray level, and V_{HIGH} the highest. Accordingly, *Rule 2* expresses the range of intensities in which a BP pixel can be found.

Rule 2 *A brain parenchyma pixel can be found between the first valley and the valley located right after the highest peak.*

Now, since the TUM gray levels are always higher than those of the BP (heuristic $H6$), and that in all cases the values of GL_{mean} of tumor population are higher than V_{HIGH} (heuristic $H7$), V_{HIGH} can be used as the lowest gray-level of tumor population. This way, *Rule 3* is defined as:

Rule 3 *The valley located right after the highest peak, indicates the lowest gray level in which a Gadolinium-enhanced tumor pixel can be found.*

Heuristic $H10$ states that the highest gray levels are those of the outside brain region; this means that the boundary of the outside brain region gray levels on the right side of histogram is already known. However, it is still necessary to identify a boundary on the left side. Taking into account that, in all cases the lowest gray-level values of OBR are higher than V_{HIGH} (heuristic $H8$), this boundary must be higher than V_{HIGH}. The immediately neighboring population to the left side is the tumor population, since the OBR gray levels are higher than the tumor gray levels (heuristic $H9$); the OBR boundary to the left indicates the end of TUM population.

Rule 4 *The highest gray level, in which a Gadolinium-enhanced tumor pixel can be found, is the lowest gray level of the outside brain region.*

Because there is no peak or valley automatically obtained which can outline the OBR boundary to the left, it is necessary to firstly define the outside brain region, and then find the lowest gray level of this region. For defining the OBR, anatomical knowledge must be included. The skull-stripping algorithm presented in Section 4.4.1 shows the steps necessary to define this region.

The following section presents the different elements of the fully automatic brain tumor segmentation framework. Section 4, also introduces a new skull stripping algorithm and the proposed membership function acquisition method.

4.4 A Fuzzy Approach to Brain Tumor Segmentation

The proposed fuzzy approach to brain tumor segmentation consists on the registration of contrast enhanced T1-weighted magnetic resonance images, an automatic fuzzy approach is defined which takes these images and produces a final segmentation without any human interaction. This excludes operations such as manual seed selection, manual contour initialization, manual prototype selection, manual contrast adjustment, manual cluster selection, or other forms of manual input or adjustment (Chapter 3). The output will be a binary segmentation of the images, where each pixel in the input image is labeled as either non-tumor or tumor. The goal of the desired output will not be defined as the determination of the absolute location of the tumor, but to perform the

segmentation as a human expert would.

According to the descriptions of radiology experts, in order to detect/segment a tumor, the most important properties to consider can be summarized as follows:

- Location (evaluation of the appearance of regions).
- Expected appearance of the tumor (expected intensity).
- Variability of normal anatomy (intensity variability in different tissues).
- Analysis of bilateral symmetry of the brain to detect abnormalities.

As the main objective of this work is to automate a task performed by human experts, two key elements in the definition of the proposed approach are the expert knowledge combined with the information derived from the images. To meet this objective, each of the previous properties (summarizing the experts knowledge) is considered to be an element in the segmentation process.

The segmentation framework is depicted in Figure 4.6 and shows the primary steps in extracting tumors from raw MR data. Firstly, when the MRI is introduced (a), a pre-processing operation is applied to extract the intracranial region from the rest of the MR image (b). The background and skull are discarded by means of a new skull stripping algorithm (Section 4.4.1). This algorithm creates an image mask of the brain that limits processing to only those pixels contained by the mask. Secondly, for defining the non-tumor and tumor populations, intensity knowledge is integrated into the system in the form of rules (Section 4.4.2). As the output of the proposed approach is a binary segmentation, the non-tumor population is comprised of the non-tumorous populations and they are directly defined by means of these rules (c). For defining the tumor population (d) it is necessary to carry out a symmetry analysis (Section 4.4.3). Subsequently, for each population its corresponding membership function is defined (e) making use of the proposed method for acquiring membership functions (Section 4.4.4), (f) finally the fuzzy classification is performed (Section 4.4.5), and the fuzzy-segmented image is obtained (g).

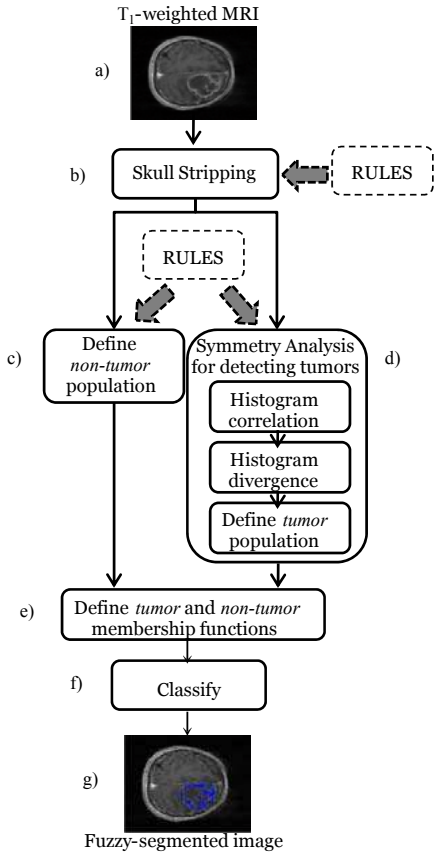

Figure 4.6: Proposed brain tumor segmentation framework. a) An MRI is introduced, b) the background and skull are discarded by means of a new skull stripping algorithm, c) the non-tumor population is directly defined by means of knowledge integrated into the system in the form of rules, d) a symmetry analysis is carried out for defining the tumor population, e) for each population its corresponding membership function is defined making use of the proposed method for acquiring membership functions, f) the fuzzy classification is performed, and the fuzzy-segmented image is obtained (g).

4.4.1 Skull Stripping Algorithm

Intracranial segmentation commonly referred to as skull stripping, aims to segment the brain tissue from the skull and non-brain intracranial tissues in

magnetic resonance images of the brain. Skull stripping is an important pre-processing step in neuroimaging analysis, because brain images must typically be skull stripped before other processing algorithms can be applied.

Numerous automated skull-stripping methods have been proposed and are widely used [Dale 1999; Hahn 2000; Sandor 1997; Segonne 2004; Smith 2002; Zhuang 2006]. Despite the clear definition of the skull stripping problem, no standardized solution has been published yet. In [Atkins 1998] is given a good survey of the work, showing strengths and weaknesses of diverse approaches, and in [Fennema 2006] it is presented a recent study where the most commonly used skull stripping algorithms are compared.

Skull stripping methods can generally be categorized into three types: intensity based, morphology based, and deformable model based. Intensity-based methods rely upon modeling the intensity distribution used for threshold classification as in [Shanthy 2007]. One limitation of intensity-based methods is that they are frequently sensitive to intensity bias caused by magnetic field inhomogeneities, sequence variations, scanner drift, or random noise.

Morphology-based methods frequently combine connectivity-based morphological operations and thresholding or edge detection to extract image features and identify brain surfaces as in [Hahn 2000, Geun 2009]. A potential disadvantage of these methods is that they are often dependent upon many parameters, and the parameters are often empirically generated and sensitive to small changes in the data.

Skull-stripping methods based upon deformable models typically evolve and deform an active contour to fit the brain surface, which is identified using selected image characteristics as in [Zhuang 2006]. In general, deformable models have the potential to produce more robust and accurate skull-stripping results than methods using edge detection and threshold classification, but they also require algorithms computationally intensive [Duncan 2000].

The main features of the skull stripping algorithm here presented are the simplicity and robustness. It is simple since neither pre-processing of the MRI data nor contour refinement is required. Furthermore, the skull stripping solely relies on one basic anatomical fact, the T1 weighted images show a distinct region of separation between the surrounding tissues and the brain tissues. This makes simple to look for this change in the intensity level and strip off this part. As long as this feature is observed in the image data, a robust segmentation can be guaranteed even in presence of severe intensity non-uniformity and

noise. The algorithm becomes totally automatic as all the intensity values are automatically determined from the histogram.

Figure 4.7 shows three T1-weighted MR images before and after the skull stripping algorithm was applied. Figure 4.7-a, presents a sample MR image with a normal brain, 4.7-c and d, present two slices of brain MRI containing a GBM tumor. The resulting images after applying the skull-stripping algorithm are shown in Figure 4.7-b, d, and f. It is observed that even in presence of severe intensity non-uniformity and noise (see background on Figure 4.7-c, and 4.7-e), a robust stripping is obtained.

To achieve the skull stripping, three steps are defined: in Step 1, the background pixels are removed, then in Step 2, the outside brain region is defined, and finally in Step 3, two morphological operations are applied to fill the gaps along the outside brain region, and to remove meningeal regions.

Figure 4.8 shows a sample slice in the T1-channel, presenting a gadolinium-enhanced GBM tumor. This slice will be used in order to show the changes that occur when implementing each of the three steps of the proposed skull-stripping algorithm. Henceforth, this slice will be referred as demonstration slice or "DSlice". The three steps are described below.

Step 1 Removing background pixels

In brain MR images there are two primary classes of pixels: "foreground" pixels are pixels of interest, while "background" pixels are not. The first step towards the skull stripping is to remove the background pixels, it is necessary to discard them, to limit processing to head pixels.

Let X be an image (slice). Making use of *Rule 1: By applying the peak-finding algorithm, all pixels whose gray level is lower than the first valley found, are considered background*, the condition in Equation (4.1) is satisfied. The valley was obtained using the peak-finding algorithm proposed by Cheng and Ying [Cheng 2000]. This way, the background pixels are defined by:

Definition 1 : *All pixels p_{ij} in image X satisfying Rule 1, are considered background pixels and thus removed.*

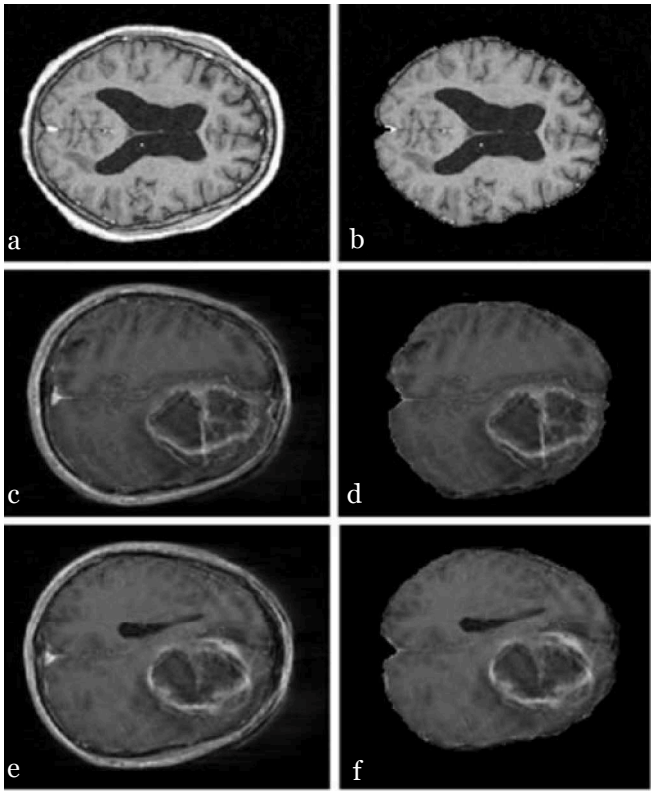

Figure 4.7: T1-weighted MR images before and after the skull stripping algorithm was applied. a)Sample MR image with a normal brain, c and d) two slices of brain MRI containing a GBM tumor. The resulting images after applying the skull-stripping algorithm are shown in b, d, and f. It can be observed that even in presence of severe intensity non-uniformity and noise in c and e, a robust stripping is obtained.

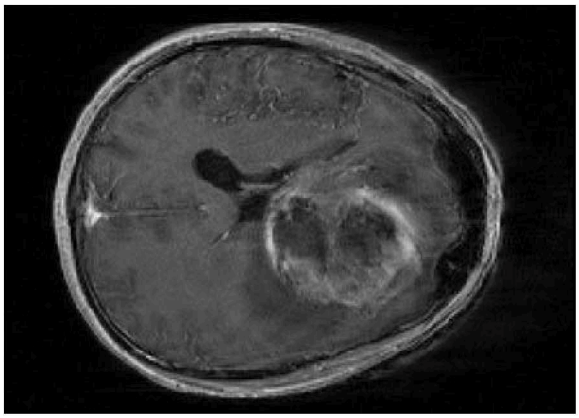

Figure 4.8: Demonstration slice *DSlice* that will be used to show the changes that occur when implementing each of the three steps of the proposed skull-stripping algorithm. A transversal T1-weighted MRI presenting an enhancing GMB tumor.

$$F(p_{ij}) = \begin{Bmatrix} X(p_{ij}) & \text{if } F(p_{ij}) \text{ satisfies } \textit{Rule 1} \\ 0 & \text{otherwise} \end{Bmatrix} \tag{4.1}$$

in which F is the "foreground" version of X, and pixels with value 0 correspond to the background. Figure 4.9 shows the demonstration slice after removing the background pixels. It can be observed that in addition to the background pixels, some of the CSF pixels were also discarded.

Step 2 Defining the outside brain region

In order to accurately detect abnormalities within the brain, analysis must be limited to pixels that correspond to the intra-cranial region, which contain the brain's soft tissues. Pixels belonging to extra-cranial tissues, such as air, skin, and fat are not of interest.

The outside brain region is a well defined and recognizable anatomical structure. The tissues surround the brain and are not found within the

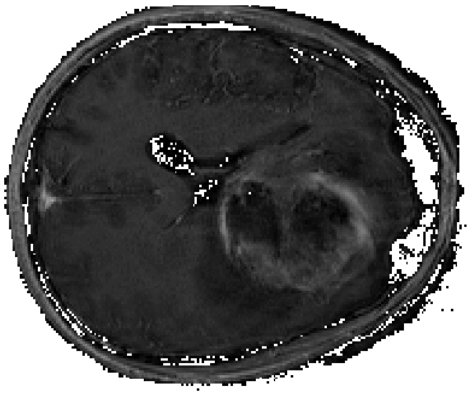

Figure 4.9: Demonstration slice *DSlice* after removing the background pixels. In addition to the background pixels, some of the CSF pixels were also discarded.

brain itself [Li 1993]; therefore, if a gross estimate of the outside brain region is created, this region can be removed.

The purpose of this step is the gross definition of the outside brain region. To achieve its definition, this step is divided into three phases. First, the head contour is localized. Then, all pixels with OBR intensity are marked. Finally, a fusion of the head contour and the OBR pixels is carried out to discard all pixels non pertaining to the outside brain region.

a Locating head contour

The first phase towards the definition of the outside brain region is to locate the head contour.

Definition 2 : *Given a foreground image F, the image is scanned from the exterior towards the interior, and the first non-zero pixel found is considered a contour pixel.*

Only the first pixel that meets the condition given in Equation (4.2) is considered a contour pixel for each row or column, and is saved in a matrix, the contour matrix C. Figure 4.10 shows the contour

matrix C for the *DSlice*. Note that in the demonstration slice, there are inhomogeneities in the background (Figure 4.8). Because of this, some false positives (pixels which are not head contour) were marked. This problem is solved in the last phase, where the fusion of the head contour and the OBR pixels is performed.

$$C(p_{ij}) = \begin{Bmatrix} 1 & \text{if} F(p_{ij})\ 0 \\ 0 & \text{otherwise} \end{Bmatrix} \tag{4.2}$$

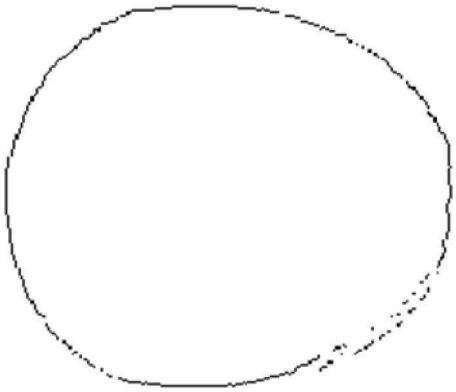

Figure 4.10: Head contour pixels for the demonstration slice. Some in homogeneities in *DSlice* were marked as contour.

b Marking outside brain region pixels

In section 4.3.2 a set of heuristics were extracted based on intensity knowledge. After analyzing these heuristics, in section 4.3.3 *Rule 3* was defined as: *The valley located right after the highest peak, indicates the lowest gray level in which a Gadolinium-enhanced tumor pixel can be found.*

Heuristics $H8$, $H9$, and $H10$, state that the OBR gray levels are higher than the tumor gray levels, and that the OBR gray levels are always higher than the lowest gray level of tumor population,

considering these heuristics, if all pixels whose gray level is higher than the indicated in *Rule 3* are saved in a matrix, this matrix will contain both: Gadolinium-enhanced pixels and outside brain region pixels.

Definition 3 : *The outside brain region matrix O is composed of all pixels p_{ij} in foreground image F, whose gray level is higher than the indicated in Rule*3*.*

The outside brain region matrix O satisfies the condition given in Equation (4.3). Figure 4.11 shows the O matrix for the demonstration slice *DSlice*. It can be observed that, as afore mentioned, the O matrix contains both, Gadolinium-enhanced pixels and OBR pixels.

$$O(p_{ij}) = \begin{Bmatrix} 1 & \text{if } F(p_{ij}) \text{ than the indicated in } Rule3 \\ 0 & \text{otherwise} \end{Bmatrix} \tag{4.3}$$

Figure 4.11: Outside brain region matrix O for the demonstration slice. The matrix contains Gadolinium-enhanced and OBR pixels.

c Fusion of contour and outside brain region pixels

The last step for the definition of the outside brain region consists on merging the contour and the outside brain region matrices obtained at the previous steps. The purpose is to exclude the OBR pixels that are within the brain parenchyma. The data obtained from this fusion, is saved in a new matrix, the merger matrix M.

Definition 4 : *The merger matrix M is composed of all pixels in contour matrix C, plus those of the outside brain matrix O, excluding the pixels that are located within the brain parenchyma.*

The merging is carried out as follows: First, all the contour pixels are added to matrix M. For each contour pixel such that $C(p_{ij}) = 1$, its eight-connected neighbor pixels are verified over O matrix. If any of its neighbors is equal to one, that pixel is added to merge matrix M, and the procedure is repeated until all possible pixels have been added. Figure 4.12 shows the M matrix for the demonstration slice *DSlice*. The Gadolinium-enhanced pixels first marked in O matrix were lost with the fusion, as well as the inhomogeneities marked as head contour in C matrix.

Figure 4.12: Merger matrix for the demonstration slice. All the Gadolinium-enhanced pixels first marked in the outside brain region matrix were lost with the fusion, as well as the inhomogeneities marked as head contour in contour matrix.

Step 3 Performing morphological operations

Morphological processing refers to operations where an input object (usually binary) is modified by another object called a structuring element to reveal a more useful or interesting shape [Jain 1995]. The two fundamental operations are erosion ($\ominus$) and dilation ($\oplus$). Let B_x denote that the structuring element is translated to point x. The erosion operator of object X by structuring element B_x is defined as the set of all points x such that B_x is included in X.

$$X \ominus B = \{x : B_x \in X\} \tag{4.4}$$

Similarly, the dilation operator of X by B_x is defined as the set of all points x such that B_x hits X (having a non-empty intersection).

$$X \oplus B = \left\{x : B_x \bigcap X \neq 0\right\} \tag{4.5}$$

By combining erosion and dilation operations, two new operators, opening and closing, can be created. The opening operator removes isolated objects and breaks weak connections in components. It is an erosion operation followed by dilation, using the same structuring element: $(X \ominus B) \oplus B$. The closing operator, a dilation followed by erosion using the same structuring element, $(X \oplus B) \ominus B$, connects small gaps in components.

The use of morphologic operations has been the basis of diverse skull-stripping approaches. In this work, the final step to achieve the skull-stripping is carried out by means of two morphological operations. First a closing is performed to fill the gaps along the outside brain region. Then, as the meningeal regions lie along the periphery of the brain in a relatively narrow margin, the periphery is created by applying an erosion operation to the outside brain region as in [Clark 1999].

a Closing to the outside brain region

In order to fill the gaps along the outside brain region, a morphological closing is performed using a disk-shaped structuring element to preserve the circular nature of the head contour, whose radius is 5 pixels. This way all pixels inside the circle are considered the first estimation of the brain mask. Figure 4.13 shows the closed outside brain region.

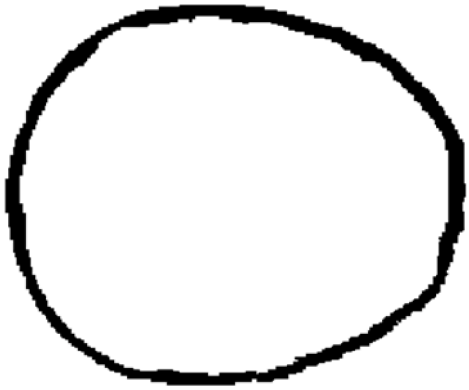

Figure 4.13: Outside brain region after applying a morphological closing.

b Erosion for removing meningeal regions

In addition to tumor, meningeal tissues immediately surrounding the brain, such as the dura or pia mater, receive gadolinium infused blood. As a result they can have a high T1 signal intensity. These tissues can be identified and removed via anatomical knowledge by noting that since they are thin membranes, meningeal regions should lie along the periphery of the brain in a relatively narrow margin [Clark 1999]. The periphery is created by applying a 7 x 7 erosion operation to the outside brain region. Figure 4.14 illustrates this erosion operation. The final definition of the brain mask is the encircled area after applying the morphological operations (Figure 4.15).

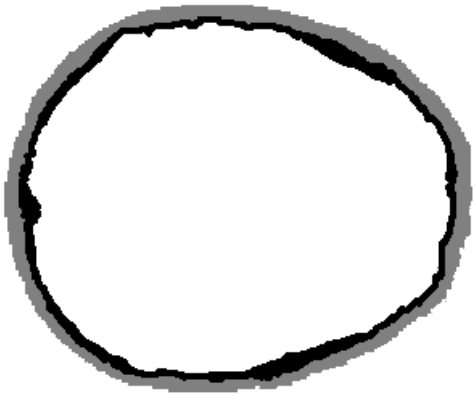

Figure 4.14: Erosion operation to the outside brain region (gray ring) for removing meningeal regions (black ring).

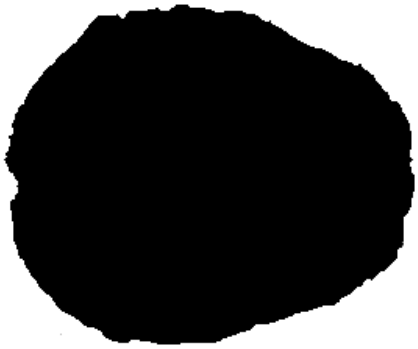

Figure 4.15: Final definition of the brain mask.

4.4.2 Defining Non-Tumor Population

The principal objective in this stage is to separate as many pixels belonging to normal tissues as possible from those belonging to tumor. In Section 4.3.3, knowledge discussed as heuristics was manually extracted and integrated into the system in the form of rules. These rules could provide a simple effective mechanism for gross separation of tumor from non-tumor pixels, which works across slices.

Since the pixels of the OBR population were removed by the skull-stripping algorithm, the non-tumor population is comprised of all the non-tumorous pixels, included in the brain parenchyma BP population. Because the tumor population is contiguous with the BP population to the left, and the OBR to the right, it is necessary to apply rules that can define the intensity ranges in which these populations fall within. Making reference to Section 4.3.3, these three populations can be defined by means of these three rules:

Rule 2 *A brain parenchyma pixel can be found between the first valley and the valley located right after the highest peak.*

Rule 3 *The valley located right after the highest peak, indicates the lowest gray level in which a Gadolinium-enhanced tumor pixel can be found.*

Rule 4 *The highest gray level, in which a Gadolinium-enhanced tumor pixel can be found, is the lowest gray level of the outside brain region.*

At this point it can be said that each population (BP, TUM, and OBR) falls within a range of gray levels. It is important to note that even though the tumor population is identified in the intensity histogram, its intensity range is not strict, since it does not guarantee that every pixel which falls within this range, is a tumor pixel. To avoid making this assumption, next section presents a symmetry analysis for determining whether the image contains a brain tumor or not.

4.4.3 Tumor Detection

As afore mentioned, the tumor population is bounded in the intensity histogram by two populations: the brain parenchyma to the left, and the outside brain region to the right. For not assuming that every pixel that falls within its range of intensity values is a tumor pixel, a symmetry analysis is performed. The tumor population will consist of all those pixels that fall within the limits of BP and OBR populations, and additionally it is found that there is an abnormality by a measure of divergence.

Using symmetry analysis of the brain to detect abnormalities in magnetic resonance images has been the basis of diverse works in the literature. Symmetry analysis is alternately referred to as left to right symmetry [Ray 2008, Cobzas 2007], symmetric bilateral [Mahajan 2008], symmetry plane [Khotan 2008], difference method [Hiong 1993], and tensor-based morphometry [Chiang 2007] among others. Symmetry analysis is a fast method for locating a region

of abnormality in the brain. The method exploits the fact that a normal brain structure is symmetric, the left part and the right part can be divided by an axis of symmetry, and abnormalities (tumors) typically disturb this symmetry.

In this work, in addition to the analysis of the left and right parts of the brain, the symmetry analysis is made dividing the brain into four parts or quadrants namely Q_1, Q_2, Q_3, and Q_4 (Figure 4.16). It would be easier to identify which part of the brain contains a larger number of tumor pixels.

Definition 5 :*In general there will be enough symmetry between the histograms of quadrants Q_1 and Q_3, and between the histograms of quadrants Q_2 and Q_4.*

Figure 4.17 shows the resulting histograms of the four quadrants of a sample image. By visual inspection of the histograms in Figure 4.17, it is clearly observed the similarity between the histograms of quadrants Q_1 and Q_3. On the contrary, histograms of quadrants Q_2 and Q_4 show a remarkable difference in the higher gray levels. This is due to the GBM tumor that this sample slice contains.

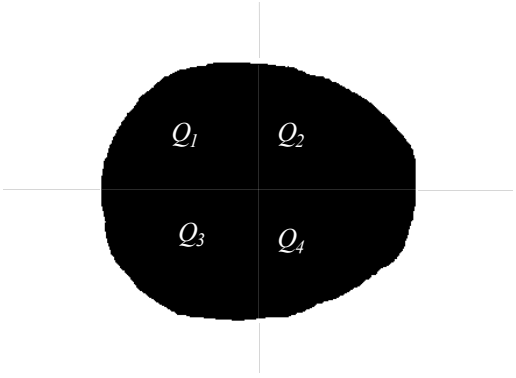

Figure 4.16: Brain mask divided into four quadrants.

The purpose of in symmetry analysis is the comparison of the histograms of symmetrical quadrants in order to identify abnormalities.

Definition 6 :*A pixel p_{ij} is tumor if it falls within the tumor intensity range, and the histograms of quadrants within that range, present a high degree*

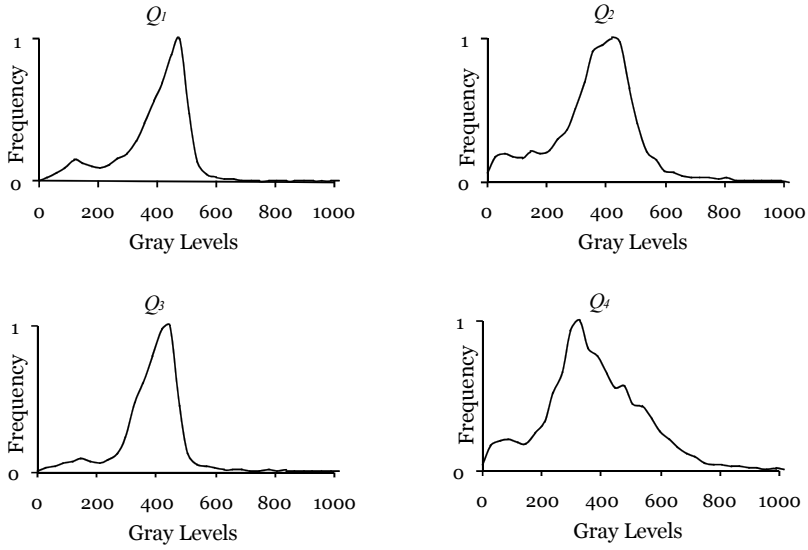

Figure 4.17: Resulting histograms of the four quadrants of a sample image.

of divergence.

In order to determine that there exists a tumor in the image based on Definition 6, the following sections show how the symmetry analysis is carried out. Before the comparison for detecting abnormalities, the histograms signatures of symmetrical quadrants are first correlated using similarity measures (Histogram Correlation). After that in "Histogram Divergence", a similarity/dissimilarity metric is presented to identify how much these histograms diverge in the tumor gray levels.

Histogram Correlation

Normal human brains possess a high degree of bilateral symmetry although they are not perfectly symmetrical. Before comparing the histograms of symmetrical quadrants for identifying tumors, it is required to assume that quadrants Q_1 and Q_3, and quadrants Q_2 and Q_4 are not perfectly symmetrical because of the morphologic nature of the brain and cranium, movements or wrong placement of the patient.

Figure 4.18 shows the histograms of the symmetrical quadrants Q_1 and Q_3 of two normal brain sample images. Note that although the histograms of symmetrical quadrants are very similar, there is some displacement between them. Considering this condition, before the comparison for detecting abnormalities, the histograms signatures of symmetrical quadrants are first correlated using similarity measures.

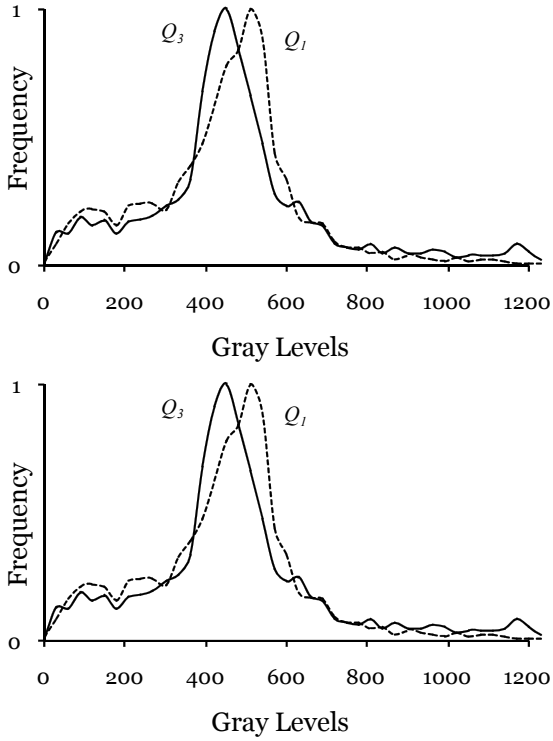

Figure 4.18: Histograms of symmetrical quadrants of two normal brain sample images. Although the histograms of symmetrical quadrants are very similar, exist some displacement between them.

The symmetrical histograms signatures' matching is achieved using the correlation coefficient. This coefficient indicates the strength and direction of a linear relationship between two random variables (in this case two histograms H and K) and is defined as:

$$\rho_{H,K} = \frac{\sigma_{HK}}{\sigma_H \cdot \sigma_K} = \frac{\frac{1}{n}\sum_{1}^{i}\left(h_i - \overline{h}\right)\left(k_i - \overline{k}\right)}{\sqrt{\frac{\sum_{1}^{i}\left(h_i - \overline{h}\right)^2}{(n-1)}}\sqrt{\frac{\sum_{1}^{i}\left(k_i - \overline{k}\right)^2}{(n-1)}}} \tag{4.6}$$

One of the two symmetrical histograms is moved over the gray-level axis until the highest correlation between these histograms is obtained as shown in Figure 4.19.

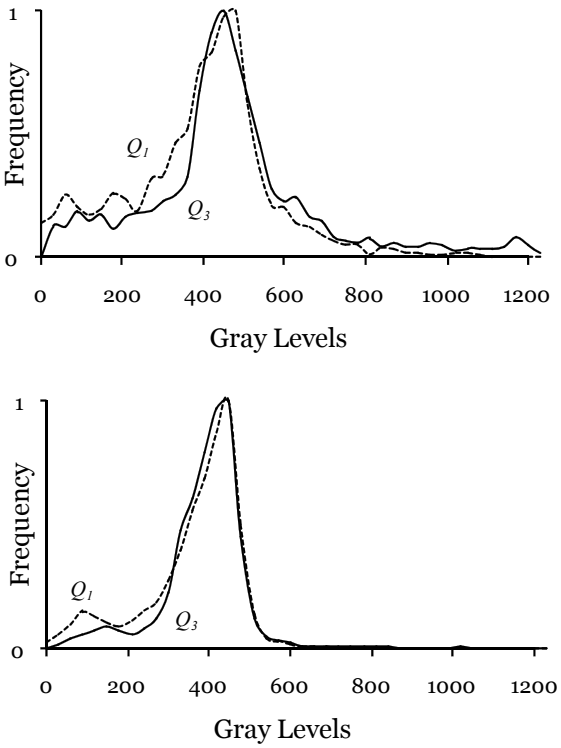

Figure 4.19: Histograms of symmetrical quadrants after correlation.

Histogram Divergence

After the symmetrical histograms are correlated, it is necessary a histogram similarity or dissimilarity metric in order to identify how much these histograms diverge in the tumor gray levels. A good overview of such metrics is given by Rubner et al. [Rubner 1998]. To determine which metric best suits this application, a number of bin-by-bin measures were investigated: $L1$ distance, $L2$ distance, histogram intersection, Jeffrey divergence, and χ^2 statistics. Diverse cross-bin measures were also tested: quadratic-form distance, match distance, and Kolmogorov-Smirnov distance. Briefly summarizing the tests, the best results were consistently obtained with the Jeffrey divergence, closely followed by the χ^2 statistics. The Jeffrey divergence was thus chosen as the dissimilarity metric that identifies if the histograms diverge in the tumor gray levels.

Given two histograms H and K, with h_i and k_i denoting the histogram entries, the Jeffrey divergence is defined as follows:

$$d_J(H,K) = \sum_i \left\{ h_i log \frac{h_i}{m_i} + k_i log \frac{k_i}{m_i} \right\} \tag{4.7}$$

where $m_i = \frac{h_i + k_i}{2}$.

Figure 4.20 shows the Jeffrey divergence values of a normal brain sample slice. It is observed that the divergence between the symmetrical quadrants Q_1 and Q_3, and quadrants Q_2 and Q_4 is not significant. On the contrary, in Figure 4.21 high divergence values between quadrants Q_2 and Q_4 are notably observed. This means that a there is a tumor in the image, and it is located on the anterior part of the right lobe.

4.4.4 Define Non-Tumor and Tumor Membership Functions

One of the biggest problems in computer vision systems, analyzing images having high uncertainty/vagueness degree, is the treatment of such uncertainty. This problem is even clearest in the segmentation process. Fuzzy set theory and fuzzy logic are ideally suited for dealing with such uncertainty [Montseny 2001].

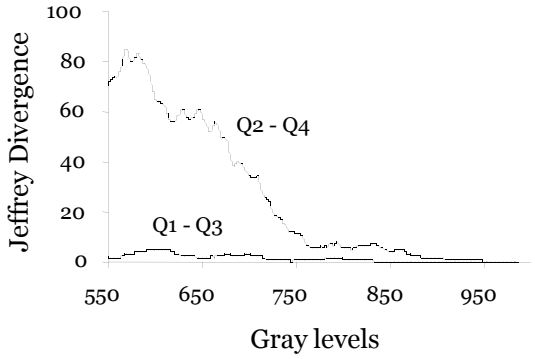

Figure 4.20: Jeffrey divergence values of a normal brain.

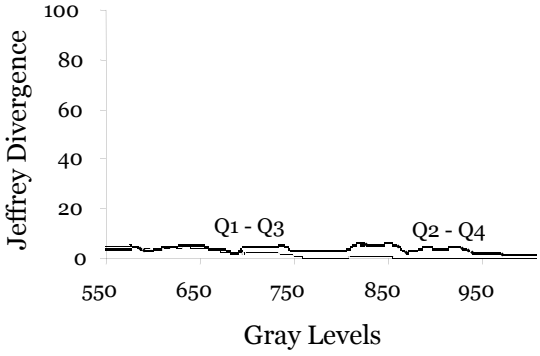

Figure 4.21: Jeffrey divergence values of a pathologic brain.

In the case here presented, the tumor itself is a vague concept modeled following expert knowledge. The purpose of this section is to represent the knowledge integrated into the system in the form of rules, by means of appropriate membership functions.

The basic element in fuzzy systems is the membership function, because the effectiveness of the extracted fuzzy feature set depends on the selection of the membership function best representing feature fuzziness. Models used for obtaining membership functions must be adaptive so that they can be easily adjusted or tuned to optimize the performance of the algorithm that uses them. Given the populations previously extracted, it is necessary to define an appropriate set of membership functions which are well adapted to MRI data, and consequently are well adapted and efficiently separate non-tumor and tumor populations.

Although it is really important to build proper membership functions, there is no single method which will work for most applications. Several approaches for building and adapting membership functions have been proposed. Next are sketched the most widely used.

Membership functions obtained from real data. These are used when data needs a framework and a methodology allowing translating raw data to membership functions. The problem is that with this approach it is also necessary to specify a performance measure to be used in the optimization procedure [Makre 2003, Moreno 2004, Pedrycz 2002].

Membership functions based on subjective perceptions of vague or imprecise categories (rather than on data). In these cases, the problem is that for assigning numbers to subjective perceptions of vague categories, it is necessary the use of various techniques of the theory of measurement and scaling.

Membership functions obtained by heuristic methods. This approach adapts well to applications where spatial relations as "above" or "to the left of", or certain properties like position, lightness, darkness, etc., have to be considered. However, as predefined shapes are considered for defining the membership functions, they are not flexible enough to model all kind of data [Ajibo 2005].

Membership functions based on transformations of probability to possibility distributions. Membership functions so obtained are intended for situations where the manipulation of randomness is hard, but it is easier to handle uncertainty via possibility distributions in the fuzzy framework [Medasani 1998].

Methods based on neural networks. Although this approach provides fairly complex membership functions, their shapes are unpredictable in regions where there is no training data. Moreover, the membership values may not be necessarily indicative of the degree of typicality of a feature with respect to a class [Cheng 2003].

Histogram-based membership functions. These methods are applied when feature values from different classes can be displayed as histograms providing information of the distribution of these features. Thus, each histogram can be modeled by parameterized functions. The most frequently used analytical non-linear functions include gaussians, sigmoids or bells.

Gaussian membership functions are quite popular in fuzzy logic literature because people often characterize their thinking process as normal distributions [Liu 1997]. Some researchers conclude that gaussian membership functions are the most adequate for representing uncertainty in measurements based on the next assertion any membership function that is adequate for describing uncertainty in measurements is equivalent to $exp(-\beta x)$ for some $\beta\, 0$ [Krein 1992]. These membership functions are best suited for off-line design of fuzzy systems such as: fuzzy nonlinear predictors [Wu 1999], fuzzy nonlinear modeling [Jin 2000], and simulation of complex fuzzy nonlinear control strategies [Green 2006, Guang 1999]. Traditionally, in computer vision, gaussian membership functions are approached by normalizing the probability density function (*pdf*) of a given frequency histogram [Cheng 2003, Hanman 2004, Hima 2001, Liu 1997]. Therefore, the membership degree of each element depends on how close this element is to the maximum. However, having only this dependency, it is not considered if the element is located close to the limits of the set of values that takes the variable.

Sigmoidal membership functions are inherently open to the right or to the left, and thus are appropriated for representing concepts such

as "very large" or "very negative". These functions can be used for constructing asymmetric fuzzy intervals, using a sigmoid on the left side and another one on the right side of the fuzzy interval, considering the data located in the limits. In general the shape of the obtained sigmoidal membership function is equivalent to the cumulative probability function of a gaussian normal distribution or probability distribution function (pDf). Sigmoidal membership functions are quite common in optimization [Dombi 2005], as well as in economical and biological models [Kodaka 2004]. In particular, most assumptions about localized distribution of input uncertainties lead to membership functions with sigmoidal shapes [Duch 2005].

Bell-shaped membership functions are symmetrical sigmoid functions around a center value c, and have a width parameter d that defines an interval $(c - d, c + d)$, in which the value of the function is greater than a threshold value. These membership functions are used for fuzzy propositions involving multiple dimensions [Lo 2002]. Moreover these membership functions can not represent fairly complex curves or asymmetric distributions.

Considering the strengths and weaknesses or failures of the above methods, the research was focused on obtaining membership functions from real data, based on the analysis of its histogram. The objective was to define membership functions that have into account not only a measure of central tendency of the data, as it is the case of membership functions defined using the mode of the distribution, but also the data variability. To this end it was proposed a method for obtaining membership functions that, unlike the majority of existing methods, it uses not only the probability density function (pdf) but also its corresponding cumulative distribution functions (cdf).

The advantage of considering the cdfs is twofold: on the one hand, they can be used to better cover the data, particularly in the case of skewed distributions; and on the other hand they provide better classification results when the histograms of the data sets are overlapped, regardless the overlapping region and the gradients of the tails that overlap. These improvements were demonstrated in [Gordillo 2009] through a comparative analysis with other widely known and used histogram-based methods. This analysis showed that the proposed method outperformed the others when considering two populations whose histograms had varying degrees of asymmetry and overlapping. This analysis also showed that the best results were obtained in cases where

the membership functions were based solely on the distribution function.

The following sections introduce the proposed method for obtaining membership functions based on the density and cumulative distribution functions.

Proposed Membership Function

Membership functions based on histograms are usually obtained approaching gaussian functions. To do so, if C is the characteristic to be assessed in a population P, c_{ij} is the value taken by C when is evaluated on the pixel p_{ij}, and $pdf_C(\cdot)$ is the probability density function obtained evaluating the characteristic over all the pixels of the population, traditionally the degree to which p_{ij} is C is derived from the following rule:

R1 : The closer $max(pdf_C)$ is to $pdf_C(c_{ij})$, the more C is p_{ij}.

The implementation of this rule, the degree to which a pixel p_{ij} is C, $\phi_C(p_{ij})$, is given by:

$$\phi_C(p_{ij}) = \mu_{1C}(c_{ij}) = \frac{pdf_C(c_{ij})}{max(pdf_C)} \tag{4.8}$$

Therefore, when using this type of membership functions, the degree to which a pixel p_{ij} satisfies a characteristic C has only into account the central tendency of the data, but not the data variability. To overcome this limitation it was proposed to consider next rule:

R2 : The closer mean(pdf_C) is to $pdf_C(c_{ij})$, the more C is p_{ij}.

where mean(pdf_C) is the mean of the distribution.

Taking advantage of the cumulative distribution functions ($cdfs$) properties, and their relation with the median of the distribution, the previous rule was implemented by means of a new membership function that is defined by:

$$\phi_C(p_{ij}) = \mu_{2C}(c_{ij}) = min\left\{1, \frac{cdf_{LC}(c_{ij})}{a_1}, \frac{cdf_{RC}(c_{ij})}{a_2}\right\} \tag{4.9}$$

where: $cdf_{LC}(c_{ij})$ and $cdf_{RC}(c_{ij})$ are the values of the left and right cumulative distribution functions associated to pixel p_{ij} for the characteristic C. a_1 and a_2 are parameters whose values are to be adjusted. As the mean of a distribution is the value for the 50^{th} percentile of the distribution (i.e., the probability that a random variable takes a value below the mean is 0.5), these parameters will be adjusted so that the number of pixels that meets the characteristic with a degree higher than 0.5 is at least Equation (4.10) per cent of the total:

$$\left(1 - \frac{a_1 - a_2}{2} \times 100\right) \tag{4.10}$$

Parameters a_1 and a_2 are adjusted based on the direct relationship between the increase in the overlapping degree of the histograms and the gradients of the tails in the overlapping area [Gordillo 2009]. This relationship is as follows:

When the tails of the histograms in the overlapping area are similar in nature, i.e. both have steep or smooth gradients (Figure 4.22-a and 4.22-b), the greater is the overlap the greater are the values of a_1 and a_2. Moreover, both values are equal.

In the cases where the tail of left histogram has steep gradient and the tail of right histogram has smooth gradient (Figure 4.22-c), or vice versa, the values of parameters a_1 and a_2 are higher where the gradient is smoother.

Considering rules $R1$ and $R2$ new membership functions can be generated that take into account both, the data variability and the complete description of the distribution of the considered characteristic. For obtaining these membership functions the first step consists in getting the approximate density and distribution functions, as explained below.

Obtaining the Density and Distribution Functions

Given a characteristic C once the frequency histogram of the values c_{ij} has been obtained, it is generated its approximate theoretical normal density func-

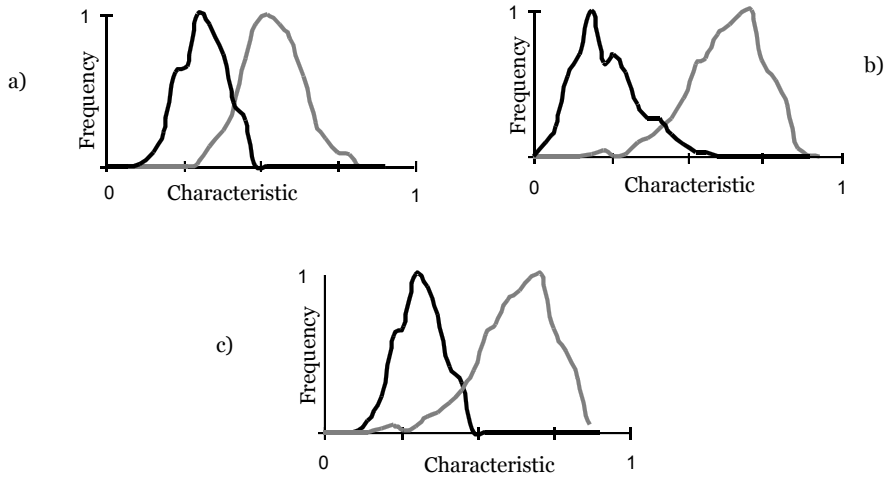

Figure 4.22: Examples of pairs of overlapped histograms of a characteristic attending to the gradient of the tails in the overlapping region: a) Both histograms have steep gradient in the overlapping zone; b) Histograms with smooth gradient; c) Histograms with steep / smooth gradient.

tion as follows:

- If the histogram is symmetric, the mean and standard deviation that define the function are obtained from the data.

- In other case the approximate normal density function is obtained using the standard deviations on the right, σ_R, and left, σ_L, sides of the histogram, and the mode, m.

It must be pointed out that the values of σ_R and σ_L, may need to be modified in order to be optimally adjusted to the shape of the histogram. From the density function obtained at previous step are obtained the right, $cdf_{LC}\,(c_{ij})$ and left $cdf_{RC}\,(c_{ij})$ cumulative distribution functions.

Obtaining the Membership Function

For getting the degree, $\psi_C(p_{ij}) = \mu_C(c_{ij})$ to which a pixel p_{ij} satisfies the characteristic C, $R1$ and $R2$ are applied by considering a weighted mean of $\mu_{1C}(c_{ij})$ and $\mu_{2C}(c_{ij})$ as follows:

$$\mu_C(c_{ij}) = (1-b)\cdot\mu_{1C}(c_{ij}) + b\cdot\mu_{2C}(c_{ij}) \tag{4.11}$$

such that $0 \leq b \leq 1$.

4.4.5 Classification

The task in classification is to use the features measured at a pixel to decide whether the pixel represents a tumor pixel or not. Therefore, it was necessary to define an appropriate set of membership functions which are well adapted to *tumor* population and efficiently separate the $non-tumor$ population using the presented model.

In a previous work [Gordillo2 2009] it was concluded that as the number of populations becomes larger, the system grows up and the classification process becomes more complicated. Thus, in order to make it simpler, the classification must be performed by pairs of populations. The author proved that in the case of having three populations, if the populations are combined by pairs obtaining three pairs of two, and then the classification is performed over these three pairs of populations, the efficiency of the classification is as good as classifying the three populations simultaneously.

Given populations BP, TUM and OBR (Figure 4.23), three pairs of two populations are obtained: Pair 1: $BPTUM$ (Figure 4.24 a), Pair 2: $BPOBR$ (Figure 4.24 b), and Pair 3: $TUMOBR$ (Figure 4.24 c).

Each pair is linked to their corresponding membership functions as follows:

$$Pair1 : \mu^1_{BP} \quad and \quad \mu^1_{TUM} \tag{4.12}$$

$$Pair2 : \mu^2_{BP} \quad and \quad \mu^2_{OBR} \tag{4.13}$$

$$Pair3 : \mu^3_{TUM} \quad and \quad \mu^3_{OBR} \tag{4.14}$$

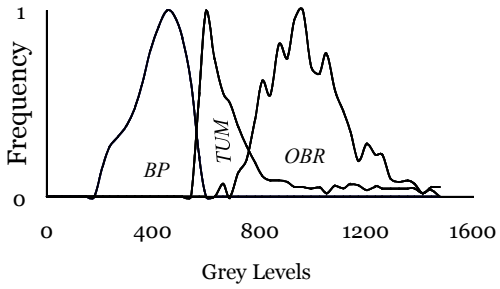

Figure 4.23: Brain parenchyma, tumor, and outside brain region populations of a sample slice.

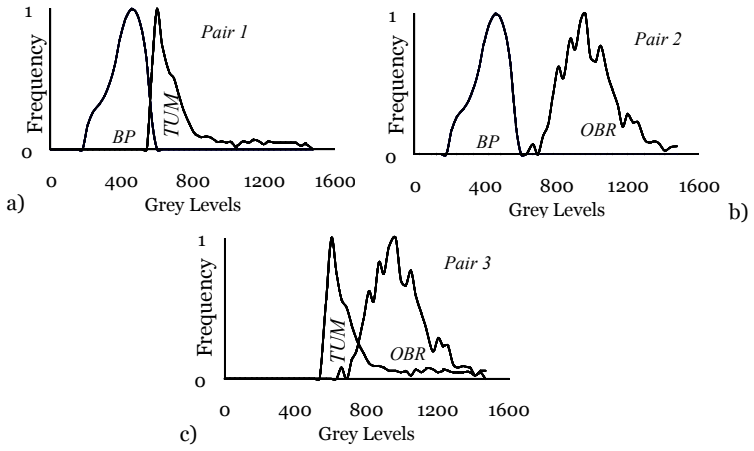

Figure 4.24: Populations combined by pairs for the classification. Pair 1 $BPTUM$ (a), Pair 2: $BPOBR$ (b), and Pair 3: $TUMOBR$ (c).

To determine these membership functions, the process described in Section 4.4 was applied. Weight b (Eq. 4.11, as well as the values of parameters a_1 and a_2 used for defining $\mu_{2C}(c_{ij})$(Eq. 4.9) were adjusted based on the direct relationship between the increase in the overlapping degree of the histograms and the gradients of the tails in the overlapping area as in [Gordillo 2009].

The binary segmentation $tumor$ and $non-tumor$ is given by the following equation:

$\forall p_{ij}$ such that $\mu^1_{TUM}(p_{ij}) > \mu^1_{BP}(p_{ij})$,

$$\left\{\begin{matrix} tumor & \text{if} \quad \mu^3_{TUM}(p_{ij}) > \mu^3_{OBR}(p_{ij}) \\ non-tumor & \text{otherwise} \end{matrix}\right\} \tag{4.15}$$

4.5 Conclusions

This chapter presented a step-by-step methodology for the automatic MRI brain tumor segmentation.

A new simple and robust skull-stripping algorithm was presented. The skull stripping solely relies on the change of intensity level between the surrounding tissues and the brain tissues in T1-weighted images. As long as this feature is observed in the image data, a robust segmentation can be guaranteed even in presence of severe intensity non-uniformity and noise. The algorithm becomes totally automatic as all the intensity values are automatically determined from the histogram.

For achieving the fully automatic and unsupervised segmentation, objective measures were delineated by means of adaptive histogram thresholds for defining the $non-tumor$ and $tumor$ populations. For defining the $tumor$ population a symmetry analysis was conducted.

The proposed brain tumor segmentation approach also introduced a new way to automatically define the membership functions from the histogram. The proposed membership functions are designed to adapt well to the MRI data

and efficiently separate the populations ($non - tumor$ and $tumor$).

The segmentation technique is simplified since neither pre- or post-processing in addition to skull stripping is necessary shortening computational times.

In this chapter it was shown how rules that attempt to capture human expertise can be used to augment low level segmentation, a step on the way towards truly automatic brain tumor segmentation.

Chapter 5

Experiments and Results

5.1 Introduction

This chapter presents some results, both qualitative and quantitative, from the experiments conducted to evaluate the performance and accuracy of the proposed approach.

5.2 Outline of the Chapter

Section 5.3 describes the image materials used in the experiments. Section 5.4 introduces the validation measure for the automatic brain tumor segmentation. The results of the conducted experiments are shown in section 5.5. They are divided in three datasets, normal dataset (NON), *glioblastoma multiforme* dataset (GBM), and *meningioma* dataset (MEN). Section 5.6 gives a general discussion. Finally section 5.7 summarizes the chapter conclusions.

5.3 Image Materials for the Experiments

The magnetic resonance imaging materials used for the experiments consists of tree datasets: normal dataset NON, *glioblastoma multiforme* dataset GBM, and *meningioma* dataset MEN. The normal dataset contains 256 slices (180 x 256 pixels) of a normal brain. The GBM dataset contains 256 slices (176 x 256 pixels) presenting a GBM brain tumor, and the *meningioma* dataset consists

of 256 slices presenting a meningioma (180 x 256 pixels).

Figures 5.1, 5.2, and 5.3 show tree $2D$ transversal MRI in the T1 channel from the image materials. Figure 5.1 shows a normal brain, Figure 5.2 a slice presenting an enhancing GBM brain tumor, and Figure 5.3 a slice containing a meningioma.

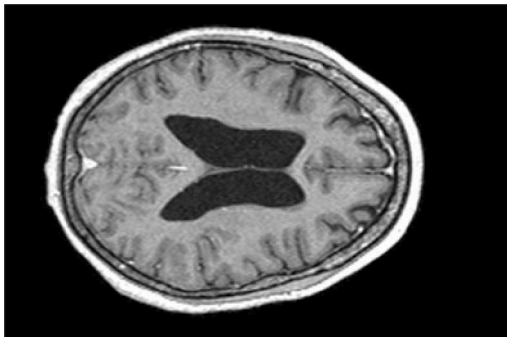

Figure 5.1: A transversal T1-weighted MRI experimental dataset of a normal brain.

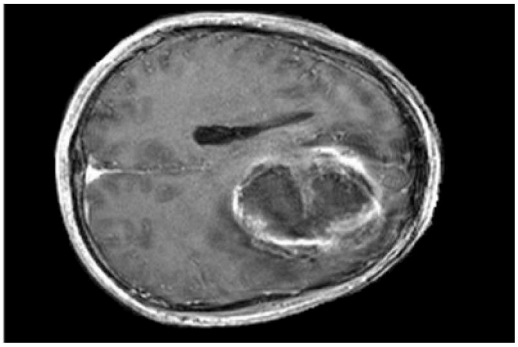

Figure 5.2: A transversal T1-weighted MRI experimental dataset of a brain presenting a GBM tumor.

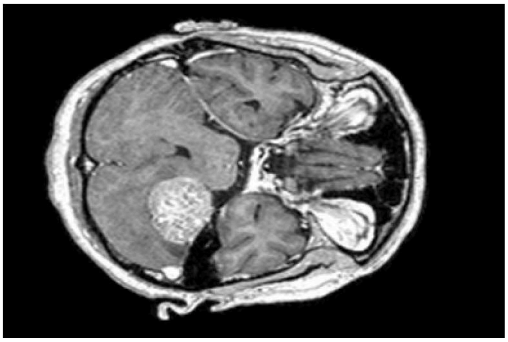

Figure 5.3: A transversal T1-weighted MRI experimental dataset of a brain presenting a meningioma.

5.4 Validation

A major issue that must be addressed in validating an automatic method for brain tumor segmentation is the means through which the segmentation is quantitatively assessed. In order to quantitatively assess the quality of an automatic binary segmentation in comparison to a manual binary segmentation produced by experts, many of the approaches in the literature [Cobzas 2007, Corso 2008, Lee 2005, Prastawa 2004] have used the Jaccard similarity measure (Eq. 5.1).

Let M be the set of manually defined tumor pixels, and A the set pixels classified as tumor by the proposed automatic method. The Jaccard similarity measure is given by:

$$J(A, M) = \frac{A \cap M}{A \cup M} = \frac{tp}{tp + fp + fn} \tag{5.1}$$

Where tp is the true positive, fp the false positive, and fn the false negative.

In order to define the M sets, the tumor pixels were manually segmented with the support of a radiology expert.

Table 5.1: Classification results of normal brain dataset (12 slices).

Slice Number	Jaccard SM
NON55	0,9226
NON60	0,9457
NON65	0,9378
NON70	0,9661
NON75	0,977
NON80	0,9803
NON85	0,9904
NON90	0,9992
NON95	0,9897
NON100	0,9884
NON105	0,9901
NON110	0,9876
Average	**0,9729**

5.5 Experiments

The experiments are divided according to their dataset. For the qualitative results, each set presents a pair of indicative slices. In the classification figures, color blue is used to represent true positives, and color red to represent false positives. For the quantitative results, each set presents a table and a chart showing the Jaccard similarity measure, and the average result of the classification for each dataset.

5.5.1 Experiments on Normal Brain Dataset

The average scores obtained in experiments on the normal brain dataset, are very accurate (Jaccard similarity measure = 0.97), these results confirm that by performing the symmetry analysis, the non-tumorous pixels whose gray level falls within the gray levels of tumor are discarded. Figure 5.4 show qualitatively this result. The quantitative results are shown in Figure 5.5.

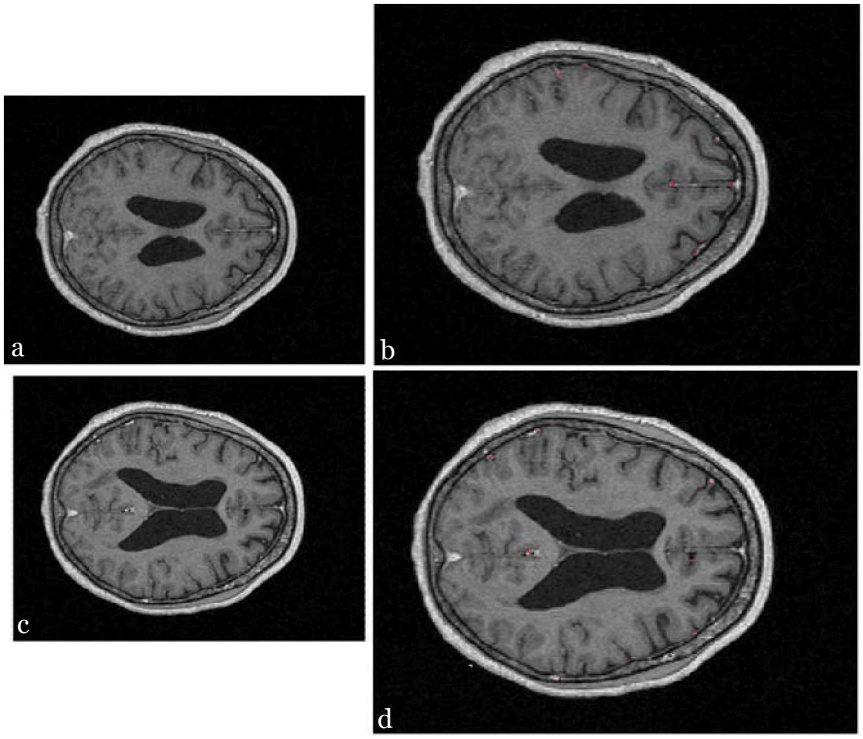

Figure 5.4: Resulting Segmentation on normal brain dataset (*NON*). The symmetry analysis discarded most of the non-tumorous pixels. A minimal amount of false positives in asymmetric areas (b,d) are shown in red.

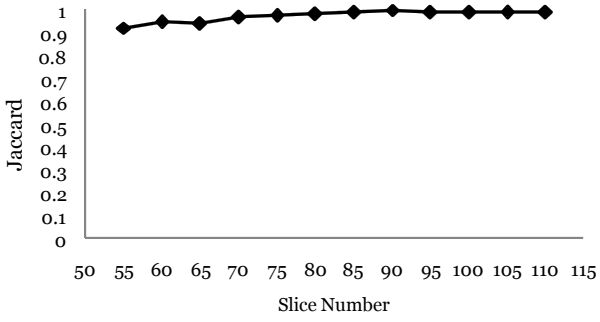

Figure 5.5: Classification results of normal brain dataset (12 slices).

5.5.2 Experiments on Glioblastoma Multiforme Dataset

The proposed system attempted to segment the enhancing GBM tumor area. In the case of slices with necrotic cores, which appear dark on T1weighted images as in Figure 5.6, only the enhancing rim of the tumor was defined as the target tumor region. The entire tumor area was defined as target in cases where ambiguous tissue between necrotic and enhancing appeared as in Figure 5.7.

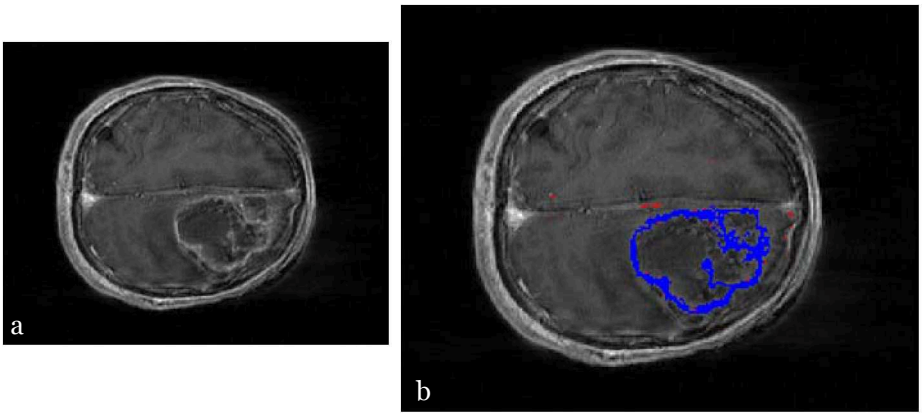

Figure 5.6: Resulting segmentation of *GBM* dataset slice 55. a) Slice 55 presenting a rim-shaped enhancing GBM tumor. b) Segmented rim-shaped enhancing GBM tumor in blue.

In general, in both cases, slices showing a rim-shaped enhancing tumor and in ambiguous cases, obtained results of about $0,83$. Problems of false negatives appeared in upper-brain slices, where non-tumorous areas where also enhanced (Figure 5.7b). Results of twelve slices are presented in table 5.2 and in Figure 5.8.

Table 5.3 shows a summary of related methods in unsupervised and supervised automatic brain tumor segmentation. These methods were applied for the segmentation of glioblastoma multiforme brain tumors, and the validation of the segmentation was measured using the Jaccard similarity measure.

The first column shows the authors' name. The second gives a brief description of the methodology. The third column indicates whether the segmentation

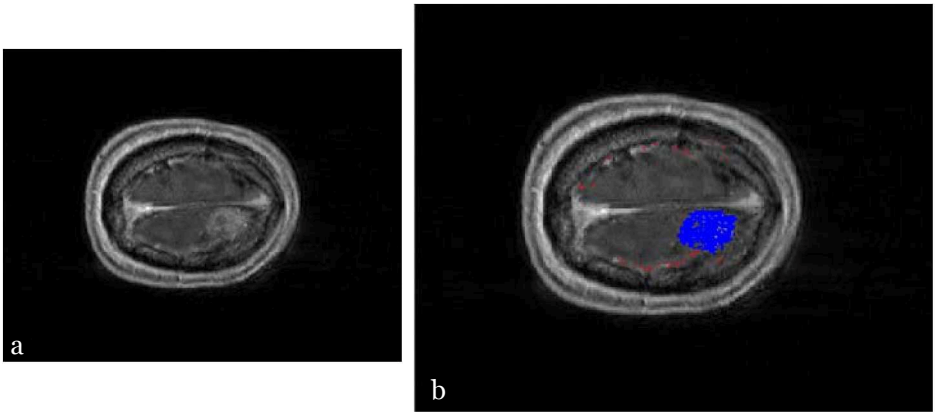

Figure 5.7: Resulting segmentation of *GBM* dataset slice 35. a) Slice 35 presenting ambiguous necrotic and enhancing GBM tumor. b) Segmented ambiguous necrotic and enhancing GBM tumor in blue. Some false negatives appeared in non-tumorous enhancing areas.

Table 5.2: Classification results of *GBM* tumor dataset (12 slices).

Slice Number	**Jaccard SM**
GBM35	0,7129
GBM40	0,7288
GBM45	0,7456
GBM50	0,7754
GBM55	0,8493
GBM60	0,8345
GBM65	0,8634
GBM70	0,8968
GBM75	0,9336
GBM80	0,9125
GBM85	0,8769
GBM90	0,9043
Average	**0,8361**

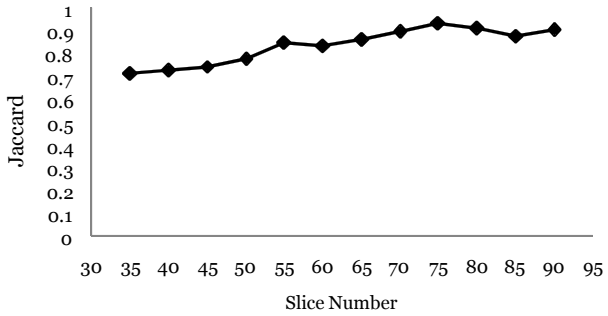

Figure 5.8: Classification results of GBM tumor dataset (12 slices).

was done in $2D$ or $3D$. In case of being performed in $2D$, and then a correlation to $3D$ was made, it is marked in the table as $2D - 3D$. The fourth column indicates whether the method is unsupervised or supervised and fully automatic. The last column shows the resulting segmentation using the Jaccard similarity measure.

Having a look to Table 5.3, the lowest results were obtained with the two supervised methods, the proposed by Cobzas with scores from 0.27 to 0.88, and the proposed by Lee (scores from 0.40 to 0.89). The highest scores were obtained with the approach proposed by Ho et al. obtaining results in the range of 0.85 the lowest, and 0.93 the highest. The work here presented obtained results similar to those of Ho, with the lowest score of 0.71 and the highest of 0.93. The lowest scores are due to false negatives, however, when this approach is extended to perform the classification in $3D$, the accuracy will be improved when the correlation between the slices is made.

5.5.3 Experiments on Meningioma Dataset

In Chapter 4, a disjoint subset of the GBM dataset was used in the histogram analysis in order to obtain intensity knowledge. It was emphasized that this set does not generate labeled training data.

The author was in the task of testing whether the knowledge obtained in the histogram analysis conducted in Chapter 4, worked on a dataset containing a different type of tumor. For this reason, the experiments in the *meningioma* dataset were carried out.

Table 5.3: Summary of related methods in unsupervised and supervised automatic brain tumor segmentation.

Authors	**Description**	$2D - 3D$	**Segmentation**	**JaccardSM**
Clark et al. [Clark 1998]	Knowledge-Based Fuzzy Clustering	2D	unsupervised / fully automatic	0,70
Corso et al. [Corso 2008]	Multilevel Bayesian	3D	supervised / fully automatic	0,27- 0,88
Ho et al. [Ho 2002]	Level Sets	3D	unsupervised / fully automatic	0,85-0,93
Lee et al. [Lee 2005]	Disc. Random Fields and SVM	3D	supervised / fully automatic	0,40-0,89
Prastawa et al. [Prasta 2004]	Knowledge-Based Outlier Detection	2D-3D	unsupervised / fully automatic	0,68-0,80
Prastawa et al. [Prasta 2003]	Statistical classification via Expec. Maximization	2D-3D	unsupervised / fully automatic	0,49-0,71
Gordillo [proposed method]	Knowledge-Based Fuzzy Clustering	2D	unsupervised / fully automatic	0,71-0,93

Table 5.4: Classification results of meningioma tumor dataset (12 slices).

Slice Number	**Jaccard SM**
MEN120	0,7989
MEN122	0,7914
MEN124	0,7743
MEN126	0,7802
MEN128	0,7893
MEN130	0,7857
MEN132	0,7432
MEN134	0,7247
MEN136	0,7426
MEN138	0,7597
MEN140	0,7651
MEN142	0,7511
Average	**0,7671**

The resulting scores show that indeed, the knowledge obtained through the histogram analysis also works for this dataset (scores in the order of 0.76). However, in order to improve the accuracy in the segmentation is necessary to include additional knowledge for discarding other tissues also contrast-enhanced as shown in Figure 5.9. The quantitative results are shown in Table 5.4 and in Figure 5.10.

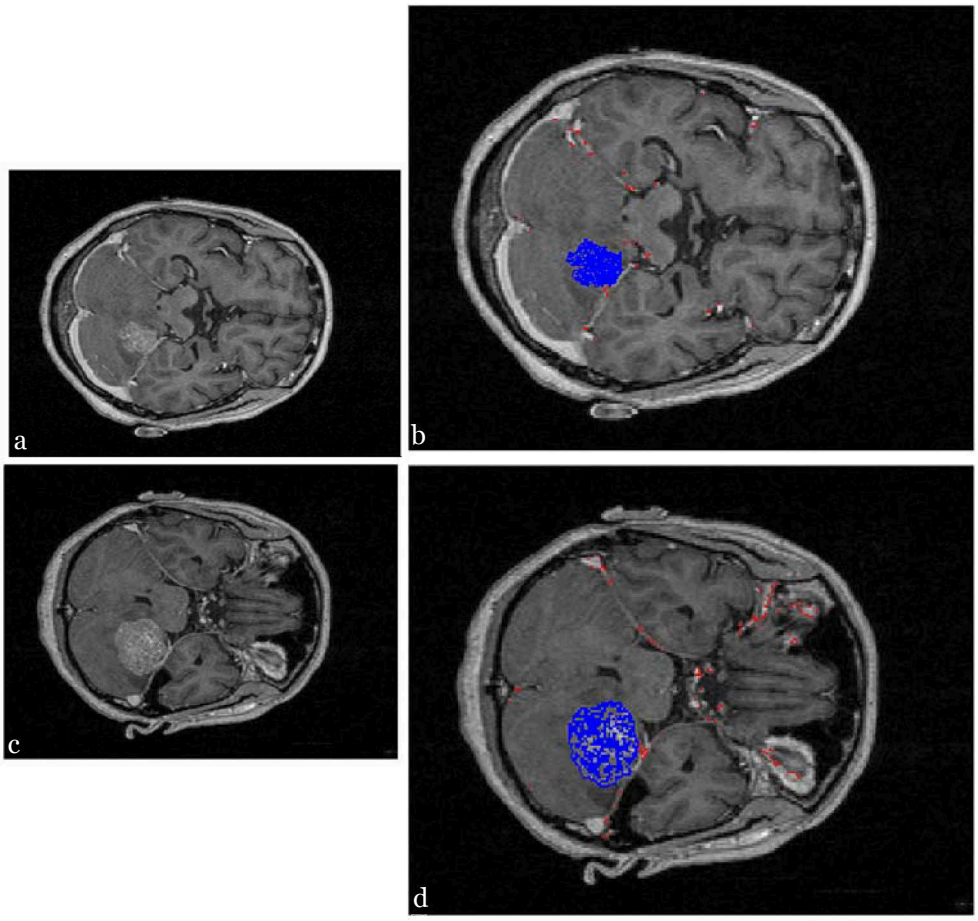

Figure 5.9: Resulting segmentation of meningioma dataset (MEN). (a,c) Slices 120 and 130 presenting ambiguous necrotic and enhancing meningiona tumor. b) Segmented ambiguous necrotic and enhancing meningioma tumor in blue. Some false negatives appeared in non-tumorous enhancing areas.

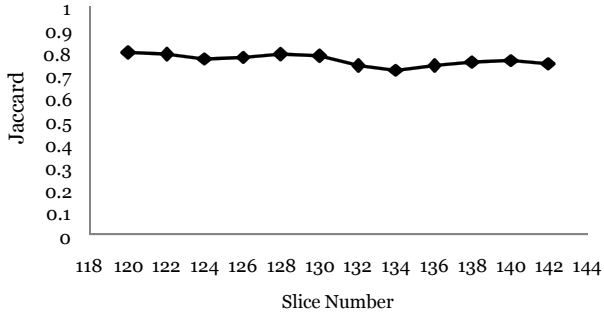

Figure 5.10: Classification results of meningioma tumor dataset (12 slices).

5.6 Conclusions

As a general conclusion of the experiments, the proposed approach is quantitatively comparable to the most accurate existing methods, even though the segmentation is done in $2D$. However, when this approach is extended to perform the classification in $3D$, the accuracy will be improved when the correlation between the slices is performed.

In this chapter the qualitative and quantitative results of three datasets were shown. Normal brain dataset achieved very accurate results close to 1 using the Jaccard similarity measure; these results confirm that the non-tumorous pixels whose gray level falls within the gray levels of tumor are discarded by means of the symmetry analysis.

The glioblastoma multiforme dataset, obtained results of about 0,83 in both cases, slices showing a rim-shaped enhancing tumor and in ambiguous cases. Some problems of false negatives appeared in upper-brain slices, where non-tumorous areas where also enhanced.

The approach was also tested on a third dataset containing a different type of tumor, a meningioma brain tumor. The resulting scores (in the order of 0.76) show that indeed, the knowledge obtained through the histogram analysis conducted in Chapter 4 also works for this dataset. However, in order to improve the accuracy in the segmentation is necessary to include additional knowledge for discarding other tissues also contrast-enhanced.

Chapter 6

Conclusions and Future Work

6.1 Conclusions

The following lines are devoted to putting together all the conclusions that were drawn in each chapter that conforms this thesis. As general conclusion, it can be summarized that the main objective was to develop a system to assist brain tumor segmentation which works in the same line of work of a technician, considering his experience and knowledge. The method successfully managed the ambiguity of MR image features, as well as the variability in tissue distribution among individuals in the human population being capable of describing knowledge about the tumors in vague terms.

The method was developed making use of the powerful tools provided by fuzzy set theory. This thesis presented a step-by-step methodology for the automatic MRI brain tumor segmentation. A new simple and robust skull-stripping algorithm was presented. For achieving the fully automatic and unsupervised segmentation, objective measures were delineated by means of adaptive histogram thresholds for defining the non-tumor and tumor populations. For defining the tumor population a symmetry analysis was conducted.

The proposed approach also introduced a new way to automatically define the membership functions from the histogram. The proposed membership functions were designed to adapt well to the MRI data and efficiently separate the populations. The segmentation technique is simplified since neither pre or post processing in addition to skull stripping is necessary shortening compu-

tational times, and is quantitatively comparable to the most accurate existing methods, even though the segmentation is done in $2D$.

6.1.1 Magnetic Resonance Imaging of Brain Tumors

The goals and requirements for brain tumor imaging are multiple and complex. They involve providing a diagnosis and a differential diagnosis, and, if possible, a specific diagnosis, as well as accurate grading of the tumor. Tumor imaging is an essential part of the decision-making process for therapy and later for precise planning of surgical or radiological interventions.

Magnetic Resonance Imaging is a powerful visualization technique that allows images of internal anatomy, metabolism, and function to be acquired in a safe and non-invasive way. It is based on the principles of Nuclear Magnetic Resonance, and allows a vast array of different types of visualizations to be performed. This imaging medium has been of particular relevance for producing images of the brain, due to the ability of MRI to record signals that can distinguish between different soft tissues such as gray matter and white matter.

MRI of the brain is a vital part of modern oncology. It is used in tumor diagnosis, monitoring tumor progression, planning treatments, and monitoring responses to treatment. From the very beginning, the technical development of MRI progressed quickly, and it seems to be continuing at an ever-increasing pace. As a result, over the last 25 years there has been an explosion in the number of clinical applications of MRI.

Due to its high tissue contrast and its noninvasiveness, MRI is accepted as the most sensitive method for diagnosing brain tumors. The very accurate MR Imaging, generally T1-weighted, T2-weighted and the proton density add diagnostic value.

6.1.2 State of the Art Survey on Brain Tumor Segmentation

Detecting the existence of brain tumors from MRI in a fast, accurate, and reproducible way is a challenging problem. Medical image processing is a very active and fast-growing field that has evolved into an established discipline. Brain tumor segmentation techniques have already shown great potential in detecting and analyzing tumors in clinical images and this trend will undoubt-

edly continue into the future.

In tumor imaging researches, one major goal is to accurately locate the cancer. Segmentation techniques have been applied according to the characteristics that allow tumors to distinguish from normal tissues. For example, some tumors can be distinguished from normal tissues by their image intensity, therefore threshold-based [Shanti 2007] or region growing [Dou 2007] techniques have been employed, others can be identified by their shapes so that a model-based technique [Chang 2008, Popuri 2009] was applied for the segmentation.

Although the reported accuracy on brain tumor segmentation of the proposed automated methods is quite promising, these approaches still have not gained wide acceptance among the pathologists, for every day clinical practice. One of the principal reasons might be the lack of standardized procedures. Another possible reason could be the substantial differences with the traditional line of work of the specialists, and the deficiency of the existing methods to assist medical decision with a transparent and interpretable way. The latter is very important for computer aided medical diagnosis where the demand for reasoning and explanation is of main priority.

Medical image analysis needs to address real-world issues that have been outside the realm of computer vision [Shen 2006]. These issues come largely from the fact that the end systems are mostly used by the physician. The human factor is essential, since any successful solution will have to be accepted by a physician and integrated into the medical procedural work flow. This put strong constraints on the type of applicable methods. Because of this, there has been a discrepancy between the advanced frameworks presented in computer vision and the low-level methods used by researchers working on real medical application solutions.

6.1.3 A New Fuzzy Approach for Automatic and Unsupervised Brain Tumor Segmentation

Chapter 4 presented a step-by-step methodology for the automatic MRI brain tumor segmentation.

A new simple and robust skull-stripping algorithm was presented. The skull stripping solely relies on the change of intensity level between the surrounding tissues and the brain tissues in T1-weighted images. As long as this feature is observed in the image data, a robust segmentation can be guaranteed even in

presence of severe intensity non-uniformity and noise. The algorithm becomes totally automatic as all the intensity values are automatically determined from the histogram.

For achieving the fully automatic and unsupervised segmentation, objective measures were delineated by means of adaptive histogram thresholds for defining the non-tumor and tumor populations. For defining the tumor population a symmetry analysis was conducted.

The proposed brain tumor segmentation approach also introduced a new way to automatically define the membership functions from the histogram. The proposed membership functions are designed to adapt well to the MRI data and efficiently separate the populations (non-tumor and tumor).

The segmentation technique is simplified since neither pre- or post-processing in addition to skull stripping is necessary shortening computational times.

In this chapter it was shown how rules that attempt to capture human expertise can be used to augment low level segmentation, a step on the way towards truly automatic brain tumor segmentation.

6.1.4 Experiments and Results

As a general conclusion of the experiments conducted in Chapter 5, the proposed approach is quantitatively comparable to the best existing methods, even though the segmentation is done in $2D$. However, when this approach is extended to perform the classification in $3D$, the accuracy will be improved when the correlation between the slices is performed.

In Chapter 5, the qualitative and quantitative results of three datasets were shown. Normal brain dataset achieved very accurate results close to 1 using the Jaccard similarity measure; these results confirm that the non-tumorous pixels whose gray level falls within the gray levels of tumor are discarded by means of the symmetry analysis.

The glioblastoma multiforme dataset, obtained results of about 0,83 in both cases, slices showing a rim-shaped enhancing tumor and in ambiguous cases. Some problems of false negatives appeared in upper-brain slices, where non-tumorous areas where also enhanced.

The approach was also tested on a third dataset containing a different type of tumor, a meningioma brain tumor. The resulting scores (in the order of 0.76) show that indeed, the knowledge obtained through the histogram analysis conducted in Chapter 4 also works for this dataset. However, in order to improve the accuracy in the segmentation is necessary to include additional knowledge for discarding other tissues also contrast-enhanced.

6.2 Future Work

The main line of future work is to implement the volumetric evaluation on the entire brain tumor collection. When performing the correlation of the $2D$ slices, false negatives will be eliminated, and the segmentation will be more accurate.

In future work, it would be interesting to include additional feature information. Besides the intensity, add more information to the pixel analysis in order to make the system more sensitive; information from the textures, or location.

It will be interesting to continue developing modeling of tumors and to study fuzzy information fusion operators for other types of brain tumors following the same line of work here presented.

Another future line would be the detection of small malignant brain tumors. It should be clear that many factors influence the appearance of tumors on images, and although there are some common features of malignancies, there is also a great deal of variation that depends on the tissue and the tumor type. Characteristic features are more likely to be found in large tumors. Small tumors may not have many of the features of malignancy and may even manifest themselves only by secondary effects such as architectural distortion.

Finally, another future line would be the development of an intelligent system which can answer questions like “Is it possible that this pixel/area has tumor?”

Bibliography

A

Adams 1994 Adams R. and Bischof L. "Seeded Region Growing," IEEE Transactions on Pattern Analysis and Machine Intelligence 16, pp. 641-647, 1994.

Allain 1992 Allain P., Travere J. and Baron J. "Entirely Automatic 3D MRI Brain Analysis as a Step In Multimodal Processing," Engineering in Medicine and Biology Society. Proceedings of the Annual International Conference of the IEEE, Vol. 3, pp. 947-949, 1992.

Albretha 2008 Albrehta T., McKeeb M., Alexec DM., Colemanc M. and Martin-Moreno J. "Making Progress Against Cancer in Europe in 2008," Europe A Journal of Cancer, pp. 1451-1456, 2008.

Ahmed 2002 Ahmed M., Yamany S., Mohamed N., Farag A. and Moriarty T. "A Modified Fuzzy C-Means Algorithm for Bias Field Estimation and Segmentation of MRI Data," IEEE Transactions on Medical Imaging 21, pp. 193-199, 2002.

Ajibo 2005 Ajiboye A. and Weir R. "A Heuristic Fuzzy Logic Approach to EMG Pattern Recognition for Multifunctional Prosthesis Control," IEEE Transactions on Neural Systems and Rehabilitation Engineering, Vol. 13, No. 3, pp. 280-291, 2005.

Archip 2007 Archip N., Jolesz F. and Warfield S. "A Validation Framework for BrainTumor Segmentation," Academic Radiology 14, pp. 1242-1251, 2007.

Atkins 1998 Atkins M. and Mackiewich B. "Fully Automatic Segmentation of the Brain in MRI," IEEE Transactions on Medical Imaging, 17(1), pp. 98-107, 1998.

B

Bamford 1998 Bamford P. and Lovell B. "Unsupervised Cell Nucleus Segmentation With Active Contours," Signal Processing Special Issue: Deformable Models and Techniques for Image and Signal Processing 71(2), pp. 203-213, 1998.

Besag 1986 Besag J. "On the Statistical Analysis of Dirty Pictures," Journal of the Royal Statistical Society B, Vol. 48, 1986.

Beyer 2006 Beyer G., Velthuizen R., Murtagh F. and Pearlman J. "Technical Aspects and Evaluation Methodology for the Application of Two Automated Brain MRI Tumor Segmentation Methods in Radiation Therapy Planning," Magnetic Resonance Imaging 24, pp. 1167-1178, 2006.

Bezdek 1993 Bezdek J, Hall L. and Clarke L. "Review of MR Imaging SegmentationTechniques Using Pattern Recognition," Medical Physics 20 (4), pp. 1033-1048, 1993.

Bezdek 1999 Bezdek J. and Sutton M. "Applications of Fuzzy Systems," Image Processing in Medicine, 1999.

Bhandar 1997 Bhandarkar S., Koh J. and Suk M. "Multiscale Image Segmentation using a Hierarchical Self-Organizing Map," Neurocomputing 14, pp. 241-272, 1997.

Bhatta 2008 Bhattacharya M. and Das A. "A Study on Seeded Region Based Improved Watershed Transformation for Brain Tumor Segmentation," The XXIX General Assembly of the International Union of Radio Science, 2008.

Bleau 2000 Bleau A. and Leon L. "Watershed-Based Segmentation and Region Merging", Computer Vision and Image Understanding, Vol. 77, No. 3, pp. 317-370, 2000.

Bloch 1946 Bloch F. "Nuclear Induction," Physical Review 70, pp. 460-474, 1946.

Butman 2006 Butman J., Koby M. and Choyke P. "Advances of MRI of the Brain," New Techniques in Oncologic Imaging, pp. 21-36, 2006.

C

Cai 2007 Cai W., Chen S. and Zhang D. "Fast and Robust Fuzzy C-Means Algorithms Incorporating Local Information for Image Segmentation," Pattern Recognition 40, pp. 825-838, 2007.

Capelle 2000 Capelle A., Alata O., Fernandez C., Lefevre S. and Ferrie J. "Unsupervised Segmentation for Automatic Detection of Brain Tumors in MRI," IEEE International Conference on Image Processing, pp. 613-616, 2000.

Capelle 2004 Capelle A., Colot O. and Fernandez-Maloigne C. "Evidential Segmentation Scheme of Multi-echo MR Images for the Detection of Brain Tumors Using Neighborhood Information," Information Fusion 5, Vol. 3, pp. 203-216, 2004.

Caselles 1993 Caselles V., Catte F., Coll T. and Dibos F. "A Geometric Model for Active Contours In Image Processing," Numerical Mathematics 66, pp. 1-31, 1993.

Chan 1996 Chan F., Lam F., Poon P., Zhu H and Chan K. "Object boundary location by region and contour deformation," IEEE Proceedings Vision, Image and Signal Processing, Vol. 143, No. 6, pp. 353-360, 1996.

Chan 2001 Chan T and Vese L., "Active Contours without Edges," IEEE Transactions on Image Processing, Vol. 10, No.2, pp. 266-277, 2001.

Chang 2006 Chang H. and Valentino D. "Image Segmentation using a Charged Fluid Method," Journal of Electroninc Imaging 15, Vol. 2, pp. 023011+, 2006.

Chang 2008 Chang H. and Valentino D. "An Electrostatic Deformable Model for Medical Image Segmentation," Computerized Medical Imaging and Graphics 32, pp. 22-35, 2008.

ChangS 2000 ChangSun Y., SunHan K., JunSong C., MooNoh S. and Won-Park J. "Threshold Estimation for Region Segmentation on MR Image of Brain having the Partial Volume Artifact," Proceedings of ICSP2000, pp. 1000-1009, 2000.

Chen 2004 Chen S. and Zhang D. "Robust Image Segmentation using FCM With Spatial Constraints Based nn New Kernel-Induced Distance Measure," IEEE. Transactions on Systems Man and Cybernetics Part. B 34, pp. 1907-1916, 2004.

Cheng 2000 Cheng H. and Sun Y. "A Hierarchical Approach to Color Image Segmentation Using Homogeneity," IEEE Transactions on Image Processing, Vol. 9, No. 12, pp. 2071-2082, 2000.

Cheng 2003 Cheng J. and Wen-Hao H. "A pseudo-Gaussian-based compensatory neural fuzzy system," IEEE International Conference on Fuzzy Systems, Vol. 1, pp. 214-219, 2003.

Chiang 2007 Chiang M., Reiss A., Lee A., Bellugi U., Galaburda A., Korenberg J., Mills D., Toga A. and Thompson P. "3D Pattern of Brain Abnormalities in Williams Syndrome Visualized using Tensor-Based Morphometry," NeuroImage Vol. 36, Issue 4, pp. 1096-1109, 2007.

Chuang 2006 Chuang K., Tzeng H., Chen S., Wu J. and Chen T. "Fuzzy C-Means Clustering with Spatial Information for Image Segmentation," Computerized Medical Imaging and Graphics 30, pp. 9-15, 2006.

Clark 1998 Clark M., Hall L., Goldgof D., Velthuizen R., Murtagh R. and Silbiger M. "Automatic Tumor Segmentation using Knowledge-Based Techniques," IEEE Transactions on Medical Imaging, Vol. 17, No. 2, pp. 187-201, 1998.

Clark 1999 Clark M, Hall L, Goldgof D, Velthuizen R, Murtagh F and Silbiger M. "Unsupervised Brain Tumor Segmentation using Knowledge Based and Fuzzy Techniques," Fuzzy and Neuro-Fuzzy Systems in Medicine, CRC Press, pp. 137-169, 1999.

Clarke 1991 Clarke, L. "MR Image Segmentation Using MLM and Artificial Neural Nets," Medical Physics, Vol. 18, No. 3, pp. 673, 1991.

Cobzas 2007 Cobzas, D., Birkbeck, N., Schmidt, M., Jagersand, M.and Murtha A. "3D Variational Brain Tumor Segmentation using a High Dimensional Feature Set," Mathematical Methods in Biomedical Image Analysis MMBIA 2007.

Coifolo 2004 Ciofolo C., Barriot C. and Hellier P. "Combining Fuzzy Logic and Level Set Methods for 3D MRI Brain Segmentation," IEEE International Symposium on Biomedical Imaging: Nano to Macro, pp. 161-164, Vol. 1, 2004.

Coifolo 2005 Ciofolo C. and Barriot C. "Bran Segmentation with Competitive Level Sets and Fuzzy Control," Information Processing in Medical Imaging 19, pp. 333-344, 2005.

Cohen 1989 Cohen L. "On active Contour Models and Balloons," Computer Vision, Graphics and Imasge Processing: Image Understanding 53 Vol. 2, pp. 211-218, 1989.

Cohen 1993 Cohen L. and Cohen I. "Finite-Element Methods for Active Contour Models and Balloons for 2-D And 3-D Images," IEEE Transactions on Pattern Analysis and Machine Intelligence 15, Vol. 11, pp. 1146-1131, 1993.

Corso 2008 Corso J., Sharon E., Dube S., El-Saden S., Sinha U., and Yuille A. "Efficient Multilevel Brain Tumor Segmentation With Integrated Bayesian Model Classification," IEEE Transactions On Medical Imaging, Vol. 27, No. 5, pp. 629-640, 2008.

D

Dale 1999 Dale A., Fischl B., Sereno M. "Cortical Surface-Based Analysis. I. Segmentation and Surface Reconstruction," Neuroimage 9(2), pp.179-194, 1999.

Dam 2004 Dam E., Loog M. and Letteboer M. "Integrating Automatic and Interactive Brain Tumor Segmentation," Proceedings of the 17th International Conference on Pattern Recognition, Vol. 3, pp. 790-793, 2004.

Damadian 1971 Damadian, R. "Tumor Detection by Magnetic Resonance," Science, 171: 1151, 1971.

DICOM 2008 Digital Imaging and Communications in Medicine (DICOM). "Part 1: Introduction and Overview," PS 3.1-2008, National Electrical Manufacturers Association, Copyright 2008.

Dickson 1997 Dickson S. and Thomas B. "Using Neural Networks to Automatically Detect Brain Tumours in MR Images," International Journal of Neural Systems 4, Vol. 1, pp. 91-99, 1997.

Dombi 2005 Dombi J. and Gera Z. "The Approximation of Piecewise Linear Membership Functions and Lukasiewicz Operators," Fuzzy Sets and Systems, Vol. 154, pp. 275-286, 2005

Dou 2007 Dou W., Ruan S., Chen Y., Bloyet D. and Constans J.M. "A framework of fuzzy information fusion for the segmentation of brain tumor tissues on MR images," Image and Vision Computing 25 , pp. 164-171, 2007.

Duch 2005 Duch W. "Uncertainty Of Data, Fuzzy Membership Functions, And Multilayer Perceptrons," IEEE Transactions on Neural Networks, Vol. 16, No. 1, pp. 10-23, 2005

Duncan 2000 Duncan J.and Ayache N. "Medical Image Analysis: Progress Over Two Decades And The Challenges Ahead. IEEE Transactions on Pattern Analysis and Machine Intelligence 22, pp. 85-106, 2000.

E

ECO 2009 European Cancer Observatory. International Agency for Research on Cancer, Lyon, 2009 (http://eu-cancer.iarc.fr, last accessed on: aug/ 2009).

Essig 2008 Essig M. "Intracranial Tumors," Magnetic Resonance Tomography, pp.243-302, 2008.

ESTRO 2009 European Society for Therapeutic Radiology and Oncology. http://www.estro.org/ , 2009

F

Farag 2005 Farag A., Ahmed M., El-Baz A. and Hassan H. "Advanced Segmentation Techniques," Handbook of Biomedical Image Analysis, Vol. I:, Segmentation Models Part A, pp. 479-533, 2005.

Fennema 2006 Fennema C., Ozyurt I., Clark C., Morris S., Bischoff A., Bondi M., Jernigan T., Fischl B., Segonne F., Shattuck D., Leahy R., Rex D., Toga A., Zou K. and Brown G. "Quantitative Evaluation of Automated Skull-Stripping Methods Applied to Contemporary and Legacy Images: Effects of Diagnosis, Bias Correction, and Slice Location," Human Brain Mapping. 27 (2), pp. 99-113, 2006.

Filippi 2005 Filippi M. and Roca M. "Multiple Sclerosis: Other MR Techniques," MR Imaging in White Matter Diseases of the Brain and Spinal Cord, pp. 225-240, Springer, 2005.

Ferlay 2007 Ferlay J, Autier P, Boniol M, et al. "Estimates of the cancer incidence and mortality in Europe in 2006," Annals of Oncology, 18, pp.581-92, 2007.

Fletcher 2001 Fletcher L., Hall L., Goldgof D. and Reed F. "Automatic segmentation of nonenhancing brain tumors in magnetic resonance images," Artificial. Intelligence in Medicine, Vol. 21, pp. 43-63, 2001.

Foo 2006 Foo J.L. "A Survey of User Interaction and Automation in Medical Image Segmentation Methods," Technical. report ISUHCI20062, Human Computer Interaction Department, Iowa State University, 2006.

G

Garcia 2004 Garcia C. and Moreno J. "Kernel based Method for Segmentation and Modeling of Magnetic Resonance Images," Lecture Notes in Computer Science 3315, pp. 636-645, 2004.

Gering 2002 Gering D., Grimson W. and Kikinis R. "Recognizing deviations from normalcy for brain tumor segmentation," Medical Image Computing and Computer-Assisted Intervention, Vol. 2488, pp. 388-395, 2002.

Giarra 2004 Giarratano J. and Riley G. "Expert Systems: Principles and Programming," Boston: PWS Publishing, Fourth Edition, 2004.

Gibbs 1996 Gibbs P., Buckley D., Blackb S. and Horsman A. "Tumour volume determination from MR images by morphological segmentation," Physics in Medicine and Biology 41, pp. 2437-2446, 1996.

Gies 2004 Gies V and Bernard T. "Statistical Solution to Watershed Oversegmentation," International Conference on Image Processing, Volume 3, pp. 1863-1866, 2004.

Gordillo 2009 Gordillo N., Montseny E. and Sobrevilla P. "Generating Histogram Based Fuzzy Membership Functions Addressed Large Data Sets," Fuzzy Sets and Systems, Manuscript number: FSS-D-08-00650, 2009.

Gordillo2 2009 Gordillo N., Montseny E. and Sobrevilla P. "Fuzzy Classification by Pairs over Three or More Populations," in press, 2009.

Green 2006 Green A. and Sasiadek J. "Heuristic Design of a Fuzzy Controller for a Flexible Robot," IEEE Transactions on Control Systems Technology, Vol. 14, Issue 2, pp. 293-300, 2006.

Guang 1999 Guang S. and Rees N. "Analysis and Design of Fuzzy Control Systems using Dynamic Fuzzy State Space Models," IEEE Transactions on Fuzzy Systems, Vol. 7, pp. 192-199, 1999.

Guru 2002 Gururangan S. and Friedman H.S. "Innovations in Design and Delivery of Chemotherapy for Brain Tumors," Neuroimaging Clinics of North America 12, pp.583-597, 2002.

H

Hahn 2000 Hahn H. and Peitgen H. "The Skull Stripping Problem in MRI Solved by a Single 3D Watershed Transform," Proceeding of MICCAI, LNCS 1935, pp.134-143, 2000.

Hanman 2004 Hanmandlu M., See J. and Vasikarla S. "Fuzzy Edge Detector using Entropy Optimization," Proceedings of International Conference on Information Technology: Coding and Computing, Vol. 1, pp. 665-670, 2004.

Hao 2006 Hao J. and Wang Q. "Watershed Based Level Set Evolution: A Novel Approach for MRA Segmentation," Proceedings of the IEEE International Conference on Mechatronics and Automation, pp. 1372-1376, 2006.

Haris 1998 Haris K., Efstratiadis S., Maglaveras N. and Katsaggelos A. "Hybrid Image Segmentation Using Watersheds and Fast Region Merging," IEEE Transactions on Image Processing, Vol. 7, No. 12, pp. 1684-1699, 1998.

Hima 2001 Himavathi S. and Umamaheswari B. "New Membership Functions for Effective Design and Implementation of Fuzzy Systems," IEEE Transactions on Systems, Man, and Cybernetics, Part A: Systems and Humans, Vol. 31, No. 6, pp. 717-723, 2001.

Hiong 1993 Hiong K. "The difference method: a way of detecting abnormalities in MRI images," Proceedings of International Joint Conference on Neural Networks, Vol. 2, Issue 25-29, pp. 1227-1230, 1993.

Ho 2002 Ho S., Bullitt E. and Gerig G. "Level Set Evolution with Region Competition: Automatic 3-D Segmentation of Brain Tumors," Proceedings of. International Conference on Pattern Recognition, Vol. I, pp. 532-535, 2002.

Hornak 2008 Hornak J. "The Basics of MRI," Copyright 1996-2008.

Hounsf 1946 Hounsfield G. "Computarised Transverse Axial Scanning (Tomography). Part 1: Description of System," The British Journal of Radiology 46, pp. 1016-1022, 1946.

I

Iftek 2009 Iftekharuddin K., Zheng J., Islam M. and Ogg R. "Fractal-Based Brain Tumor Detection in Multimodal MRI," Applied Mathematics and Computation 207, pp. 23-41, 2009.

J

Jain 1995 Jain R., Kasturi R. and Schunck B. "Machine Vision," McGraw-Hill, Inc., 1995.

Jin 2000 Jin Y. "Fuzzy Modelling of High-Dimensional Systems: Complexity Reduction and Interpretability Improvement," IEEE Transactions on Fuzzy Systems, Vol. 8, pp. 212-220, 2000.

K

Kang 1999 Kang D. "Stable Snake Algorithm for Convex Tracking of MRI Sequences," Electronic Letters, Vo1.35, pp. 1070-107I, 1999.

Kannan 2008 Kannan S. "A New Segmentation System for Brain MR Images Based on Fuzzy Techniques," Applied Soft Computing 8, pp. 1599-1606, 2008.

Kass 1987 Kass M., Witkin A. and Terzopoulos D. "Snake: Active Contour Models," Proceedings of the First International Conference on Computer Vision, pp.259-268, 1987.

Kaus 2001 Kaus M., Warfield S., Nabavi A., Black P., Jolesz F. and Kikinis R. "Automated Segmentation of MRI of Brain Tumors," Radiology 218 2, pp. 586-591, 2001.

Kato 2007 Kato H., Kanematsu M., Zhang X., Saio M., Kondo H., Goshima S. and Fujita H. "Computer-Aided Diagnosis of Hepatic Fibrosis: Preliminary Evaluation of MRI Texture Analysis Using the Finite Difference Method and an Artificial Neural Network," American Journal of Roetgenology 189, pp.117-122, 2007.

Khotan 2009 Khotanlou H., Colliot O., Atif J. and Bloch I. "3D Brain Tumor Segmentation in MRI using Fuzzy Classification, Symmetry Analysis and Spatially Constrained Deformable Models," Fuzzy Sets and Systems, Vol. 160, Issue 10, pp. 1457-1473, 2009.

Kichen 1995 Kichenassamy S., Kumar A., Olver P., Tannenbaum A. and Yezzi A. "Gradient Flows and Geometric Active Contour Models," IEEE Proceedings of the International Conference on Computer Vision, pp. 810-815, 1995.

Kohonen 2000 Kohonen T, Kaski S, Lagus K, Salojarvi J, Paatero V and Saarela A. "Self-organization of a Massive Document Collection," IEEE Transactions on Neural Networks 11, pp. 574-585, 2000.

Kodaka 2004 Kodaka M. "Requirements for Generating Sigmoidal Time-course Aggregation in Nucleation-Dependent Polymerization Model," Biophysical Chemistry Vol. 107, pp. 243-253, 2004

Kong 2006 Kong J., Wang J., Lu Y., Zhang J., Li Y. and Zhang B. "A Novel Approach for Segmentation of MRI Brain Images," IEEE Mediterranean Electrotechnical Conference, MELECON pp. 525-528, 2006.

Krein 1992 Kreinovich V., Quintana C. and Reznik L. "Gaussian Membership Functions are Most Adequate in Representing Uncertainty in Measurements," Proceedings of North American Fuzzy Information Processing Society Conference, Vol. 2, pp. 618-624, 1992.

Kumar 2006 Kumar S. and Hebert M. "Discriminative Random Fields: A Discriminative Framework for Contextual Interaction in Classification," International Journal of Computer Vision, Vol. 68, No. 2, pp. 179-201, 2006.

Kundel 2002 Kundel H. and Dean P. "Tumor Imaging," Image-Processing Techniques for Tumor Detection, ISBN: 0-8247-0637-4, pp. 1-17, 2002.

L

Lafferty 2001 Lafferty J., McCallum A. and Pereira F. "Conditional random fields: Probabilistic Models for Segmenting and Labeling Sequence Data," Proceedings of the International Conference on Machine Learning, pp. 282-289, 2001.

Lakare 2000 Lakare S. "3D Segmentation Techniques for Medical Volumes," Center of Visual Computer, state university of NY, Stony Brooks, 2000.

Law 2001 Law A., Zhu H., Lam F. and Chan F. "Tumor Boundary Extraction in Multislice MR Brain Images using Region and Contour Deformation," Proceedings of the International Workshop on Medical Imaging and Augmented Reality, pp. 183-187, 2001.

Law 2002 Law A., Lam F. and Chan F. "A Fast Deformable Region Model for Brain Tumor Boundary Extraction," International Conference of the Engineering in Medicine and Biology Society, Vol. 2, pp. 1055-1056, 2002.

Lazaro 2005 Lazaro J., Arias J., Matin J., Cuadrado C. and Astarloa A. "Implemenation of a Modified Fuzzy C-Means Clustering Algorithm for Real-Time Applications," Microprocessors and Microsystems, Vol. 29, Issues 8-9, pp. 375-380, 2005.

Letteboer 2001 Letteboer M., Niessen W., Willems P., Dam E. and Viergever M. "Interactive Multi-Scale Watershed Segmentation of Tumors in MR Brain Images," Proceedings. of the IMIVA workshop of MICCAI, 2001.

Lee 2005 Lee C. H., Schmidt M., Murtha A., Bistritz A., Sander J. and Greiner R. "Segmenting Brain Tumor with Conditional Random Fields and Support Vector Machines," Computer Vision for Biomedical Image Applications, pp. 469-478, 2005.

Lefohn 2003 Lefohn A., Cates J. and Whitaker R. "Interactive, GPU-based Level Sets For 3D Brain Tumor Segmentation," Technical Report, University of Utah, April 2003.

Li 1993 Li C., Goldgof D., and Hall L. "Automatic Segmentation and Tissue Labeling of MR Brain Images. IEEE TMI, 12(4), pp.740-750, 1993.

Li 2000 Li S. "Markov Random Field Modeling in Image Analysis, Springer-Verlag, New York, 2001.

Li 2001 Li S. "Markov Random Field Modeling" Image Analysis. Springer-Verlag, Tokyo, 2001.

Links 1998 Links J., Beach L. and Subramaniam B. "Edge complexity and partial volume effects," Journal of Computer Assisted Tomography, Vol. 22, No.3, pp. 450-458, 1998.

Liu 1997 Liu X. and Chai T. "Fuzzy Logic Strategy on Boiler Control Problem," Proceedings of the American Control Conference, pp. 1264-1266, 1997.

Lo 2002 Lo S. "The Application of an ANFIS and Grey System Method in Turning Tool-Failure Detection," The International Journal of Advanced Manufacturing Technology, Vol. 19, No. 8, pp. 564-572, 2002.

Luger 2008 Luger G. "Artificial Intelligence: Structure and Strategies for Complex Problem Solving," Addison-Wesley, Sixth Edition, 2008.

Luo 2003 Luo S., Li R. and Ourselin S. "A New Deformable Model Using Dynamic Gradient Vector Flow and Adaptive Balloon Forces," APRS Workshop on Digital Image Computing, pp. 9-14., 2003.

Luo 2006 Luo S. "Automated Medical Image Segmentation Using a New Deformable Surface Model,"International Journal of Computer Science and Network Security, Vol.6, No.5A, pp. 109-115, 2006.

M

Mahajan 2008 Mahajan S. and Schucany W. "Symmetric Bilateral Caudate, Hippocampal, Cerebellar, and Subcortical White Matter MRI Abnormalities in in Adult Patient With Heat Stroke," Baylor University Medical Center Proceedings, 21(4), pp. 433-436, 2008.

Makre 2003 Makrehchi M. and Kamel M. "An Information Theoretic Approach to Generating Membership Functions from Real Data," International Conference of the North American Fuzzy Information Processing Society, pp. 44-49, 2003.

Malladi 1995 Malladi R., Sethian J. and Vemuri B. "Shape Modeling with Front Propagation: A Level Set Approach," IEEE Transactions on Pattern Analysis and Machine Intelligence 17 Vol. 02, pp. 158-175, 1995.

Mansfield 1977 Mansfield P. "Multi-planar Image Formation using NMR Spin Echoes," Journal of Physics C: Solid State Physics 10, 55, 1977.

Mayer 2009 Mayer A. and Greenspan H. "An Adaptive Mean-Shift Framework for MRI Brain Segmentation," IEEE Transactions on Medical Imaging, 28 (8), pp. 1238-1250, 2009.

Mazzara 2004 Mazzara, G., Velthuizen, R., Pearlman, J., Greenberg, H., and Wagner, H. "Brain Tumor Target Volume Determination for Radiation Treatment Planning through Automated MRI Segmentation," International Journal of Radiation Oncology*Biology*Physics, 59(1), pp. 300-312, 2004.

Medasani 1998 Medasani S., Kim J. and Krishnapuram R. "An Overview of Membership Function Generation Techniques for Pattern Recognition," International Journal of Approximate Reasoning, pp. 391-417, 1998.

McIner 1996 McInerney T. and Terzopoulos D. "Deformable Models in Medical Image Analysis: A Survey," Medical Image Analysis 1, Vol. 2, pp. 91-108, 1996.

McIner 2000 McInerney T. and Terzopoulos D. "Deformable Models," Handbook of Medical Imaging Processing and Analysis, pp. 127-145, 2000.

Montsen 2001 Montseny E. and Sobrevilla P. "On Fuzzy Rule-Based Algorithms for Image Segmentation using Gray-Level Histogram Analysis," Proceedings of the 2nd International Conference in Fuzzy Logic and Technology, pp. 59-62, 2001.

Moreno 2004 Moreno F., Baturone I., Solano S. and Barriga A. "The Parametric Definition of Membership Functions in XFL3," IEEE International Conference on Fuzzy Systems, Vol. 2, pp. 761-766, 2004.

Muroff 1995 Muroff L.R. and Runge V.M. "The Use of MR Contrast in Neoplastic Disease of the Brain," Top Magnetoc Resonance Imaging 7, pp. 137-157, 1995.

Muruga 2007 Murugavalli S. and Rajamani V. "An Improved Implementation of Brain Tumor Detection Using Segmentation Based on Neuro Fuzzy Technique," Journal of Computer Science 3, Vol.11, pp. 841-846, 2007.

N

Neuwelt 2004 Neuwelt E.A. "Mechanisms of Disease: the Blood-Brain Barrier," Neurosurgery 54, pp. 131-140, 2004.

Nobel 2003 Nobel Prize in Physiology or Medicine. "Discoveries Concerning the Use of Magnetic Resonance to Visualize Different Structures," 2003.

Novell 1987 Novelline R. and Squire L. "Living Anatomy," Hanley and Belfus, 1987.

O

Ohgaki 2005 Ohgaki H. and Kleihues P. "Population-Based Studies on Incidence, Survival Rates, and Genetic Alterations in Astrocytic and Oligodendroglial Gliomas," Journal of Neuropathology and Experimental Neurology 64, pp. 479-489, 2005.

Olaba 2001 Olabarriaga S. and Smeulders A. "Interaction in the Segmentation of Medical Images: A Survey," Medical Image Analysis 5, pp. 127-142, 2001.

Osher 1988 Osher S. and Sethian, J. A. "Fronts propagating with curvature-dependent speed: Algorithms based on Hamilton-Jacobi formulations," Journal of Computational. Physics, Vol. 79, No. 1, pp. 12-49, 1988.

Osher 2003 Osher S. and Fedkiw R. "Level Set Methods and Dynamic Implicit Surfaces," New York: Springer-Verlag; 2003.

OsherP 2003 Osher S. and Paragios N. "Geometric Level Set Methods in Imaging, Vision, and Graphics," New York: Springer-Verlag; 2003.

Ott 1988 Ott R., Flower M., Babich J. and Marsden P. "The Physics of Radioisotope Imaging," The Physics of Medical Imaging, pp. 142-318, 1988.

Ozkan 1993 Ozkan M., Dawant B. and Maciunas R. "Neural-Network-Based Segmentation of Multi-Modal Medical Images: A Comparative and Prospective Study," IEEE Transactions on Medical Imaging, 12(3), pp. 534-544, 1993.

P

Papage 2008 Papageorgiou E., Spyridonos P., Glotsos D., Stylios C., Ravazoula P., Nikiforidis G. and Groumpos P. "Brain Tumor Characterization using the Soft Computing Technique of Fuzzy Cognitive Maps," Applied Soft Computing 8, pp. 820-828, 2008.

Patel 2004 Patel M. and Tse V. "Diagnosis and Staging of Brain Tumors," Seminars in Roentgenology, Vol. 39, No. 3, pp. 347-360, 2004.

Pedrycz 2002 Pedrycz W. and Vukovich G. "On Elicitation of Membership Functions," IEEE Transactions on Systems, Man, and CyberneticsPart A: Systems And Humans, Vol. 32, No. 6, pp. 761-767, 2002.

Pham 1999 Pham D. and Prince J. "Adaptive Fuzzy Segmentation of Magnetic Resonance Images," IEEE Transactions on Medical Imaging 18, pp. 737-752, 1999.

Pham 2003 Pham D. "Unsupervised Tissue Classification in Medical Images using Edge-Adaptive Clustering," Proceedings of the International Conference IEEE EMBS, Vol. 25, pp. 634-637, 2003.

Phillips 1995 Phillips W., Velthuizen R., Phupanich S., Hall L., Clarke L. and Silbiger M. "Application of Fuzzy C-Means Segmentation Technique for Tissue Differentiation in MR Images of a Hemorrhagic Glioblastoma Multiforme," Magnetic Resonance Imaging., Vol. 13, No. 2, pp. 277-290, 1995.

Popuri 2009 Popuri K., Cobzas D., Jagersand M, Shah S. and Murtha A. "3D Variational Brain Tumor Segmentation on a Clustered Feature Set," SPIE Medical Imaging 2009.

Prasad 2006 Prasad P.V. "Magnetic Resonance Imaging: Methods and Biologic Applications," Vol. 124, Humana Press; 2006.

Prastawa 2003 Prastawa M., Bullitt E., Moon N., Van Leemput K. and Gerig G. "Automatic Brain Tumor Segmentation by Subject Specific Modification of Atlas Priors," Academic Radiology, Vol. 10, Issue 12, pp. 1341-1348, 2003.

Prastawa 2004 Prastawa M., Bullitt E., Ho S. and Gerig G. "A Brain Tumor Segmentation Framework based on Outlier Detection," Medical Image Analysis, Vol. 8, No. 3, pp. 275-283, 2004.

Purcell 1946 Purcell E., Torrey H. and Pound R. "Resonance Absorption by Nuclear Magnetic Moments in a Solid," Physical Review 69, pp.37-38, 1946.

Q

Quian 1991 Qian W. and Titterington D. "Estimation of Parameters in Hidden Markov Models," Philosophy Transactions of the Real Society of London A, Vol. 337, pp.407-428, 1991.

R

Ratan 2009 Ratan R., Sharma S. and Sharma S.K. "Multiparameter Segmentation and Quantization of Brain Tumor from MRI Images," Indian Journal of Science and Technology, Vol.2, No 2, pp. 11-15, 2009.

Ray 2008 Ray N., Greiner R. and Murtha A. "Using Symmetry to Detect Abnormalies in Brain MRI," Computer Society of India Communications, 31(19), pp 7-10, 2008.

Reddick 1997 Reddick W., Glass J., Cook E., Elkin T. and Deaton R. "Automated Segmentation and Classification of Multispectral Magnetic Resonance Images of Brain Using Artificial Neural Networks," IEEE Transactions on Medical Imaging16, Vol. 6, pp. 911-918.

Reiser 2008 Reiser M.F, Semmler W. and Hricak H: "Magnetic Resonance Tomography," ISBN 978-3-540-29354-5, 2008.

Rexilius 2007 Rexilius J., Hahn H., Klein J., Lentschig M. and Peitgen H. "Multispectral Brain Tumor Segmentation based on Histogram Model Adaptation," Proceedings of SPIE Conference on Medical Image Computing, pp. 65140V-1-65140V-10, 2007.

Rubner 1998 Rubner Y., Tomasi C. and Guibas L. "The Earth Mover's Distance as a Metric for Image Retrieval," STAN-CS-TN-98-86, Stanford University, 1998.

S

SalBad 2005 Salman Y. and Badawi A. "Validation Techniques for Quantitative Brain Tumor Measurements," The 27th Annual International Conference of the IEEE Engineering in Medicine and Biology Society, pp. 7048-7051, 2005.

Salman 2005 Salman Y., Badawi A., Assal M. and Alian S. "New automatic technique for tracking brain tumor response," International Conference on Biological and Medical Physics, UAE, 2005.

Sammou 1996 Sammouda R., Niki N. and Nishitani H. "A Comparison Of Hopfield Neural Network And Boltzmann Machine In Segmenting Mr Images Of The Brain," IEEE Transactions on Nuclear Science 43, Vol. 6, pp. 3361-3369, 1996.

Sandor 1997 Sandor S. and Leahy R. "Surface-Based Labeling of Cortical Anatomy using a Deformable Database," IEEE Transactions on Medical Imaging 16, pp. 41-54, 1997.

Sato 2000 Sato M., Lakare S., Wan M. and Kaufman A. "A Gradient Magnitude Based Region Growing Algorithm For Accurate Segmentation," Proceedings of the International Conference on Image Processing, Vol.3, pp. 448-451, 2000.

Schmi 2005 Schmidt M., Levner I., Greiner R., Murtha A. and Bistritz A. "Segmenting Brain Tumors using Alignment-Based Features," International Conference on Machine Learning, 2005.

SchmiT 2005 Schmidt M. "Automatic Brain Tumor Segmentation," Master's thesis, University of Alberta, 2005.

Seghier 2008 Seghier M., Ramackhansingh A., Crinion J., Lett A. and Price C. "Lesion Identification using Unified Segmentation-Normalisation Models and Fuzzy Clustering," Neuroimage 41, pp. 1253-1266, 2008.

Seghier 2007 Seghier M., Friston K. and Price J. "Detecting Subject-Specific Activations using Fuzzy Clustering," Neuroimage 36, pp. 594-605, 2007.

Segonne 2004 Segonne F., Dale A., Busa E., Glessner M., Salat D., Hahn H. and Fischl B. "A Hybrid Approach to the Skull Stripping Problem in MRI," Neuroimage 22(3), pp. 1060-1075, 2004.

Shanthi 2007 Shanthi K. J and Sasi Kumar M. "Skull Stripping and Automatic Segmentation of Brain MRI Using Seed Growth and Threshold Techniques," Conference on Intelligent and Advanced Systems ICIAS 2007, pp. 422-426, 2007.

Shen 2006 Shen H. "Methods and Applications for Segmenting 3D Medical Image Data," Addvances in Image and Video Segmentation, IRM Press, pp. 250-269, 2006.

Siddiqi 1998 Siddiqi K., Lauziere Y., Tannenbaum A. and Zucker S. "Area and Length Minimizing Flows for Shape Segmentation," IEEE Transactions on Image Processing 7, Vol. 3, pp. 433-443, 1998.

Siyal 2005 Siyal M. andYu L. "An Intelligent Modified Fuzzy C-Means Based Algorithm for Bias Field Estimation and Segmentation of Brain MRI," Pattern Recognition Letters 26, pp. 2052-2062, 2005.

Smirnio 1999 Smirniotopoulos J. "The New WHO Classification of Brain Tumors," Neuroimaging Clinics of North America, Vol. 9, No. 4, pp. 595-613, 1999.

Smith 2002 Smith S. "Fast Robust Automated Brain Extraction," Human Brain Mapping 17(3), pp.143-155, 2002.

Stad 2004 Stadlbauer A., Moser E., Gruber S., Buslei R., Nimsky C., Fahlbusch R. and Ganslandt O. "Improved Delineation of Brain tumors: An Automated Method for Segmentation based on Pathologic Changes of 1H-MRSI Metabolites in Gliomas," NeuroImage 23, pp. 454-461, 2004.

Supot 2007 Supot S., Thanapong C., Chuchart P. and Manas S. "Segmentation of Magnetic Resonance Images Using Discrete Curve Evolution and Fuzzy Clustering," Proceedings of the 2007 IEEE International Conference on Integration Technology, pp. 697-700, 2007.

Szilgyi 2003 Szilgyi L., Beny Z., Szilgyi S. and Adam H. "MR Brain Image Segmentation using an Enhanced Fuzzy C-Means algorithm," Proceedings of the International Conference IEEE EMBS, Vol. 25, pp. 724-726, 2003.

Szilgyi 2007 Szilgyi L., Szilgyi S. and Beny Z. "A Modified Fuzzy C-Means Algorithm for MR Brain Image Segmentation," Lecture Notes in Computer Science, Vol. 4633, pp. 866-877, 2007.

T

Tayel 2006 Tayel M. and Abodou M. "A Neuro-Difference Fuzzy Technique for Automatic Segmentation of Region of Interest in Medical Imaging," Proceedings of the Twenty Third National Radio Science Conference NRSC, pp. 1-7, 2006.

Tran 2005 Tran T., Wehrens R. and Buydens L. "Clustering Multispectral Images: A Tutorial," Chemometrics and Intelligent Laoratory Systems, Vol. 77, pp. 3-17, 2005.

V

Valsasina 2005 Valsasina P., Rocca M., Agosta F., Benedetti B., Horsfield M., Gallo A., Rovaris M., Comi G. and Filippi M. "Mean Diffusivity and Fractional Anisotropy Histogram Analysis of the Cervical Cord in MS Patients," NeuroImage, Vol. 26, Issue 3, pp. 822-828, 2005.

Vander 1990 Vander A., Sherman J. and Luciano D. "Human Physiology: The Mechanisms of Body Function," McGraw-Hill Publishing Co., Fifth edition, 1990.

Veloz 2008 Veloz A., Chabert S., Salas R., Orellana A. and Vielma J. "Fuzzy Spatial Growing for Glioblastoma Multiforme Segmentation on Brain Magnetic Resonance Imaging," Lecture Notes in Computer Science, Vol. 4756, pp. 861-870, 2008.

Vernon 1991 Vernon D. "Image Analysis," Machine Vision: Automated Visual Inspection and Robot Vision, pp. 118-136, 1991

Vijaya 2007 Vijayakumar C., Damayanti G., Pant R. and Sreedhar C. "Segmentation and Grading of Brain Tumors on Apparent Diffusion Coefficient Images Using Self-Organizing Maps," Computerized Medical Imaging and Graphics 31, pp. 473-484, 2007.

Vincent 2004 Vincent F., Chong H., Zhou J., James B., Khoo K., Huang J. and Lim T. "Tongue Carcinoma: Tumor Volumen Measurement," International Journal of Radiation Oncology Biology Physics, Vol. 59, No. 1, pp. 59-66, 2004.

W

Walter 2007 Walter A. "Brain Tumors," The Neumours Foundation, Reviewed in 2007.

Wiselin 2005 Wiselin G. and Ganesan L. "Unsupervised Segmentation using Fuzzy Logic based Texture Spectrum for MRI Brain Images," World Academy of Science, Engineering and Technology 5, pp. 155-157, 2005.

White 1999 White D., Houston, A., Sampson, W. and Wilkins, G. "Intra and Interoperator Variations in Region-Of-Interest Drawing and Their Effect on the Measurement of Glomerular Filtration Rates," Clinical. Nuclear Medicine, Vol. 24, pp. 177-181, 1999.

Wong 2005 Wong K. "Medical Image Segmentation: Methods and Applications in Functional Imaging," Handbook of Biomedical Image Analysis, Vol. 2, Segmentation Models Part B, pp. 111-182, 2005.

WHO 2008 World Health Organization. "Statistical Information System, Mortality statistics,", 2008.

Wootton 2003 Wootton D., Guez A., Vaidyanathan P., Avinash D., Stablum J., McDonough J. Udupa J. and Arens R. "Model of Upper Airway Flow Restriction in Children with Obstructive Sleep Apnea," IEEE Proceedings of the Bioengineering Conference, pp. 217-218, 2003.

Wu 1999 Wu T. and Chen S. "A New Method for Constructing Membership Functions and Fuzzy Rules from Training Examples," IEEE Transactions on Systems, Man, Cybernetics, B, Vol. 29, pp. 25-40, 1999.

X

Xie 2005 Xie K., Yang J., Zhang Z. and Zhu Y. "Semi-Automated Brain Tumor and Edema Segmentation using MRI," European Journal of Radiology 56 , pp. 12-19, 2005.

Xu 1998 Xu C. and Prince J. "Generalized Gradient Vector Flow External Forces for Active Contours," Signal Processing 71, pp. 131-139, 1998.

XuPrince 1998 Xu C. and Prince J. "Snakes, Shapes, and Gradient Vector Flow," IEEE Transactions on Images Processing 7, Vol. 3, pp. 359-369, 1998.

Xu 2000 Xu C., Pham D. and Prince J. "Current Methods in Medical Image Segmentation," Annual Review of Biomedical Engineering, Annual Reviews, Vol. 2, pp. 315-337, 2000.

Y

Yao 2006 Yao J. "Image Processing in Tumor Imaging," New Techniques in Oncologic Imaging, pp. 79-102, 2006.

Yezzi 1997 Yezzi A., Kichenassamy S., Kumar A., Olver P. and Tannenbaum A. "A Geometric Snake Model for Segmentation of Medical Imagery," IEEE Transactions on Medical Imaging 16, Vol. 2, pp. 199-209, 1997.

Yong 2004 Yong Y., Chongxun Z. and Pan L. "A Novel Fuzzy C-Means Clustering Algorithm for Image Thresholding," Measurement Science Review, Vol. 4, Section 1, pp. 11-19, 2004.

Z

Zhang 2001 Zhang X., and Roy R. "Derived Fuzzy Knowledge Model for Estimating the Depth of Anesthesia," IEEE Transaction on Biomedical Engineering 48(3), pp. 312-323, 2001.

Zhang 2004 Zhang J., Ma K., Er M. and Chong V. "Tumor Segmentation from Magnetic Resonance Imaging by Learning Via One-Class Support Vector Machine," Proceedings of International Workshop on Advanced Image Technology, pp. 207-211, 2004.

Zhu 1997 Zhu Y. and Yan H. "Computerized Tumor Boundary Detection using a Hopfield Neural Network," IEEE Transactions on Medical Imaging 16, pp. 55-67, 1997.

Zhuang 2006 Zhuang A., Valentino D. and Toga A. "Skull-Stripping Magnetic Resonance Brain Images using a Model-Based Level Set," Neuroimage. 32 (1), pp. 79-92, 2006.

Publications Derived From the Thesis

Gordillo N. , Montseny E. and Sobrevilla P. "On the Use of the Distribution Function for Generating Fuzzy Membership Functions Adressed to Image Processing," II Symposium on Fuzzy Logic and Soft Computing. Pg 229-236. LFSC (EUSFLAT) 2007.

Gordillo N. , Montseny E. and Sobrevilla P. "Generating Histogram Based Fuzzy Membership Functions Addressed Large Data Sets," Fuzzy Sets and Systems, Manuscript number: FSS-D-08-00650, 2009.

López J. and Gordillo N. Pupil Detection Algorithm Addressed to Drowsiness Detection based on Computer Vision and Fuzzy Techniques, Thesis 66044, Universidad Autónoma de Ciudad Juárez, Nov. 2009.

Gordillo N. , Montseny E. and Sobrevilla P. "Fuzzy Classification by Pairs over Three or More Populations," Manuscript Submitted IEEE Transactions on Fuzzy Systems, Manuscript Number TFS-2010-0130, 2010.

Gordillo N. , Montseny E. and Sobrevilla P. "A New Fuzzy Approach to Brain Tumor Segmentation," IEEE International Conference on Fuzzy Systems, Barcelona, 2010.

Appendix A

Nuclear Magnetic Resonance Phenomena and MR Image Formation

A.1 Nuclear Magnetic Resonance

Nuclear Magnetic Resonance is a physical phenomenon of the magnetic property of nuclei, which have a positive nuclear spin quantum number. Under the influence of an external static magnetic field, these nuclei will precess about the direction of the magnetic field with an angular frequency, the $Larmor frequency$. Through absorption (excitation) and emission (relaxation) of radio frequency energy at the resonance frequency, the Larmor equation, and the processing of this raw data by the Fourier transformation, physical, chemical, electronic, and structural information about molecules can be obtained.

A.1.1 Behavior of Nuclei in a Magnetic Field

The phenomenon of NMR derives from the fact that certain nuclei possess tiny magnetic moments. In the presence of an applied magnetic field, the magnetic moments undergo a rotational motion known as precession. The explanation of nuclear precession lies in the relationship between the magnetic moment of the nucleus and its intrinsic spin.

Spin is a fundamental property of certain nuclei, particularly hydrogen, that

contain unpaired protons or neutrons. Although spin is an essentially quantum mechanical property, it can be visualized as the rotation of the nucleus about its own axis. Because the nucleus is positively charged, its spin entails a circulation of charge. The circulation of charge associated with the nuclear spin similarly endows the nucleus with a magnetic moment. The nucleus therefore produces its own tiny magnetic field, and is subject to a torque in the presence of an external field. The torque attempts to turn the magnetic moment of the nucleus into alignment with the external field, where its energy is a minimum. Because the magnetic moment of the nucleus is derived from its spin, the orientation of the magnetic moment is locked to the spin axis. This is expressed through next equation:

$$\mu = \gamma I \tag{A.1}$$

where μ is the magnetic moment of the nucleus and I is its spin. The factor γ is known as the gyromagnetic ratio, and is a property of the nucleus. I is a vector quantity, and thus has both magnitude and direction. The direction of I is given by the spin axis. μ is parallel to I and determines the orientation of the nucleus' intrinsic magnetic field.

Because the magnetic moment of the nucleus is parallel to its spin, any change in the direction of the magnetic moment requires a corresponding reorientation of the spin axis. When a nucleus is subjected to a magnetic field, its magnetic moment does not simply swing into alignment with the field but also precesses about the direction of the field. The frequency at which the nucleus precesses about the magnetic field is known as the $Larmor frequency$, ω_L. It can be shown, using classical mechanics, that the value of the $Larmor frequency$ is proportional to the strength of the magnetic field in the z component, B_0, and the gyromagnetic ratio of the nucleus:

$$\omega_L = \gamma B_0 \tag{A.2}$$

This is the angular frequency of precession. Additionally, the precession of vector μ around vector B_0 is done clockwise.

The nuclei most commonly visualized by magnetic resonance imaging are those of the hydrogen atoms, because they are present throughout the body in

water and fat.

The net magnetic field experienced by the nucleus is a sum of the external field applied to the tissue and the much smaller fields generated by the electrons surrounding the nucleus. These additional fields alter the precession frequency of the nucleus by a tiny fraction known as the chemical shift. The value of the chemical shift is characteristic of the molecular group in which the nucleus resides, and thus provides a distinctive signature for each metabolite. By analyzing the frequencies present in the MR signal, the examiner can identify the metabolites in the tissue and estimate their concentration.

A.1.2 Excitation and Signal Detection

The net magnetic field of all the nuclei in a given volume of tissue can be specified by the vector sum of their magnetic moments. The sum is known as the nuclear magnetization, and denoted by M. The component of M that lies in the transverse plane (perpendicular to the static field B_0) rotates at the $Larmor frequency$, as the nuclei precess. This produces an oscillating magnetic field that can be detected with a Radio Frequence (RF) receiver coil. As the transverse magnetization rotates, the magnetic flux through the loop oscillates, inducing a small alternating voltage in the coil. The MR signal is thus proportional to the transverse component of M.

At equilibrium, the nuclei precess with random phases. The transverse components of their magnetic moments, therefore, cancel out and produce no detectable signal. There is, however, a small net magnetization, M_0, in the longitudinal direction (parallel to B_0) that cannot be detected directly, because it does not oscillate, but is necessary for producing the signal, as we will soon show. The equilibrium magnetization arises because the nuclei exhibit a slight preference for being aligned along the direction of the external magnetic field. This can be explained on the basis of energy considerations. The energy of a magnetic moment depends on its orientation in the magnetic field, through the equation:

$$E = -\mu_z B_0 \tag{A.3}$$

The more closely the magnetic moment is aligned to the field, the lower its energy. The nuclei exhibit a slight preference for being tilted toward the

external field (up) rather than away from it (down). At equilibrium, therefore, a slightly more quantity of nuclei are oriented upwards than downwards. The small excess of nuclei pointing upwards gives rise to the equilibrium magnetization M_0.

By applying a transverse oscillating magnetic field to the tissue, at exactly the $Larmor frequency$, the nuclear magnetization can be tipped away from the longitudinal axis, so producing a finite component in the transverse plane. The excess nuclei that had been pointed upwards at equilibrium precess in synchrony, emitting a detectable signal. The process is a resonant excitation, and is similar to the mechanism involved in pushing a childs swing.

The equilibrium state of a swing is that in which it rests at the lowest point of its arc. Energy can be transferred to the swing by pushing it at its natural or resonant frequency. As the swing gains energy it begins to oscillate back and forth, and its amplitude of motion gradually increases. The resonant frequency of the swing is identical to the frequency at which it will oscillate by itself when the driving force is stopped.

Just as the swing can be made to oscillate by applying a periodic force, the nuclei in a sample of tissue can be made to precess in synchrony by applying a rotating magnetic field in the transverse plane. The applied field is denoted $B_1(t)$, and its frequency of rotation must exactly match the $Larmor frequency$ of the nuclei to satisfy the resonance condition. Because the $Larmor frequency$ falls in the RF regime, the process is described as RF excitation, and the resonance condition is written as $\omega_{RF} = \omega_L$. As the $B_1(t)$ field transfers energy to the nuclei, the amplitude of their transverse magnetization gradually increases. When the $B_1(t)$ field is switched off, the transverse magnetization continues to rotate at the $Larmor frequency$, producing an oscillating magnetic field that can be detected by the RF receiver coil. Eventually, however, the transverse magnetization will decay back to zero and the signal will disappear.

A.1.3 Quantum Mechanical Description

According to quantum mechanics, neither matter nor energy can be divided indefinitely into ever-smaller parts; on a sufficiently tiny scale can be found fundamental units, or quanta, which cannot be further divided. Electromagnetic energy, such as X-rays, light, and radio waves, exists in discrete energy packets, called photons. The energy of an individual photon, E_{photon}, coincides with the frequency, ω, of the electromagnetic wave:

$$E_{photon} = \omega \tag{A.4}$$

Whenever an atom or nucleus absorbs or emits electromagnetic waves, an entire photon is consumed or created. To conserve the total energy of the system, the atom or nucleus must simultaneously undergo a quantum jump to a state of different energy. However, a nucleus has just a few different states available to do it, because a separate quantization condition governs the angular momentum. This restricts the possible frequencies of the electromagnetic waves that the nucleus can absorb or emit.

Angular momentum is a vector quantity, whose direction is determined by the axis of rotation. The quantization condition for angular momentum stipulates that its component along any given measurement axis may adopt only certain discrete values. Because nuclear spin I is a form of angular momentum, this rule applies to the component of spin along the longitudinal axis, conventionally denoted I_z. The difference in the z-component of spin between adjacent states is ΔI_z.

When the nucleus is subjected to an external magnetic field, the energies of the states differ, and the energy differences among them can be used to derive the resonance condition governing RF excitation and signal emission.

As previously discussed, the energy of a nucleus depends on the orientation of its magnetic moment with respect to the external magnetic field, as given in Eq. (A.3). However, because the magnetic moment is proportional to the spin, through Eq. (A.1), the energy of the nucleus varies with the spin direction according to:

$$E = -\gamma I B_0 \tag{A.5}$$

The energy is thus proportional to the component of spin in the longitudinal direction,

$$E = -\gamma I_z B_0 \tag{A.6}$$

This relation shows that states with different I_z values have different energies when subjected to an external magnetic field. Because the angular momentum differs between adjacent spin-states by ΔI_z, the energy separation between the states is equal to:

$$\Delta E = \gamma B_0 \tag{A.7}$$

According to Eq. (A.2), the product γB_0 equals the $Larmor frequency$, ω_L, the energy difference can be written as:

$$\Delta E = \omega_L \tag{A.8}$$

Moreover, the excitation of the nucleus to the next energy level requires the absorption of a photon, whose energy equals this energy difference,

$$E_{photon} = \Delta E \tag{A.9}$$

Then, by substituting Eqs. (A.8) and (A.4) into (A.9), the frequency of the photon must exactly match the $Larmor frequency$. Because the value of the $Larmor frequency$ is typically on the order of MHz, the photon represents an RF wave of frequency:

$$\omega_{RF} = \omega_L \tag{A.10}$$

This is the resonance condition, which is derived here using the law of energy conservation, together with the rules of quantization.

The quantum mechanical interpretation of NMR is that a photon at the $Larmor frequency$ excites the nucleus to a higher energy state. The excited

nucleus may lose its energy through frictional processes to the environment, or it may decay back to its initial state, releasing a photon of the same frequency, which contributes to the observed MR signal.

A.1.4 Spin Relaxation

Excitation of nuclei by means of an RF pulse makes a macroscopic number of spins precess in synchrony, producing a rotational magnetic field that can be detected with an RF coil. However, the signal will not persist indefinitely because internuclear and intermolecular forces will cause loss of phase coherence among the spins, and a corresponding attenuation of the transverse magnetization. The nuclei lose energy to their surroundings, resulting in a recovery of the longitudinal magnetization to its equilibrium value. These processes are termed transverse and longitudinal relaxation, respectively. Relaxation processes limit the available acquisition time, and broaden the spectroscopic line-widths. However, because their relaxation rates depend on the molecular environment of the nuclei, they can be exploited to produce signal contrast among different tissues in MR imaging.

This section provides a brief discussion of the physical mechanisms underlying relaxation processes, and the means by which they can be harnessed to produce signal contrast.

Longitudinal relaxation, Basics of T1-Weighted Images

Excitation by an RF pulse, $B_1(t)$, increases the net energy of the nuclei above its equilibrium value. The nuclei will eventually lose that additional energy through interactions with neighboring nuclei and molecules, and the system will return to equilibrium. Because the net energy of the system is related to the longitudinal nuclear magnetization, the processes that cause loss of energy are collectively termed longitudinal relaxation. The timescale on which longitudinal relaxation occurs is denoted T1, and defined as the reciprocal of the rate of energy loss. The longitudinal relaxation time, T1, gives the time required for the longitudinal magnetization after a 90° pulse to grow to 63% of its equilibrium value, M_0, as depicted in Figure A.1-(a).

Because longitudinal relaxation is caused by interactions between the nuclei and their environment, the value of T1 varies according to the molecule in which the nucleus is bound, and the type of tissue in which it is present. For example, the T1 of tissue water tends to be longer in body fluids, such as blood

and cerebrospinal fluid, than in more solid tissues, such as the white matter of the brain. Intensity differences between these tissues can be achieved on an MR image by tailoring the acquisition so that it is sensitive to T1.

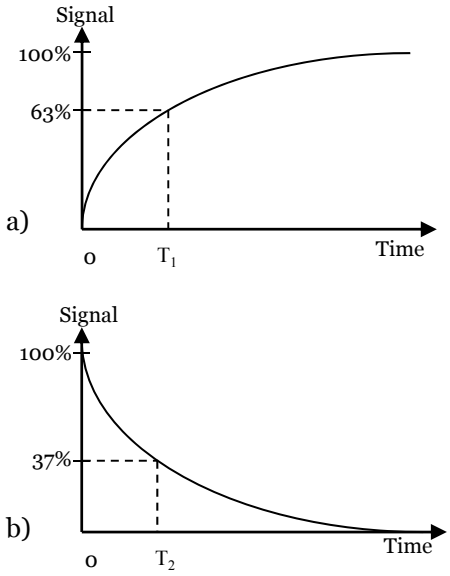

Figure A.1: Relaxation of the longitudinal (a) and transversal (b) magnetization after excitation by a 90° pulse.

Longitudinal relaxation arises from fluctuations in the local magnetic field at the site of each nucleus. The local magnetic field is a sum of the applied field, B_0, and the smaller secondary fields generated by the surrounding electrons, neighboring nuclei, and nearby molecules. As the host molecule moves and tumbles within the medium, the position of each nucleus varies randomly with respect to adjacent nuclei and molecules. As a result, the nucleus experiences a fluctuating magnetic field. If the fluctuations have frequency components equal to the $Larmor frequency$, they can induce transitions between nuclear energy states. Excited nuclei will, on average, lose energy to their surroundings. The energy loss continues until the nuclei reach thermal equilibrium with their environment, and the magnetization returns to its equilibrium value, M_0. The recovery of the longitudinal magnetization follows an exponential curve, given by next expression:

$$M_\zeta(t) = M_0 + [M_\zeta(0) - M_0]e^{-\frac{t}{T_1}} \tag{A.11}$$

where M_ζ denotes the longitudinal magnetization, and t is the time after the RF excitation. The value of $M_\zeta(0)$ is determined by the longitudinal magnetization available before the excitation and by the flip angle (FA) of the RF pulse.

Longitudinal relaxation occurs most efficiently when the molecular tumbling rate is near the $Larmor frequency$. Therefore, the value of T1 depends on the mobility of the host molecule, which, in turn, varies with molecular weight and tissue type. It turns out that the tumbling rate is closest to the $Larmor frequency$ for medium-sized molecules, such as lipids. Therefore, fat has a relatively short T1. By contrast, the free water in body fluids has a relatively long T1, because its molecular tumbling rate is much faster than the $Larmor frequency$. However, the T1 of water is shortened in solid tissues, where its motion is more restricted.

T1 differences among tissues are exploited to produce signal contrast on MR images. MRI involves the collection of a large amount of spatial information, what requires excitation and signal acquisition processes to be repeated many times in succession. The repetition time, TR, between successive excitations is important in determining the signal amplitude from a given tissue type. If the TR is short with respect to the T1 of the tissue, the longitudinal magnetization will not be fully recovered to its equilibrium value, M_0, before the next excitation. Because the magnetization remains partially saturated, the signal from the tissue is reduced accordingly. By comparison, a tissue with a faster relaxation rate will be less saturated and will exhibit a relatively higher signal. In general, the degree of magnetization recovery depends on the factor $exp^{(TR/T1)}$. If TR is chosen to be sufficiently short that the signal from each tissue depends heavily on its T1 value, the resulting image is described as being T1-weighted.

Transverse relaxation, Basics of T2-Weighted Images

The MR signal is produced by the transverse component of the magnetization, whose amplitude depends on the degree of phase coherence among the nuclei. The transverse magnetization is zero at equilibrium, and attains a finite value only through RF excitation by the $B_1(t)$ field. After excitation,

its amplitude gradually decays back to zero. The signal must, therefore, be acquired during the short period after the excitation pulse, but before the transverse magnetization has disappeared. Transverse relaxation occurs more rapidly than longitudinal relaxation, because it involves additional mechanisms that are related to dephasing among the spins, and originate from a variety of microscopic and mesoscopic processes. The component caused by microscopic processes depends on intrinsic factors, such as molecular size and tissue type, and occurs on a timescale denoted T2. Dephasing over a larger scale is a result of effects such as magnetic field inhomogeneity. This further shortens the coherence time of the transverse magnetization, within a given volume of tissue, until a value denoted by T2*. Tissue-dependent differences in both T2 and T2* can be exploited to produce signal contrast on MR images. Figure A.1-(b) shows the transverse relaxation. T2 gives the time required for the transverse magnetization after a 90° pulse drop to 37% of its original magnitude.

Variations in the magnetic local field's strength cause dephasing among the spins by making them precess at slightly different rates. On a microscopic scale, the variations are caused by the presence of neighboring nuclei and molecules, which produce their own tiny magnetic fields. Dephasing also arises when energy is exchanged between identical nuclei. These two processes contribute to T2 relaxation, and occur most efficiently if the molecular tumbling rate is low. Rapid motion tends to inhibit T2 relaxation by averaging out the effects of microscopic interactions over time. Free water in body fluids, for example, relaxes relatively slowly, because its molecules are in constant rotation. By comparison, molecules that are very large or bound to cell membranes have very short T2 values, because of their relative immobility. In diseased tissues, for any pathological process (inflammatory, tumor, degenerative, traumatic, etc.), cells have greater permeability to water, and consequently the content of free water is greater. For this reason, most tumors have low signal intensity on T1-weighted images, and high signal intensity on T2-weighted images.

Figure A.2 shows a graphical representation of the relationship of pathologic cells with relaxation times T1 and T2, where pathologic cells show lower signal intensity on T1 than healthy cells, and higher signal intensity on T2.

Dephasing also results from larger-scale variations in magnetic field strength, which arise from inhomogeneities in the applied field and differences in magnetic susceptibility among the tissues themselves. These effects contribute to T2* relaxation. Magnetic susceptibility refers to the tendency of a material to become magnetized in the presence of an external magnetic field. This alters the strength of the field both within the material itself and in its immediate

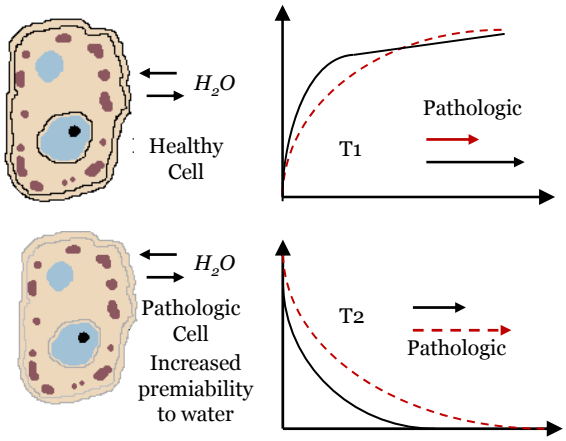

Figure A.2: Relationship of pathologic cells with relaxation times T1 and T2. As pathologic cells have greater permeability to water, they show lower signal intensity on T1 than healthy cells, and higher signal intensity on T2.

neighborhood. Ferromagnetic materials, such as iron, have very high susceptibility, and cause substantial distortions in the local magnetic field.

Air, by contrast, has almost zero susceptibility. Most biological materials are diamagnetic, what means that have a small negative susceptibility; while a few biological substances, mostly blood proteins such as deoxyhemoglobin and hemosiderin, are paramagnetic i.e. have a small positive susceptibility. Whenever a sample contains tissues of different susceptibility, the strength of the magnetic field changes across their boundaries, causing spin dephasing and shortening the T2* value. This occurs around air-filled cavities, as sinuses and petrous bones in the head, and in tissues containing deoxygenated blood or byproducts of hemorrhage.

A.1.5 The Free Induction Decay and the Spin Echo

The attenuation of the transverse magnetization following RF excitation is known as the free induction decay (FID). It results from both microscopic interactions and larger-scale field variations, and occurs on a timescale T2*. The value of T2* varies according to the host molecule and tissue type, but, in each case, the transverse magnetization follows an exponential decay:

$$M_\zeta(t) = M_\zeta(0)e^{-\frac{t}{T_{2^*}}} \tag{A.12}$$

Here, M_ζ is the amplitude of the transverse magnetization and t is the time following the RF excitation. The value of $M_\zeta(0)$ is determined by the longitudinal magnetization available before the excitation and by the FA of the RF pulse.

The dephasing caused by macroscopic and mesoscopic field inhomogeneities is considered reversible, because it can be undone using a simple refocusing procedure. The technique relies on the use of a $180°RF$ pulse (the refocusing pulse) to reverse the phase differences that have accumulated among the spins. The refocusing pulse effectively resets the phase evolution, giving the faster spins a handicap and the slower spins a head start. As the spins continue to precess under the influence of the same field inhomogeneities, they gradually come back into phase, producing a brief signal recovery known as a *spinecho*. The time taken for the spins to rephase exactly equals the time during which they were allowed to dephase, and the total is known as the *echotime*, TE.

The procedure is only able to compensate for magnetic field inhomogeneities on a mesoscopic and macroscopic scale, which remain relatively constant with time. Microscopic interactions, which vary as the molecules rotate and diffuse, produce irreversible dephasing that cannot be undone by the refocusing procedure. The amplitude of the spin echo is therefore attenuated by T2 relaxation, and equals:

$$M_\zeta(TE) = M_\zeta(0)e^{-\frac{TE}{T_2}} \tag{A.13}$$

Both $spin-echo$ and FID acquisition techniques are used in imaging offering alternative types of signal contrast among tissues. Spin-echo acquisitions provide T2 weighting, whereas FID acquisitions provide T2* weighting. The degree of T2 or T2* weighting depends on the time delay between RF excitation and signal acquisition. A longer delay allows more time for transverse relaxation, so that tissues with short T2 or T2* will appear darker than those with longer relaxation times. Note that to obtain pure T2 weighting, the signal must be acquired during the spin echo. The TE can, however, be controlled

via the timing of the refocusing pulse.

A.2 Image Formation

To reconstruct an image the signal from each point within the tissue must be correctly identified and mapped onto the corresponding point within the image. This is achieved with the use of magnetic field gradients, which alter the $Larmor frequency$ of the nuclei in a spatially dependent manner. The signal contrast between different tissues can be controlled via the timing and amplitude of the RF excitation pulses, and through the use of exogenous (injected) contrast agents.

Imaging can be formed using $2D$ or $3D$ acquisitions, which involve the excitation of nuclei in a specified slice or slab of tissue, respectively. Once excited, all the tissues within the slice or slab emit a signal simultaneously. To produce images it is, therefore, necessary to identify the contribution from each point. This is carried out by encoding spatial information into the phase and frequency of the signal. Both slice-selective excitation and spatial encoding involve the use of magnetic field gradients.

A.2.1 Slice-Selective Excitation

Nuclei can absorb energy from the RF field, $B_1(t)$, only if their $Larmor frequency$ exactly matches the frequency of the RF field. Slice-selective excitation is achieved by applying the RF field in the presence of a magnetic field gradient. The gradient introduces a small spatial variation into the strength of the B_0 field (growing arrows in Figure A.3), producing a corresponding variation in the $Larmor frequency$. Only those nuclei whose $Larmor frequency$ ω_L equals the frequency of the applied RF field, ω_{RF}, will be excited. The condition $\omega_L = \omega_{RF}$ is satisfied for nuclei lying in a particular slice of tissue perpendicular to the magnetic field gradient. The thickness of this slice is determined by the bandwidth of the RF pulse and the amplitude of the gradient, each of which can be selected independently. Thin slices are chosen for $2D$ imaging, and thicker slabs for $3D$ imaging. The location of each slice along the direction of the gradient is controlled via the frequency of the RF field. Increasing the RF frequency will excite nuclei in a slice of tissue where the $Larmor frequency$ is correspondingly higher. Finally, the orientation of the slice is determined by the direction of the magnetic field gradient (horizontal arrows representing nuclear magnetization M in Figure A.3). The gradient coils can be used singly

or in combination to excite a slice in any oblique plane.

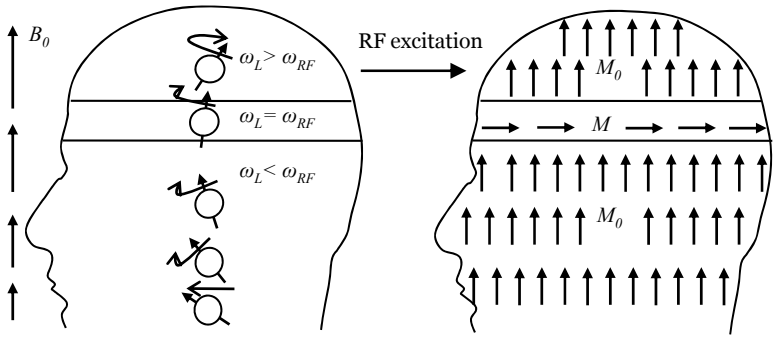

Figure A.3: Slice-selective excitation is achieved by applying a radio frequency pulse in the presence of a magnetic field gradient. The gradient produces a linear variation in the strength if the static field B_0 (growing arrows to the left), which gives rise to a spatial variation in the value of the $Larmor frequency$. Only those spins whose $Larmor frequency$, ω_L, exactly matches the frequency of the applied radio frequency field, ω_{RF}, will be excited. The orientation of the slice is determined by the direction of the magnetic field gradient (horizontal arrows representing nuclear magnetization M).

A.2.2 Spatial Encoding

Because the RF pulse excites all the tissue in the selected slice, where $\omega_L = \omega_{RF}$ in Figure A.3, the emitted signal is a sum of contributions from all the spins within that slice. To identify the contribution from each tissue element, spatial information is encoded into the signal by means of magnetic field gradients that are applied after the RF excitation. By applying a magnetic field gradient during data acquisition, position information is encoded into the frequency of the signal. Tissue located at points where the B_0 field is slightly stronger will emit the signal at a fractionally higher frequency than tissue located at points where it is weaker. Because the detected signal comes from the entire slice, it will contain a range of different frequencies, corresponding to contributions from different tissue elements. The amplitude of each component indicates how much signal came from each position along the direction of the gradient. The technique is known as frequency encoding, because the origin of the signal can be identified by its frequency. However, frequency encoding is not sufficient by

itself to reconstruct an image, because it provides position information in only one direction.

Position information in the perpendicular direction of the $Larmor frequency$ ω_L is obtained through a mechanism known as phase encoding, which is used in combination with frequency encoding to produce an image in $2D$. A gradient pulse is applied in the phase encoding direction before signal acquisition. The gradient pulse alters the $Larmor frequency$ of the spins, but only for a brief period, resulting in a relative phase shift among the spins as depicted with curved arrows in Figure A.4. The detected signal, therefore, contains components with different phases, which originate from different positions along the direction of the gradient. To extract the amplitude of each component, the entire process of excitation and signal acquisition must be repeated many times, with gradient pulses of incrementally different strengths. The change in phase between successive acquisitions uniquely identifies the position of the tissue along the direction of the gradient. Phase encoding is, in fact, mathematically equivalent to frequency encoding, except that the data are acquired in a discrete rather than continuous manner.

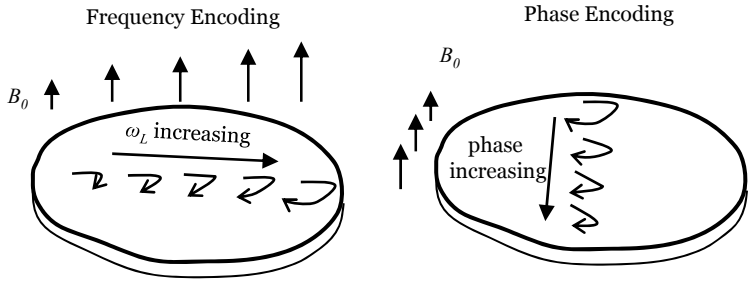

Figure A.4: Having excited the nuclear magnetization within a desired slice of tissue, the position of the spins within the imaging plane must be determined. This is carried out using frequency encoding in one direction (horizontal arrow) and phase encoding in the perpendicular direction (vertical downward arrow). A gradient pulse is applied in the phase encoding direction before signal acquisition. The gradient pulse alters the $Larmor frequency$ of the spins, but only for a brief period, resulting in a relative phase shift among the spins (this shift is represented with curved arrows).

A.2.3 Image Reconstruction

Frequency and phase encoding are used in combination to produce a $2D$ image. The directions of frequency and phase encoding are conventionally denoted x and y, respectively, and the through-slice direction is denoted z. However, these labels are completely arbitrary, and are not connected with the physical axes of the scanner or the gradient coils. In fact, the gradient coils can be used in combination to form an image of the tissue in any oblique plane.

To produce an image, the same slice of tissue is excited repeatedly, and the signal is sampled as a function of time after each excitation. The amplitude of the frequency-encoding gradient remains constant with each repetition, whereas that of the phase-encoding gradient is incremented from one repetition to the next, as shown in Figure A.5.

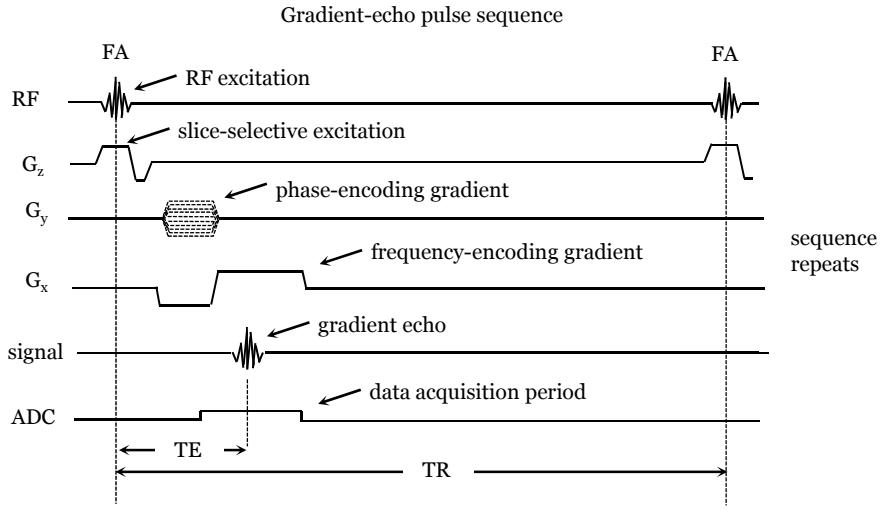

Figure A.5: A simple pulse sequence illustrating the implementation of slice selection and spatial encoding. The top line illustrates the radio frequency pulses produced by the transmitter, which have flip angle, FA. The lines marked G_z, G_y, and G_x indicate the magnetic field gradients in the slice-select, phase-encoding, and frequency-encoding directions, respectively. The label ADC denotes the analog-to-digital converter, which is turned on during signal acquisition.

The resulting data are recorded as a series of lines in a $2D$ array known

as $k-space$. By applying a $2D$ Fourier transform to the $k-space$ data, the spatial distribution of the signal is recovered. The phase information is usually discarded at that stage, leaving a map of the signal amplitude, which constitutes the image. Figure A.6 shows the process of image reconstruction.

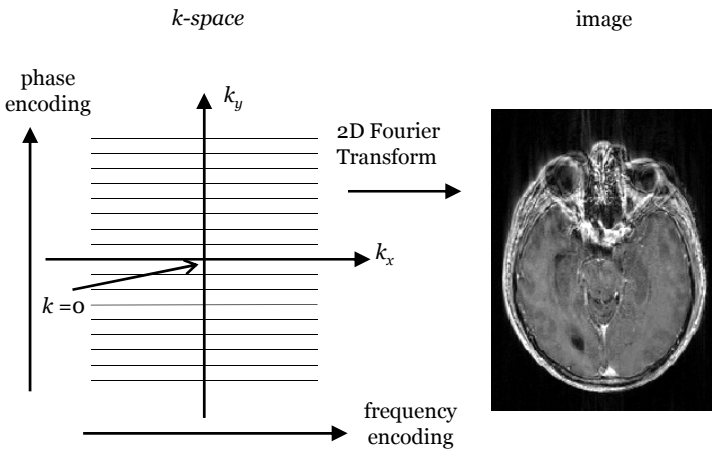

Figure A.6: Process of image reconstruction. After each excitation, the magnetic resonance signal is acquired as a function of time and recorded as a row of numbers in a data array known as $k-space$. The process is repeated with phase-encoding gradients of incrementally different amplitudes, and each time the signal is recorded as an adjacent line in $k-space$. After all of the $k-space$ data have been collected, the image is extracted by means of a $2D$ fast Fourier transform.

The resolution of the image in the phase-encoding direction is determined by the number of $k-space$ lines collected. For example, an image with a resolution of 256 pixels in the phase-encoding direction for example requires the acquisition of 256 $k-space$ lines. Resolution in the frequency-encoding direction is determined by the amplitude of the frequency-encoding gradient and the duration of the acquisition period.

For $3D$ acquisitions, phase encoding is used in the through-slab direction as well as one of the inplane dimensions. This produces a $3D$ set of k-space data, which can be reconstructed into a $3D$ map of the tissue by means of a $3D$ Fourier transform. The results are typically displayed as a stack of $2D$ images, but can be reconstructed along any plane.

It is useful to note that data in a k-space can be interpreted as spatial-frequency components of the image. Data near the center of $k - space$ $(k = 0)$ correspond to low spatial-frequency components and represent the large-scale or coarse spatial structure in the image. Data near the outer edges of $k - space$ correspond to high spatial-frequency components, and represent the fine structure in the image.

This document was finished
in September 2009